

論文 / 著書情報
Article / Book Information

題目(和文)	量子計算に基づく画像データ探索、電子透かし及び感情空間の表現法
Title(English)	Quantum Computation based Image Data Searching, Image Watermarking, and Representation of Emotion Space
著者(和文)	閻 飛
Author(English)	Yan Fei
出典(和文)	学位:博士(工学), 学位授与機関:東京工業大学, 報告番号:甲第9544号, 授与年月日:2014年3月26日, 学位の種別:課程博士, 審査員:廣田 薫,新田 克己,室伏 俊明,長谷川 修,小野 功
Citation(English)	Degree:Doctor (Engineering), Conferring organization: Tokyo Institute of Technology, Report number:甲第9544号, Conferred date:2014/3/26, Degree Type:Course doctor, Examiner:,,,,,
学位種別(和文)	博士論文
Type(English)	Doctoral Thesis

Quantum Computation based Image Data Searching, Image Watermarking, and Representation of Emotion Space

「量子計算に基づく画像データ探索、
電子透かし及び感情空間の表現法」

Yan Fei

閻 飛

Supervisor: Prof. Kaoru Hirota

Doctoral Thesis

Tokyo Institute of Technology

東京工業大学

Interdisciplinary Graduate School of Science and Engineering

大学院総合理工学研究科

Department of Computational Intelligence and Systems science

知能システム科学専攻

March 2014

Abstract

Quantum computation is a promising and rapidly growing field that has witnessed a series of significant breakthroughs in the last several decades. While some practitioners envision the realization of complete quantum computing devices, the research presented in the thesis focusses on the works that we can do with quantum computing hardware when they are realized. One of such areas is that of quantum image processing. A Flexible Representation of Quantum Images (FRQI) allows us to dedicate n -qubits and 1-qubit to capturing the information about the position and color of every pixel in the image, respectively.

A method to compare multiple pairs of quantum images in parallel is proposed, where the similarities of the images are estimated according to the probability distributions of the readouts from quantum measurements. It offers a significant speed-up in comparison to performing the same task on traditional computing devices by means of a single Hadamard gate with control-conditions to transform the entire information encoding the quantum images in a strip. The simulation experiments comprising of the comparison of two images, multiple pairs of images, and the sub-blocks from two images are implemented to demonstrate the feasibility and efficiency of the parallel comparison. On the basis of such a comparison strategy, a quantum image searching method is presented where the image in a 4×4 binary image database with the highest similarity value to the particular test image is retrieved as the search result using low computational resources. To process the RGB-like quantum image, the representation for Multi-Channel Quantum Images (MCQI) is given, and a double-key, double-domain watermarking strategy for

MCQI images is stated. It protects the security of quantum images by embedding the watermark image into both the spatial domain and the frequency domain of carrier image with different keys. A Tokyo Tech logo as the watermark information is embedded into nine building images which yields an great improvement in terms of the visible quality of the watermarked images. Inspired by the quantum image processing, the representation of emotion space is modestly extended into quantum field that a Bloch Sphere based Emotion Space (BSES) is presented, where two angles φ and θ in Bloch sphere represent the emotion (such as happiness, surprise, anger, sadness, expectation, and relaxation in $[0, 2\pi)$) and its intensity (from neutral to maximum in $[0, \pi]$), respectively. It takes advantage of the psychological interpretation of color to assign the basic colors to each emotion subspace so that the BSES space can be visualized, and by using the quantum gates, changes in emotions can be tracked and recovered. In the experimental validation of the proposal, two typical human emotions, i.e. happiness and sadness, are analyzed and visualized in BSES space according to a preset emotional transition model.

These proposals in the thesis extend classical-like image and emotion processing applications to the quantum computing domain. They provide a basic step for designing a search engine on quantum computing devices. In addition, the watermarking strategy sets a stage for other applications aimed at quantum data protection. The transition matrix that tracks the emotional change in BSES space could be used to control quantum robots in order to make them adaptive and responsive to human emotions.

Acknowledgements

As the Chinese saying goes, ‘Good honing gives a sharp edge to a sword; Bitter cold adds keen fragrance to plum blossom’. During the past three years, I kept challenging myself with unremitting efforts and persistence, and taking every difficulty as the chance to make me better. When I am Looking back the days that I strove, many people have helped and supported me to this success story. It is therefore a great pleasure to thank them in these opening remarks.

First and foremost, I must start by expressing my sincere appreciation and profound gratitude to my advisor and supervisor, Prof. Kaoru Hirota, for not only his devotion in the guidance to me, but for also helping me to get to know Japan and even the whole world. My appreciation must also go to Prof. Fangyan Dong, for her thoughtful kindness both in my work and life all the time. Nothing is impossible because I know she is always waiting over there. My gratitude goes to Ms. Harumi Hoshino for always making the lab’s miscellaneous jobs methodically. My examiners: Profs. Katsumi Nitta, Toshiaki Murofushi, Osamu Hasegawa, and Isao Ono, deserve special commendation for their professional comments and criticisms, which helped to shape my research and improve the content of this thesis to a large extent.

I want to appreciate the Quantum Computation Group (QCG) members at Hirota lab, Drs. Phuc Q. Le, Abdullah M. Ilyasu, Bo Sun, and Jesus A. Garcia. In addition to the loads of fun we had together, they helped tremendously in exploring my potential for which I thank them enormously. Worthy of special mention is Dr. Ilyasu, my senpai, my research pioneer, my English teacher, and the most important is that my best friend. I

will never forget the intense discussions with him at the coffee shops; I will never forget his assistance and encouragement when I wrote my first paper; and surely I will never forget those calls from overseas for urging me to continue my research even after his graduation. He always makes things much easier, and I would like to use the word he created to express my gratitude to him ‘Thanksdoomshukrangracias’.

I am also grateful for the past members of Hirota lab that deserve my special appreciation include: Drs. Jingpei Dan, Chastine Fatichah, Zhentao Liu, Martin L. Tangel, and Mr. Yojiro Adachi. Among the present members of the lab, I must acknowledge the friendship and comradeship of my tutor on arrival to Japan, Dr. Yongkang Tang, and my good friends Drs. Janet P. Betancourt, Kazuhiro Ohnishi, Luefeng Chen, and Jiajun Lu. And beyond our lab, kudos must go to my numerous friends in my ‘pingpong group’ and Chinese Scholars and Students Association of Tokyo Institute of Technology.

I am forever indebted to the Japanese Government and people for not only shouldering the huge burden of sponsoring my programme over the past three years but for also being friendly and accommodating hosts for me. As my culture and Japanese language learning, I would like to express my gratitude to the senseis in the Japanese follow up class, e.g. Yasuaki Itoh sensei, for teaching me and showing me around.

Finally, no amount of words can convey my appreciation and gratitude to my parents. The patience, support, understanding, and perseverance of my parents and relatives throughout this 3 years are the reason I have survived to tell my story.

Contents

1	Introduction	1
2	A flexible representation of quantum images and its processing operations	6
2.1	Introduction	6
2.2	Quantum bits and qubit gates	7
2.3	Quantum image processing framework for FRQI, GTQI, and CTQI	10
2.3.1	Flexible representation for quantum images	10
2.3.2	Fast geometric transformations on quantum images	11
2.3.3	Efficient color transformations on quantum images	14
2.4	Multi-channel representation for quantum images	15
2.5	Conclusion	17
3	A parallel comparison of multiple pairs of images on quantum computers	19
3.1	Introduction	19
3.2	Representation of strip encoding multiple FRQI images	20
3.3	Parallel comparison of multiple pairs of quantum images	22
3.3.1	Scheme to compare images in parallel on quantum computers	23
3.3.2	Evaluation of the similarity between two quantum images	25
3.3.3	A parallel comparison of multiple pairs of images in a strip	28

3.3.4	Comparison between two arbitrary quantum images and the sub-blocks	33
3.4	Simulation experiments to assess the similarity of quantum images	36
3.4.1	Comparison of two synthetic quantum images	36
3.4.2	Parallel comparison of four quantum images in a strip	37
3.4.3	Comparison of sub-blocks from two quantum images	38
3.5	Conclusion	41
4	Quantum image searching based on probability distributions	45
4.1	Introduction	45
4.2	Representation of Z-strip to indicate multiple FRQI images	46
4.3	Image searching on quantum mechanical systems	48
4.4	A simulation experiment to search quantum images from database	53
4.5	Conclusion	55
5	A double-key, double-domain watermarking strategy for multi-channel quantum images	57
5.1	Introduction	57
5.2	General schematic of watermarking strategy for MCQI images	58
5.3	Double-key generation and double-domain embedding procedure	62
5.3.1	Two watermark information generation	62
5.3.2	Spatial domain embedding and CIK generation	63
5.3.3	Frequency domain embedding and PIK generation	66
5.3.4	Embedding and extracting procedure of watermark image	66
5.4	Simulation experiments of watermarking for MCQI images	68
5.5	Conclusion	69
6	Bloch sphere based representation for quantum emotion space	71
6.1	Introduction	71
6.2	Bloch sphere based emotion space	73
6.2.1	Qubit and human emotion	73

6.2.2	Representation of BSES space	74
6.3	Quantum Emotion in BSES space	77
6.3.1	Definition of quantum emotion	78
6.3.2	Generation of quantum emotion	80
6.4	Experiment of representing human emotion in BSES space	81
6.5	Conclusion	84
7	Conclusions	86
	Bibliography	97
	Related Publications	98

List of Figures

1.1	Outline of thesis.	5
2.1	Bloch sphere representation of a qubit.	8
2.2	NOT, Z, Hadamard, CNOT, and Toffoli gates.	9
2.3	Quantum circuit symbol for measurement.	9
2.4	A 2×2 FRQI image, its circuit structure and FRQI state.	11
2.5	Generalized circuit design for geometric transformations on quantum images.	12
2.6	An example of two-point swapping operation.	13
2.7	An example of two sub-blocks swapping operation.	13
2.8	Single qubit gates applied on the color wire.	14
2.9	The 8×8 images before and after the application of the gate X on the color wire.	15
2.10	General circuit of MCQI images.	17
2.11	A 2×2 MCQI image, its circuit structure and MCQI state.	17
3.1	Circuit structure to encode the strip input.	22
3.2	Scheme to compare quantum images in parallel on quantum computers.	25
3.3	Generalized circuit structure for comparing two FRQI images.	26
3.4	Four strips where each comprises two images are considered in order to compare the four pairs of images.	28
3.5	Generalized circuit structure for a parallel comparison of $2^m - 1$ pairs of images.	29

3.6	An example to realize the simultaneous comparison of two pairs of images.	32
3.7	Generalized circuit structure for parallel comparison of FRQI images. . . .	34
3.8	Comparison of two sub-blocks, ‘C’ and ‘M’ from images $ I_0\rangle$ and $ I_3\rangle$ in strip $ \varphi_0\rangle$. Strip $ \varphi_1\rangle$, $ \varphi_2\rangle$, and $ \varphi_3\rangle$ in (a) are the midterm states when applying the circuit in (b).	35
3.9	Two synthetic 8×8 FRQI images and the circuit structure for their comparison.	37
3.10	Two synthetic 256×256 FRQI images and the circuit structure for their comparison.	38
3.11	The strip on the left and the images being compared in the strip.	39
3.12	Circuit structure of comparing the images in Figure 3.11.	40
3.13	Histogram of the probabilities of the readouts in the measurements.	41
3.14	Parallel comparison of two Lena images and two ‘Man’ images.	41
3.15	Circuit structure for realizing the comparison in Figure 3.14.	42
3.16	Histogram of the probabilities of the readouts in the measurements.	43
4.1	Circuit structure to encode the Z-strip input.	48
4.2	An example of Z-strip, its circuit structure and Z-FRQI state.	49
4.3	Generalized circuit structure for parallel comparison of quantum images in Z-strip.	50
4.4	Block diagram of scheme to realize image searching on quantum mechanical systems.	52
4.5	Image searching from database $ D\rangle$	53
4.6	Circuit structure for realizing the image searching in Figure 4.5.	54
4.7	Similarities among different pairs of images in Z-strip.	55
4.8	The test image $ D(2)\rangle$ and the retrieved image $ D_{37}(2)\rangle$	55
5.1	General schematic for MC-WaQI.	60
5.2	The watermark image and its separations in 4 channels.	62
5.3	Watermark image $ SW\rangle$ in spatial domain.	62

5.4	(a) Watermark image $ FW\rangle$ and (b) resized version $ FW'\rangle$ in frequency domain.	63
5.5	Generation procedure of CIK.	64
5.6	The rule of applying CIK operations.	65
5.7	(a) Watermark image $ SW\rangle$ and (b) result image $ SW'\rangle$ by applying CIK operations.	65
5.8	(a) Scrambled image $ FW''\rangle$ and (b) scrambled image $ SW''\rangle$	66
5.9	(a) Resized image $ FW'''\rangle$ and (b) resized image $ SW'''\rangle$	68
5.10	All the carrier images in the simulation experiments.	70
5.11	(a) The carrier image, (b) watermark image, and (c) watermarked image.	70
6.1	Pleasure-arousal judgment space for affective feelings.	75
6.2	Pleasure-arousal judgment space with continuous color disc for affective feelings.	76
6.3	Human emotional space expressed using the Bloch sphere.	77
6.4	Generation of human emotion in BSES space.	81
6.5	‘Happy’ emotion and its representation in the BSES space.	83
6.6	‘Sad’ emotion and its representation in the BSES space.	83

List of Tables

3.1	Image comparison by applying Hadamard operation on different strip wires.	33
3.2	Summary of comparison results for synthetic images in Figures 3.9 and 3.10.	37
3.3	Comparison results for the images encoded in the strip in Figure 3.11.	38
3.4	Comparison results for the sub-blocks from two images.	42
6.1	Different emotions expressed by colors [50][19][35].	75
6.2	Quantum emotion scores for single Action Units adapted from [53].	79
6.3	Quantum emotion scores for the two emotions in Figures 6.5 and 6.6.	82

Chapter 1

Introduction

Computer science and computer engineering are disciplines that have transformed every aspect of human endeavor. In these fields, novel methods for speeding-up certain tasks, and building bridges between computer science and several other scientific fields are attracting the gaze of scientists. Quantum computation is such a thriving and advancing field with a considerable number of evolutions in the past several decades [56][25][11]. In 1982, Feynman proposed a novel computation model named quantum computers based on principles of quantum physics which seemed to be more powerful than classical ones [20]. Subsequently, Shor's polynomial time algorithm for the integer factoring problem [56][51] and Grover's database search algorithm [25][17] are essential evidences supporting the superiority of quantum computers.

A quantum computer is a physical machine that can accept input states which represent a coherent superposition of many different inputs and subsequently evolve them into a corresponding superposition of outputs [6][55]. Computation, i.e. a sequence of unitary transformations, affects simultaneously each element of the superposition, generating a massive parallel data processing albeit within one piece of hardware. The smallest unit to facilitate such computation, the qubit, has logical properties that are inherently different from their classical counterparts. While bits and their manipulation can be described using two constants (0 and 1) and the tools of boolean algebra, qubits, on the other hand must be discussed in terms of vectors, matrices, and other linear algebraic constructions [33][7]. The current paradigm for implementing quantum algorithms is the quantum

circuit model [7], in which the algorithms are compiled into a sequence of simple gates acting on one or more qubits. Many of these quantum algorithms are expressed in terms of uniform special-purpose circuits that depend strongly on the problem at hand. These circuits comprise various levels of abstraction and combinations of the universal gates: NOT, Hadamard, Controlled-NOT, and Toffoli gates. These gates combine to form what is often referred to in the literature as the NCT library [33][3].

Quantum computation and quantum information have appeared in various areas of computer science such as information theory, cryptography, image processing, and emotion representation because the inefficient tasks on classical computers can be overcome by exploiting the power of the quantum computation [49][13]. Quantum image processing, which utilizes the characteristic of quantum parallelism [20] to speed up many processing tasks, is a subfield of quantum information processing [31]. Because the first step in quantum image processing field involves proposals on representations to capture and store the image on quantum computers, various representations for images on quantum computer were proposed, such as Qubit Lattice [63], Real Ket [36], Grid Qubit [62], the Flexible Representation of Quantum Image (FRQI) [37][41], and Multi-Channel Quantum Image (MCQI) [60][59]. Many image processing strategies exploiting these representations are also developed to process transformations that target the geometric information and the color information [38][39][57][58]. In addition, applications based on these representations are presented such as the digital watermarking and the framework of producing quantum movies [29][32][33][28].

The smallest unit of information in a quantum system, a qubit, is a unit vector in a two-dimensional Hilbert space that can exist in a superposition state. It only ever gives ‘0’ or ‘1’ as the measurement result probabilistically when a qubit is measured [49]. These are analogous to the human’s behavior where in the inside of human mind there are a number of emotions, but the final course of action taken typically represents one emotion [52]. An emotion space is always used to represent the emotion in terms of quantitative analysis and visualization which is critical to facilitate a smooth communication in face-to-face communication. In 1997, pleasure-arousal judgment space [53] was proposed to

represent not only specific emotions but also continuous variations in emotions, in which each emotion can be placed when stimuli are translated into appropriate values. On the basis of the pleasure-arousal space, a certainty axis was added to produce smooth and effective communication between humans and robots [46]. After that in order to consider about the rapid variations in the mentality state due to real time human-robot interaction, affinity pleasure-arousal space [66] was proposed where the affinity axis was used to describe the transition from one mentality state to another according to the progress of the conversation and repetitive interaction.

The thesis tries to extend classical-like image and emotion processing applications to the quantum computing domain which is organized as follows:

In Chapter 2, the basic knowledge and notations in quantum computation are introduced first. In addition, the Flexible Representation of Quantum Images (FRQI) which captures two fundamental information (i.e. its color and position) about an image, the general framework and classification of all geometric transformations on FRQI image, and the efficient color transformations on FRQI image are reviewed. Finally, the extension of FRQI image which is for processing the color image, the Multi-Channel representation for Quantum Images (MCQI), is introduced.

In Chapter 3, a method to compare multiple pairs of quantum images in parallel is proposed, where the similarities of the images are estimated according to the probability distributions of the readouts from quantum measurements. The proposed method by means of a single Hadamard gate with control-conditions to transform the entire information encoding the quantum images in a strip, offers a significant speed-up in comparison to performing the same task on traditional computing devices. Three simulation experiments comprising of the comparison of two images, multiple pairs of images, and the sub-blocks from two images are implemented to demonstrate the feasibility and efficiency of the parallel comparison. The proposal advances a fundamental step towards image searching on quantum computers in which the image with the highest similarity to a particular reference image is retrieved as a search result from a database.

In Chapter 4, a quantum image searching method is proposed based on the probability

distributions of the readouts from the quantum measurements. It is achieved by using low computational resources which are only a single Hadamard gate combined with $m + 1$ quantum measurement operations. To validate the proposed method, a simulation experiment is used where the image with the highest similarity value of 0.93 to the particular test image is retrieved as the search result from 4×4 binary image database. The proposal provides a basic step for designing a search engine on quantum computing devices where the image in the database is retrieved based on its similarity to the test image.

In Chapter 5, based on the representation of MCQI, a new watermarking strategy (MC-WaQI) is proposed where the double-key and double-domain idea makes the watermarking more secure. The strategy realizes the watermarking method to protect the copyright of the quantum images, which embeds the specific quantum symbolic information (such as the logo representing the image's owner) into color quantum images.

In Chapter 6, a Bloch Sphere based Emotion Space (BSES), where two angles φ and θ in Bloch sphere represent the emotion (such as happiness, surprise, anger, sadness, expectation, and relaxation in $[0, 2\pi)$) and its intensity (from neutral to maximum in $[0, \pi]$), respectively is proposed. It takes advantage of the psychological interpretation of color to assign the basic colors to each emotion subspace so that the BSES space can be visualized and changes in emotions can be tracked and recovered by using the quantum gates. In the experimental validation of the proposal, two typical human emotions, i.e. happiness and sadness, are analyzed and visualized in BSES space according to a preset emotional transition model. The transition matrix that tracks the emotional change could be used to control quantum robots in order to make them adaptive and responsive to human emotions.

In Chapter 7, the proposals and related works in the thesis are summarized, in addition, new extensions and applications are discussed for the future work.

The road map visualizes the dependence among the individual chapters, and summarizes the thesis organization as shown in Figure 1.1.

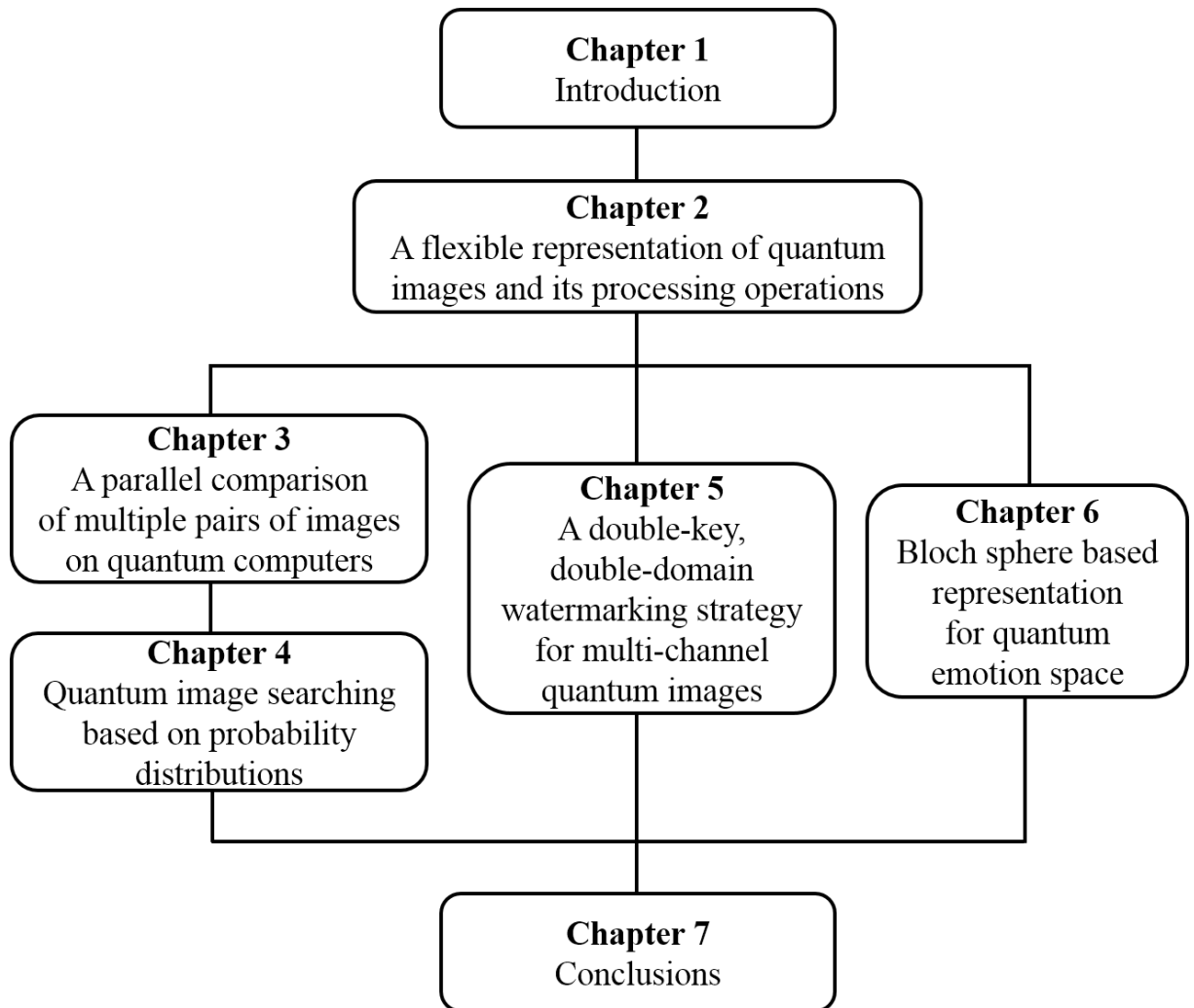


Figure 1.1: Outline of thesis.

Chapter 2

A flexible representation of quantum images and its processing operations

2.1 Introduction

A Flexible Representation of Quantum Images (FRQI) [37][41] that captures information about colors and corresponding positions of every point in an image into a normalized quantum state is reviewed in this chapter. By using such a representation, some basic image processing operations such as image rotation and color transformation can be done through applying the elementary gates combined with appropriate quantum measurements. Furthermore, some image processing based framework to produce application-specific quantum computing software and hardware can be designed based on FRQI representation. As the basis of quantum research, the quantum bits and qubit gates are reviewed first as shown in Section 2.2, where the quantum state, its specialized properties as well as often-used quantum gates, and its visualization in Bloch sphere are brushed up. In addition, the general scheme and classification of geometric transformations and the efficient color transformations on FRQI images are reviewed in Section 2.3, from which we can see how our familiar image processing operations in classical computing devices are realized to the quantum images in FRQI representation. The last part of this chapter is the extension of FRQI images which is for processing the color image, the Multi-Channel representation for Quantum Images (MCQI). It is introduced in Section 2.4 for the prepa-

ration of its watermark processing in Chapter 5.

2.2 Quantum bits and qubit gates

The basic notations used in this thesis are introduced below. The state of a quantum system is described as a vector in a Hilbert space which is called a ket in quantum mechanical notation. The ket and its adjoint, bra, notations are defined as

$$|u\rangle = \begin{pmatrix} u_0 \\ u_1 \\ \vdots \\ u_{n-1} \end{pmatrix}, u_i \in C, i = 0, 1, \dots, n-1, \quad (2.1)$$

$$\langle u| = |u\rangle^* = [u_0^* u_1^* \cdots u_{n-1}^*] \quad (2.2)$$

where u^* is the notation of complex conjugate of u .

The smallest unit of information in a quantum system is a qubit, which is a unit vector in two dimensional Hilbert space defined by

$$\psi = \begin{pmatrix} \alpha \\ \beta \end{pmatrix} = \alpha \begin{pmatrix} 1 \\ 0 \end{pmatrix} + \beta \begin{pmatrix} 0 \\ 1 \end{pmatrix} = \alpha|0\rangle + \beta|1\rangle, \quad (2.3)$$

where α and β are complex numbers.

On the consideration of the normalized state of qubits, $|\alpha|^2 + |\beta|^2 = 1$, and ignoring the factor which has no observable effects, one picture useful in thinking about qubits is the following geometric representation,

$$\psi = \cos \frac{\theta}{2} |0\rangle + e^{i\varphi} \sin \frac{\theta}{2} |1\rangle, \quad (2.4)$$

where θ and φ are real numbers that define a point on the unit three-dimensional sphere, i.e. Bloch sphere in Figure 2.1, which provides a useful means of visualizing the state of a single qubit, and often serves as an excellent test-bed for ideas about quantum

computation and quantum information. Many of the operations on single qubits can be neatly described within the Bloch sphere picture [49].

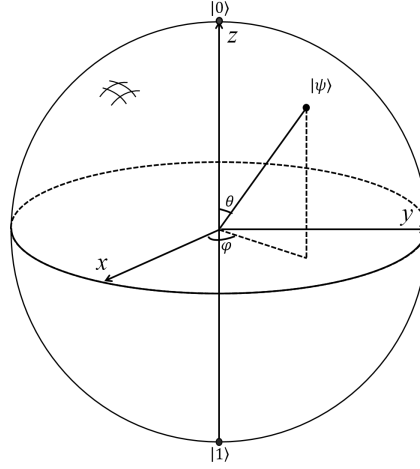


Figure 2.1: Bloch sphere representation of a qubit.

The notation for the tensor product, \otimes , is used to express the composition of quantum systems. The tensor product of two matrices is defined as follows:

$$A = \begin{pmatrix} a_{11} & a_{12} & \cdots & a_{1m} \\ a_{21} & a_{22} & \cdots & a_{2m} \\ \vdots & \vdots & \ddots & \vdots \\ a_{n1} & a_{n2} & \cdots & a_{nm} \end{pmatrix}, B = \begin{pmatrix} b_{11} & b_{12} & \cdots & b_{1q} \\ b_{21} & b_{22} & \cdots & b_{2q} \\ \vdots & \vdots & \ddots & \vdots \\ b_{p1} & b_{p2} & \cdots & b_{pq} \end{pmatrix}, \quad (2.5)$$

$$A \otimes B = \begin{pmatrix} a_{11}B & a_{12}B & \cdots & a_{1m}B \\ a_{21}B & a_{22}B & \cdots & a_{2m}B \\ \vdots & \vdots & \ddots & \vdots \\ a_{n1}B & a_{n2}B & \cdots & a_{nm}B \end{pmatrix}. \quad (2.6)$$

The short notation for tensor product $|u\rangle \otimes |v\rangle$ of two vectors or two kets, $|u\rangle$ and $|v\rangle$, is $|uv\rangle$ or $|u\rangle|v\rangle$ and $A^{\otimes n} = A \otimes A \otimes \cdots \otimes A$ is used to denote the tensor product of a matrix A for n times.

In the quantum circuit model, a complex transform is broken down into simpler gates such as the commonly used NOT, Hadamard, CNOT, and Toffoli gates which are shown in Figure 2.2. The gate which acts on k qubits is usually represented by a $2^k \times 2^k$

unitary matrix, and the number of qubits in the input and output of the gate have to be equal. The final step in quantum simulation is the measurement which converts the quantum information into the classical information in form of probability distributions, i.e. it converts a single qubit state $|\psi\rangle = \alpha|0\rangle + \beta|1\rangle$ into a probabilistic classical bit M (distinguished from a qubit by drawing it as a double-line wire), which is 0 with probability $|\alpha|^2$ or 1 with probability $|\beta|^2$ as shown in Figure 2.3.

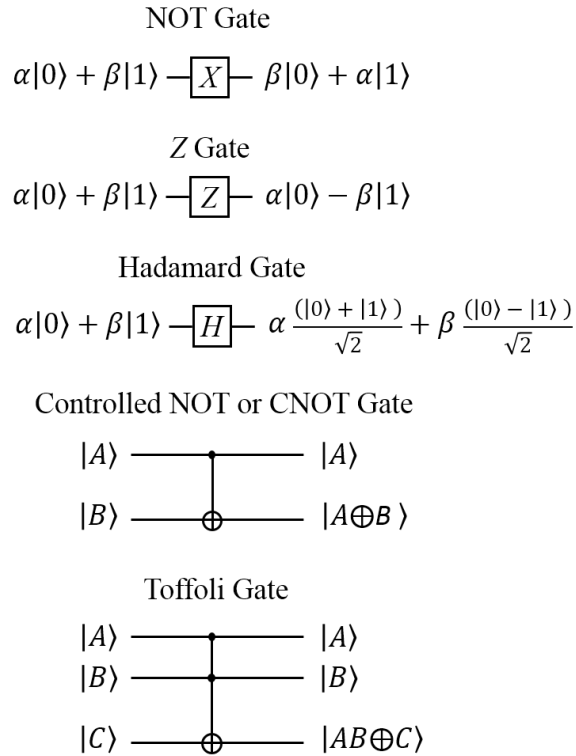


Figure 2.2: NOT, Z, Hadamard, CNOT, and Toffoli gates.

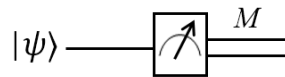


Figure 2.3: Quantum circuit symbol for measurement.

2.3 Quantum image processing framework for FRQI, GTQI, and CTQI

The realization of most quantum image processing applications will undoubtedly rely on using their corresponding classical operations as reference. In this section, a Flexible Representation for Quantum Images, FRQI, which is similar to the pixel representation for images on conventional computers is introduced initially, in addition, the geometric transformation based on FRQI images (GTQI) which can swap two points, even two sub-blocks in an image and the transformation focusing on the color information (CTQI) are reviewed.

2.3.1 Flexible representation for quantum images

The Flexible Representation for Quantum Images, FRQI [37][41], captures the essential information about the colors as well as the corresponding positions of every point in an image and integrates them into a quantum state having its formula in Equation (2.7),

$$|I(n)\rangle = \frac{1}{2^n} \sum_{i=0}^{2^{2n}-1} |c_i\rangle \otimes |i\rangle, \quad (2.7)$$

where

$$|c_i\rangle = \cos \theta_i |0\rangle + \sin \theta_i |1\rangle, \quad (2.8)$$

$$\theta_i \in [0, \frac{\pi}{2}], i = 1, 2, \dots, 2^{2n} - 1, \quad (2.9)$$

where $|0\rangle$ and $|1\rangle$ are 2-D computational basis quantum states, $|i\rangle$, $i = 1, 2, \dots, 2^{2n} - 1$, are $2n$ -D computational basis quantum states and $\theta = (\theta_0, \theta_1, \dots, \theta_{2^{2n}-1})$ is the vector of angles encoding colors. There are two parts in the FRQI representation of an image; $|c_i\rangle$ and $|i\rangle$ which encode information about the colors and corresponding positions in the image, respectively. For the 2-D images, the position information $|i\rangle$ includes two parts, the vertical and horizontal co-ordinates. In $2n$ -qubit systems for preparing quantum

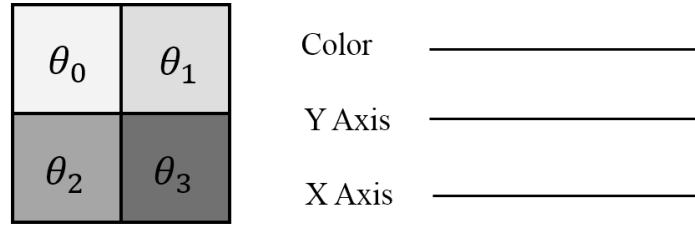
images, or n -sized images, the vector

$$|i\rangle = |y\rangle|x\rangle = |y_{n-1}y_{n-2}\cdots y_0\rangle|x_{n-1}x_{n-2}\cdots x_0\rangle, \quad (2.10)$$

$$x_j, y_j \in \{0, 1\}, \quad (2.11)$$

for every $j = 0, 1, \dots, n$, encodes the first n -qubit $y_{n-1}y_{n-2}\cdots y_0$ along the vertical location and the second n -qubit $x_{n-1}x_{n-2}\cdots x_0$ along the horizontal axis. An example of a 2×2 FRQI image is shown in Figure 2.4. The FRQI state is a normalized state, i.e. $\|I(\theta)\| = 1$ as given by

$$\|I(n)\| = \frac{1}{2^n} \sqrt{\sum_{i=0}^{2^{2n}-1} (\cos^2 \theta_i + \sin^2 \theta_i)} = 1. \quad (2.12)$$



$$|I(1)\rangle = \frac{1}{2} [(\cos \theta_0 |0\rangle + \sin \theta_0 |1\rangle) \otimes |00\rangle + (\cos \theta_1 |0\rangle + \sin \theta_1 |1\rangle) \otimes |01\rangle + (\cos \theta_2 |0\rangle + \sin \theta_2 |1\rangle) \otimes |10\rangle + (\cos \theta_3 |0\rangle + \sin \theta_3 |1\rangle) \otimes |11\rangle]$$

Figure 2.4: A 2×2 FRQI image, its circuit structure and FRQI state.

2.3.2 Fast geometric transformations on quantum images

Geometric Transformations on Quantum Images (GTQI) [38] are the operations which focus on manipulating the geometric information of the FRQI images, i.e. information about position of every point in the image. These transformations are akin to ‘shuffling’ the image content point-by-point. The global effect being a transformation of the original image to a new state whose nature is determined by the gate sequence of the operation needed to accomplish the desired transformation [29]. Such transformations are referred to as geometric transformations, G_I , which on FRQI images can be defined as in Equation

(2.13),

$$G_I(|I(n)\rangle) = \frac{1}{2^n} \sum_{i=0}^{2^{2n}-1} |c_i\rangle \otimes G(|i\rangle), \quad (2.13)$$

where $|I(n)\rangle$ is of the form defined in Equation (2.7) and $G(|i\rangle)$ for $i = 0, 1, \dots, 2^{2n} - 1$ is the unitary transformation performing geometric exchanges based on the vertical and horizontal information represented by $|i\rangle$. The general structure of circuits for geometric transformations on FRQI images is shown in Figure 2.5.

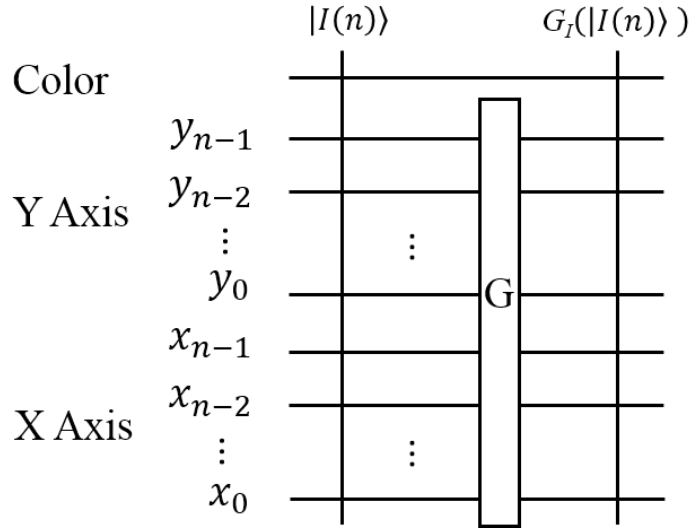


Figure 2.5: Generalized circuit design for geometric transformations on quantum images.

Using the GTQI operations, classical-like transformations such as flipping, swapping, or rotating an image can be performed on quantum computers using images encoded in the FRQI representation. An example of two-point swapping between the content of the image located in $|001\rangle|100\rangle$ and $|010\rangle|000\rangle$ as well as the corresponding circuit structure to accomplish the swapping operation are shown in Figure 2.6. The input and output images are shown in (a) and (c), respectively, and the corresponding circuit structure to accomplish the swapping operation is presented in (b). The complexity of two-point swapping operation on n -sized FRQI images ($n \geq 2$) is $O(n^2)$ [38].

When geometric transformations are well-understood, often designers of new operations would want to use smaller versions of the transformations as the main components to realize more complex operations. Restricted geometric transformations on FRQI images were proposed in [40] in order to constrain the desired geometric transformation to

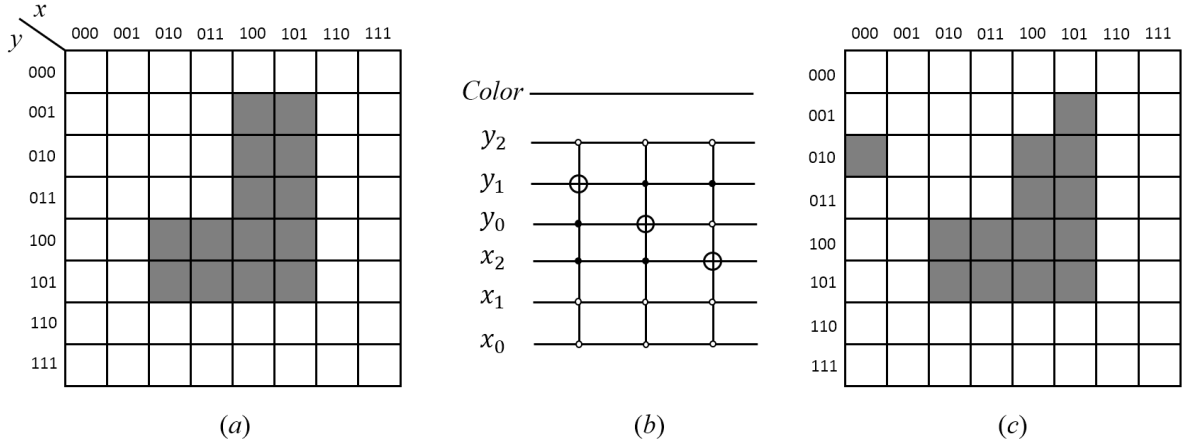


Figure 2.6: An example of two-point swapping operation.

a smaller sub-block of the image by imposing additional restrictions to indicate specific locations. An example for swapping two sub-blocks where the first comprises the positions labelled 1, 2, 3, and 4, and the other consists of the positions labelled 5, 6, 7, and 8 is presented in Figure 2.7. The input and output image are shown in (a) and (c), respectively, and the corresponding circuit structure to accomplish the swapping operation is presented in (b).

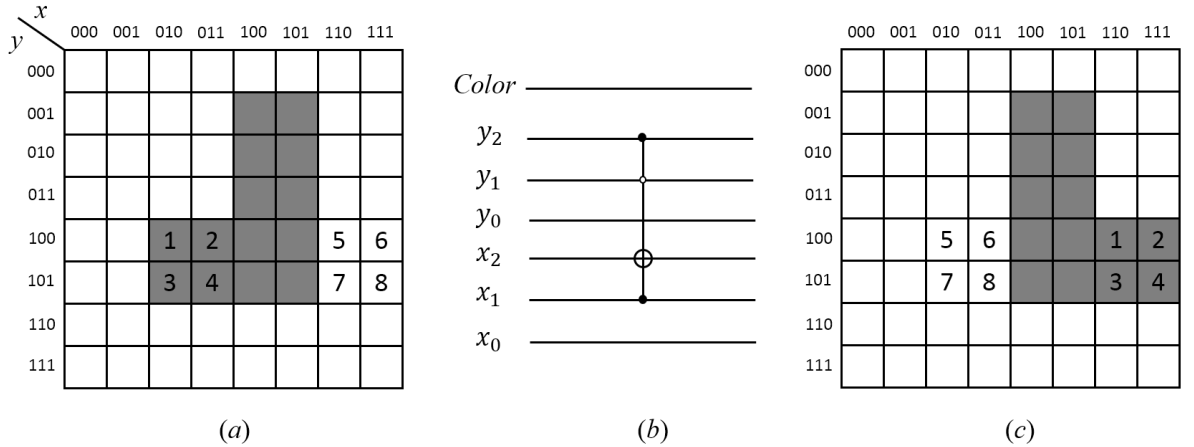


Figure 2.7: An example of two sub-blocks swapping operation.

In order to account for the change in complexity of the circuit caused by applying additional control on the original operations, some properties of FRQI related to the number of controls and the size of affected sub-blocks were analyzed in the Remark of [40]. It is known that the more the number of controls the transformations have, the less

the size of the affected areas.

2.3.3 Efficient color transformations on quantum images

When a single qubit gate, C , is applied with control conditions on the color wire in FRQI representation as shown in Figure 2.8, the colors of every controlled position in the image are changed. Such a color transformation can be defined as

$$C_I(|I(n)\rangle) = \frac{1}{2^n} \sum_{i=0}^{2^{2n}-1} C(|c(\theta_k)\rangle) \otimes |i\rangle, \quad (2.14)$$

where C_I is the qubit gate to transform the color information in quantum image $|I(n)\rangle$ and $|c(\theta_k)\rangle$ encodes the color information which is presented as

$$|c(\theta_k)\rangle = \cos \theta_k |0\rangle + \sin \theta_k |1\rangle. \quad (2.15)$$

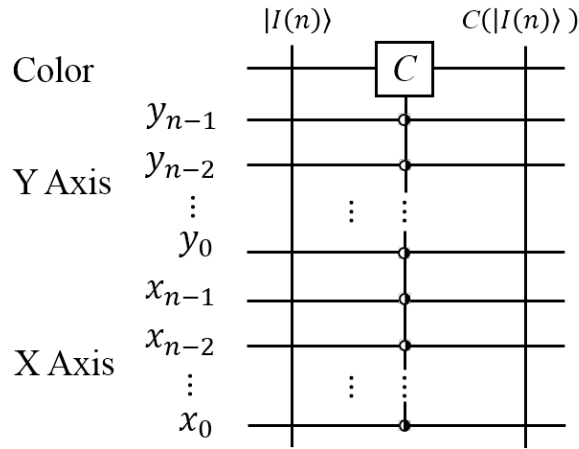


Figure 2.8: Single qubit gates applied on the color wire.

A single qubit gate NOT gate or X gate is taken as an example to explain how the color transformation works. Its function is defined as

$$X = \begin{pmatrix} 0 & 1 \\ 1 & 0 \end{pmatrix}, \quad (2.16)$$

and its property is apparently to switch the value $|0\rangle$ and $|1\rangle$ as $X|0\rangle = |1\rangle$, $X|1\rangle = |0\rangle$.

When the NOT or X gate is applied on the color wire, its performance is

$$X(|c(\theta_k)\rangle) = |c(\frac{\pi}{2} - \theta_k)\rangle, \forall k \in 0, 1, \dots, 2^{2n} - 1, \quad (2.17)$$

where $|c(\theta_k)\rangle$ is the color information as defined in Equation (2.15).

If we apply X gate on an 8×8 image having 4 gray levels, comprising black, dark, light, and white colors, as shown in Figure 2.9 (a). The color information is transformed based on the circuit in Figure 2.9 (b) with the X gate applied on the color wire and the resulting image is shown in Figure 2.9 (c). The function of the X gate is like the color invert operation, which inverts the color of entire image from black to white and vice versa.

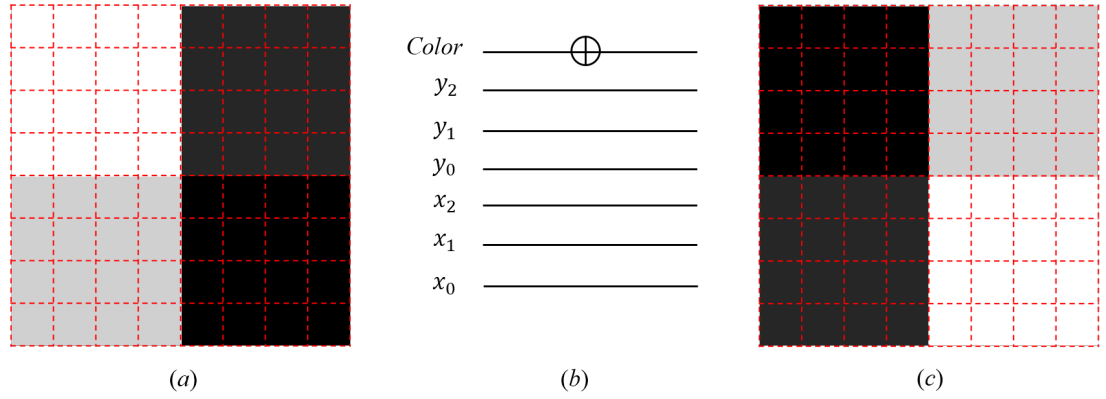


Figure 2.9: The 8×8 images before and after the application of the gate X on the color wire.

2.4 Multi-channel representation for quantum images

To process color images on quantum computers, a new representation encoding information from R, G, and B channels should be established, and these multi-channel information should be stored in quantum states simultaneously. Based on the FRQI representation [37] in Section 2.3.1, the Multi-Channel representation for Quantum Images (MCQI) is proposed to capture RGB channel information [60][59]. This is accomplished by assigning three qubits to encode color information about images. The Multi-Channel

representation for Quantum Images (MCQI) is presented as

$$|I(\theta)_{mc}\rangle = \frac{1}{2^{n+1}} \sum_{i=0}^{2^{2n}-1} |C_{RGB}^i\rangle \otimes |i\rangle, \quad (2.18)$$

where the color information $|C_{RGB}^i\rangle$ encoding the RGB channels information is defined as

$$\begin{aligned} |C_{RGB}^i\rangle = & \cos \theta_R^i |000\rangle + \cos \theta_G^i |001\rangle + \cos \theta_B^i |010\rangle + \cos \theta_O |011\rangle \\ & + \sin \theta_R^i |100\rangle + \sin \theta_G^i |101\rangle + \sin \theta_B^i |110\rangle + \sin \theta_O |111\rangle, \end{aligned} \quad (2.19)$$

where $|000\rangle, |001\rangle, \dots,$ and $|111\rangle$ are 8-D computational basis and $\{\theta_R^i, \theta_G^i, \theta_B^i\} \in [0, \pi/2]$ are three angles encoding the colors of the R, G, and B channels of the i^{th} pixel, respectively. θ_O is set as 0 to make the two coefficients constant ($\cos \theta_O = 1$ and $\sin \theta_O = 0$) to carry no information which is discussed in [60][59]. Specifically, there are two parts in the MCQI image: $|C_{RGB}^i\rangle$ and $|i\rangle$, which encode information about colors and their corresponding positions in the image, respectively. The general MCQI circuit is shown in Figure 2.10, where the first 3 qubits ($c_1, c_2,$ and c_3) are color qubits that encode RGB color information for an image and the remaining $2n$ qubits ($y_{n-1}, y_{n-2}, \dots, y_0$ and $x_{n-1}, x_{n-2}, \dots, x_0$) are used to encode position information (Y Axis and X Axis) about pixels of a $2^n \times 2^n$ image. A simple 2×2 MCQI image, its circuit structure, and its quantum state are shown in Figure 2.11. The methods for storing and retrieving quantum images are discussed in [60][37][63]. Like FRQI, the MCQI state is also a normalized state, i.e. $\| |I(\theta)_{mc}\rangle \| = 1$, as given by

$$\begin{aligned} \| |I(\theta)_{mc}\rangle \| &= \frac{1}{2^{n+1}} \times \\ & \sqrt{\sum_{i=0}^{2^{2n}-1} (\cos^2 \theta_R^i + \sin^2 \theta_R^i + \cos^2 \theta_G^i + \sin^2 \theta_G^i + \cos^2 \theta_B^i + \sin^2 \theta_B^i + \cos^2 0 + \sin^2 0)} = 1. \end{aligned} \quad (2.20)$$

Certainly, we can also do the geometric operations on the position wires, and color transformations on the three color wires like how the GTQI and CTQI works [57][58].

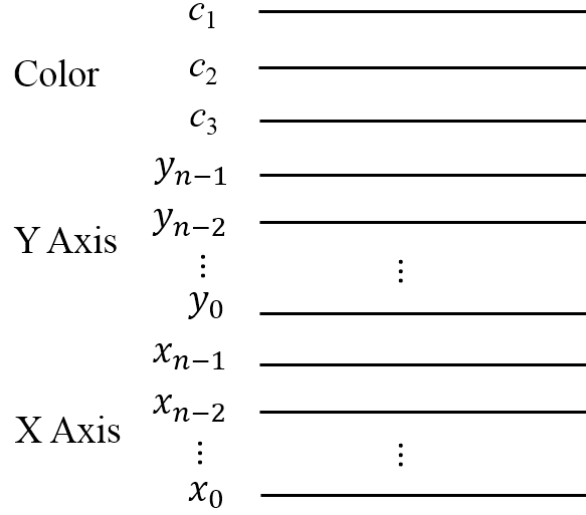


Figure 2.10: General circuit of MCQI images.

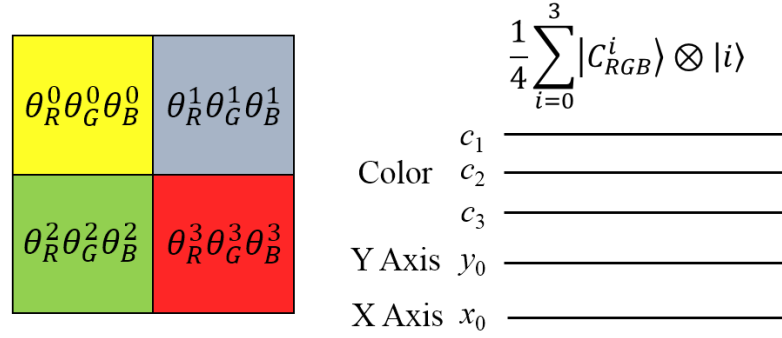


Figure 2.11: A 2×2 MCQI image, its circuit structure and MCQI state.

2.5 Conclusion

A Flexible Representation of Quantum Images (FRQI) is introduced in this chapter, and based on such an representation, the geometric transformation and color transformation could be applied on it. The parallel comparison of multiple pairs of quantum images in Chapter 3 and the quantum image data searching in Chapter 4 are realized based on such an image representation and its related operations. The extension of FRQI, Multi-Channel representation for Quantum Images (MCQI), is also reviewed, and for the information protection, a double-key, double-domain watermarking strategy is proposed based on MCQI images in Chapter 5. Finally, a Bloch sphere based representation for quantum emotion space is proposed in Chapter 6, which is on the basis of the visualiza-

tion of quantum bit as introduced at the beginning of this chapter. The thesis is unfolded based on these proposals.

Chapter 3

A parallel comparison of multiple pairs of images on quantum computers

3.1 Introduction

A Flexible Representation of Quantum Image (FRQI) [37][41] has been proposed and some image processing operations can be executed by applying the elementary gates such as Pauli-X and Hadamard gates combined with appropriate quantum measurements [10] on it. For example, several processing transformations have been proposed based on the FRQI representation among them are the geometric transformations, GTQI [38] and the CTQI [37] that are focused on the color information of the images. Moreover, applications such as a scheme to watermark and authenticate quantum images [29][32] and a framework to produce movies on quantum computers [33], have also been suggested based on the FRQI representation for the images.

Most of the operations on FRQI images [38][39][29], however, are focused on single images. This chapter presents an attempt to extend this in order to compare multiple pairs of FRQI images encoded in parallel. Succinctly put, the main contributions of this work include the following:

- Proposing a scheme for the parallel comparison of images on quantum computers;

- Ascertaining the relationship between the similarity of two quantum images and the probability of their post-measurement states;
- Analyzing the similarities of multiple pairs of images and the sub-blocks from two images in parallel.

The comparison process is executed using low computational requirements, and hence, offers a significant speed-up in comparison with performing the same task on traditional computing devices, since only a single Hadamard gate as well as several control-conditions (when sub-blocks of two images are compared) could transform the entire information encoding the quantum images in a strip, simultaneously. The quantum image processing framework for the FRQI, GTQI, and strip are reviewed in Section 3.2. The parallel comparison of multiple pairs of quantum images is analyzed in Section 3.3. Three simulation experiments for different cases of image comparison are presented in Section 3.4.

3.2 Representation of strip encoding multiple FRQI images

The Flexible Representation for Quantum Images, FRQI, is proposed in [37][41]. It encodes the color and corresponding position's information of every point in an image and integrates them into a quantum state as given by

$$|I(n)\rangle = \frac{1}{2^n} \sum_{i=0}^{2^{2n}-1} |c_i\rangle \otimes |i\rangle, \quad (3.1)$$

where

$$|c_i\rangle = \cos \theta_i |0\rangle + \sin \theta_i |1\rangle, \quad (3.2)$$

$$\theta_i \in [0, \frac{\pi}{2}], i = 1, 2, \dots, 2^{2n} - 1, \quad (3.3)$$

where $|i\rangle$, $i = 1, 2, \dots, 2^{2n} - 1$, are $2n$ -D computational basis quantum states and $\theta = (\theta_0, \theta_1, \dots, \theta_{2^{2n}-1})$ is the vector of angles encoding colors.

A dextrous property of the strip representation [33][2] to encode 2^m -ending FRQI images lies in its ability to utilize the parallelism inherent to quantum computation in order to transform multiple images using very few quantum resources. The definition of the strip and its properties are introduced in this section.

Definition 3.1 A strip, $|S(m, n)\rangle$, is an array comprising 2^m FRQI images, which is defined by

$$|S(m, n)\rangle = \frac{1}{2^{m/2}} \sum_{s=0}^{2^m-1} |I_s(n)\rangle \otimes |s\rangle, \quad (3.4)$$

where

$$|I_s(n)\rangle = \frac{1}{2^n} \sum_{i=0}^{2^n-1} |c_{s,i}\rangle \otimes |i\rangle, \quad (3.5)$$

$$|c_{s,i}\rangle = \cos \theta_{s,i} |0\rangle + \sin \theta_{s,i} |1\rangle, \quad (3.6)$$

$$\theta_{s,i} \in [0, \frac{\pi}{2}], i = 1, 2, \dots, 2^n - 1, s = 1, 2, \dots, 2^m - 1, \quad (3.7)$$

where $|s\rangle$ is the position of each image in the strip, m is the number of qubits required to encode the images being compared, $|I_s(n)\rangle$ is a FRQI image as defined in Equation (3.1) at position $|s\rangle$, $|c_{s,i}\rangle$ and $|i\rangle$ encode the information about the colors and their corresponding positions in the image $|I_s(n)\rangle$. The state $|S(m, n)\rangle$ is normalized, which can be confirmed by

$$\begin{aligned} \||S(m, n)\rangle\| &= \frac{1}{2^{m/2}} \sqrt{\sum_{s=0}^{2^m-1} \||I_s(n)\rangle\|^2} \\ &= \frac{1}{2^{m/2+n}} \sqrt{\sum_{s=0}^{2^m-1} \sum_{i=0}^{2^n-1} (\cos^2 \theta_{s,i} + \sin^2 \theta_{s,i})} = 1. \end{aligned} \quad (3.8)$$

As seen in Figure 3.1, the size of a strip in the representation captures the input state of the strip comprising 2^m quantum images. Each image in the strip is an FRQI state while the combination of such states in the strip is best represented as a multiple FRQI or simply m FRQI state. The m FRQI state can represent 2^m quantum images using only $m+2n+1$ qubits since all of the images are of the same size in this strip.

The 2^m -ending FRQI images encoded in a strip can be horizontally-oriented or vertically-oriented [69]. The latter case, the vertically-oriented strip, is implied throughout the ensuing discussion. Control-conditions on strip wires could control the image which is

being processed, combining with the control-conditions from the position $|y\rangle|x\rangle$ to the color wire; every pixel in this strip can be accessed.

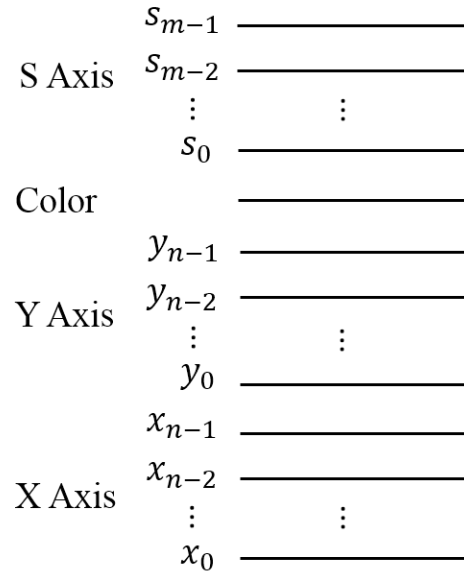


Figure 3.1: Circuit structure to encode the strip input.

3.3 Parallel comparison of multiple pairs of quantum images

Inspired by the importance of image searching and how it is accomplished on conventional computers, quantum image searching from a database appears to be an indispensable application in quantum image processing [4][9]. It is envisaged that quantum image searching from a database will be faster than the classical ones because of the inherent parallelism of quantum computation [47][8]. A first step towards realizing that would be to propose a scheme to evaluate the extent to which two or more images are similar to one another [14]. The main contribution of this chapter is tailored towards achieving this essential step of quantum image searching. In the sub-sections that follow, we present the scheme to compare images in parallel on quantum computers, and the different cases in the comparison process such as the comparison of sub-blocks from two images.

3.3.1 Scheme to compare images in parallel on quantum computers

The scheme to compare quantum images on quantum computers, together with several momentous definitions as the basis of the ensuing discussions is presented in this subsection. It starts with the introduction of comparison for two quantum images. The comparison of two FRQI images $|I_k(n)\rangle$ and $|I_t(n)\rangle$,

$$|I_k(n)\rangle = \frac{1}{2^n} \sum_{i=0}^{2^{2n}-1} (\cos \theta_{k,i}|0\rangle + \sin \theta_{k,i}|1\rangle) \otimes |i\rangle, \quad (3.9)$$

$$|I_t(n)\rangle = \frac{1}{2^n} \sum_{i=0}^{2^{2n}-1} (\cos \theta_{t,i}|0\rangle + \sin \theta_{t,i}|1\rangle) \otimes |i\rangle, \quad (3.10)$$

is that obtain the similarity, which is in the interval from 0 to 1, between them through the quantum operations. In addition, given a strip comprising 2^m quantum images, parallel comparison of quantum images retrieves the similarities between $2^m - 1$ pairs of images in the strip simultaneously.

Definition 3.2 The difference between the i^{th} pixels of two FRQI images $|I_k(n)\rangle$ and $|I_t(n)\rangle$, as defined in Equations (3.9) and (3.10), is given by

$$\sigma_{k,t}^i = |\theta_{k,i} - \theta_{t,i}|, \sigma_{k,t}^i \in [0, \pi/2], \quad (3.11)$$

where $\theta_{k,i}$ and $\theta_{t,i}$ represent the color information at position i of the two images, respectively.

Definition 3.3 The similarity between two FRQI images $|I_k(n)\rangle$ and $|I_t(n)\rangle$, as defined in Equations (3.9) and (3.10), is a function of pixel difference $\sigma_{k,t}$ at every position of the image given by

$$\text{sim}(|I_k\rangle, |I_t\rangle) = f(\sigma_{k,t}^0, \sigma_{k,t}^1, \dots, \sigma_{k,t}^{2^{2n}-1}), \quad (3.12)$$

where $\text{sim}(|I_k\rangle, |I_t\rangle) \in [0, 1]$.

Two special cases of the similarity between two quantum images are listed as follows:

- if $\forall i, \sigma_{k,t}^i = \pi/2$, then $\text{sim}(|I_k\rangle, |I_t\rangle) = 0$ and the two images are totally different;

- if $\forall i, \sigma_{k,t}^i = 0$, then $\text{sim}(|I_k\rangle, |I_t\rangle) = 1$ and the two images are exactly the same,

where $i = 0, 1, \dots, 2^{2n} - 1$, $\sigma_{k,t}^i$ is the pixel difference at position i as defined in Definition 3.2.

Combining the properties of quantum computation, superposition and entanglement, the representation of strip which is introduced in Section 3.2 is supposed to be used for comparing quantum images of equal size because an operation on the strip wires can transform the information in all the images in the strip simultaneously. The strip does not only make the comparison of quantum images possible but it also provides an efficient way to compare multiple pairs of quantum images in parallel. The scheme to compare quantum images in parallel consists of three steps as detailed in Figure 3.2. These steps are outlined in this sub-section.

Step1: Preparation of the strip comprising 2^m quantum images

The quantum images are prepared into FRQI states using their classical versions images. The color information as well as the corresponding positions of every point in the classical version is integrated into the quantum state, and 2^m quantum images being compared are combined to form a vertically-oriented strip. The routine involved in preparing FRQI images and its extension to encode multiple FRQI images as a single register, called the strip, are discussed thoroughly in [37][33][69]. In all these instances, the availability of a classical version of each image from which the quantum versions of the images are prepared is implied.

Step2: Comparison of quantum images through quantum operations

The strip as prepared in the preceding period is transformed using a gate array comprising geometric, GTQI [38] and color, CTQI, [39], transformations on all the images in the strip. For this particular application, the transformations are built in a way to allow the recovery of the pixel difference as defined in Equation (3.11). This transformation step combines with measurement operations that follow it to convert the quantum information into the classical form as probability distributions. Since measurements are known to destroy the superposition state in quantum systems [49], in order to compare the similarity between two FRQI images (in parallel), the strip has to be prepared n ($n > 1$) times.

Step 3: Observation of readouts from quantum measurements

The readouts from the n quantum measurements build up a histogram that implicitly reflects the probability distributions. Extracting and analyzing these distributions gives information that the similarity values between the quantum images being compared. The strip preparation will be continued until $\min(P(|s_{m-1}, \dots, s_0\rangle)) \geq \delta$, where $\min(P(|s_{m-1}, \dots, s_0\rangle))$ is the minimum of the probabilities of the readouts from the experiments, $\delta \in [0, 1]$ is a pre-set threshold, which can be read as the reasonable estimation for the similarity between two quantum images being compared.

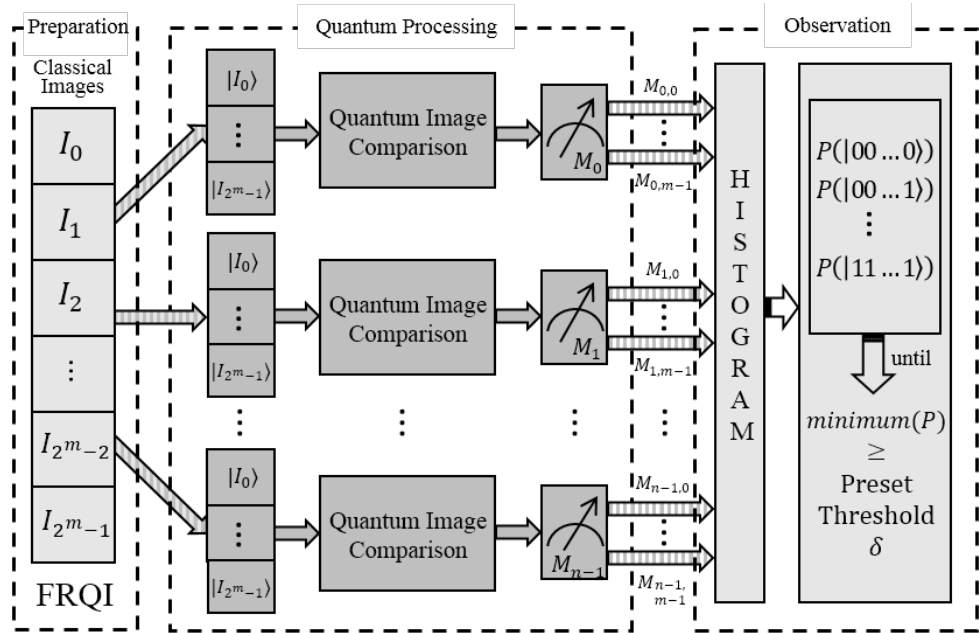


Figure 3.2: Scheme to compare quantum images in parallel on quantum computers.

The comparison of quantum images in this scheme is especially specified in the ensuing sub-sections which are the evaluation of the similarity between two images, parallel comparison of multiple pairs of images, and the comparison of sub-blocks from two images.

3.3.2 Evaluation of the similarity between two quantum images

As the basis of discussing parallel quantum image comparison, the comparison between two quantum images should come first [69]. According to Equations (3.4), (3.9), and (3.10),

the state of the strip comprising two images ($m = 1, k = 0, t = 1, s = 0, 1$) becomes

$$|S(1, n)\rangle = \frac{1}{\sqrt{2}}(|I_0(n)\rangle \otimes |0\rangle + |I_1(n)\rangle \otimes |1\rangle), \quad (3.13)$$

where

$$|I_0(n)\rangle = \frac{1}{2^n} \sum_{i=0}^{2^{2n}-1} (\cos \theta_{0,i}|0\rangle + \sin \theta_{0,i}|1\rangle) \otimes |i\rangle, \quad (3.14)$$

and

$$|I_1(n)\rangle = \frac{1}{2^n} \sum_{i=0}^{2^{2n}-1} (\cos \theta_{1,i}|0\rangle + \sin \theta_{1,i}|1\rangle) \otimes |i\rangle, \quad (3.15)$$

are the two FRQI images being compared, which are located in the upper part and lower part of the strip, respectively.

The circuit structure to compare these two FRQI images is shown in Figure 3.3. A Hadamard gate, $H = \frac{1}{\sqrt{2}} \begin{pmatrix} 1 & 1 \\ 1 & -1 \end{pmatrix}$, which maps the basis state $|0\rangle$ to $(|0\rangle + |1\rangle)/\sqrt{2}$ and $|1\rangle$ to $(|0\rangle - |1\rangle)/\sqrt{2}$, is applied on the strip wire s_0 to obtain the recombination of $|I_0(n)\rangle$ and $|I_1(n)\rangle$, it is then followed by a measurement operation M_0 .

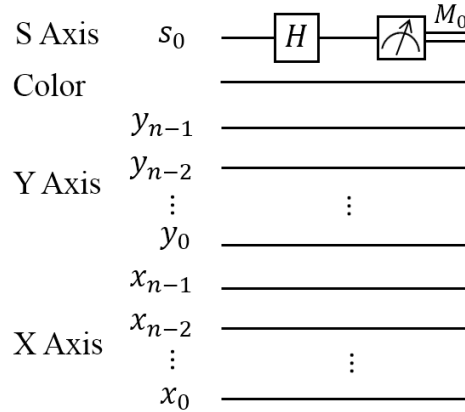


Figure 3.3: Generalized circuit structure for comparing two FRQI images.

Corresponding to the circuit shown in Figure 3.3, the new state of the quantum system after applying the Hadamard gate on the strip wire s_0 (expressed by $H_0|S(1, n)\rangle$) can be

given as follows:

$$\begin{aligned}
 H_0|S(1, n)\rangle &= \frac{1}{\sqrt{2}}(|I_0(n)\rangle \otimes H|0\rangle + |I_1(n)\rangle \otimes H|1\rangle) \\
 &= \frac{1}{2}[|I_0(n)\rangle \otimes (|0\rangle + |1\rangle) + |I_1(n)\rangle \otimes (|0\rangle - |1\rangle)] \\
 &= \frac{1}{2}[(|I_0(n)\rangle + |I_1(n)\rangle) \otimes |0\rangle + (|I_0(n)\rangle - |I_1(n)\rangle) \otimes |1\rangle]
 \end{aligned} \tag{3.16}$$

where

$$|I_0(n)\rangle \pm |I_1(n)\rangle = \frac{1}{2^n} \sum_{i=0}^{2^{2n}-1} [(\cos \theta_{0,i} \pm \cos \theta_{1,i})|0\rangle + (\sin \theta_{0,i} \pm \sin \theta_{1,i})|1\rangle]|i\rangle. \tag{3.17}$$

It is obvious that the result of the measurement M_0 depends on the disparities between $|I_0(n)\rangle$ and $|I_1(n)\rangle$. The state $|0\rangle$ and $|1\rangle$ exist on strip wire s_0 at a certain probability. In accordance with the measurement postulate in [48], the probability of state $|0\rangle$ on this strip wire is

$$\begin{aligned}
 P_{s_0}(|0\rangle) &= \left(\frac{1}{2^{n+1}}\right)^2 \sum_{i=0}^{2^{2n}-1} [(\cos \theta_{0,i} + \cos \theta_{1,i})^2 + (\sin \theta_{0,i} + \sin \theta_{1,i})^2] \\
 &= \frac{1}{2^{n+1}} \sum_{i=0}^{2^{2n}-1} [1 + \cos(\theta_{0,i} - \theta_{1,i})] \\
 &= \frac{1}{2} + \frac{1}{2^{2n+1}} \sum_{i=0}^{2^{2n}-1} \cos \sigma_{0,1}^i.
 \end{aligned} \tag{3.18}$$

In the same manner, that of state $|1\rangle$ on the same wire is

$$P_{s_0}(|1\rangle) = \frac{1}{2} - \frac{1}{2^{n+1}} \sum_{i=0}^{2^{2n}-1} \cos \sigma_{0,1}^i. \tag{3.19}$$

The probabilities of these two states sum up to 1, i.e. $P_{s_0}(|0\rangle) + P_{s_0}(|1\rangle) = 1$, as they should.

It is apparent that, arising from Equation (3.19) the pixel difference $\sigma_{0,1}^i$ is related to the probability of getting readout of 1 from the strip wire s_0 , $P_{s_0}(|1\rangle)$, in the measurement and $P_{s_0}(|1\rangle)$ will increase when pixel difference increases. Furthermore, the similarity between two images, which is a function of the pixel differences at every position, depends

on $P_{s_0}(|1\rangle)$ as given by

$$\text{sim}(|I_0\rangle, |I_1\rangle) = 1 - 2P_{s_0}(|1\rangle) = \frac{1}{2^{2n}} \sum_{i=0}^{2^{2n}-1} \cos \sigma_{0,1}^i. \quad (3.20)$$

where $|I_0\rangle$ and $|I_1\rangle$ are the two images being compared, $P_{s_0}(|1\rangle)$ is in the form defined in Equation (3.19), and $\text{sim}(|I_0\rangle, |I_1\rangle) \in [0, 1]$. The similarity between $|I_0\rangle$ and $|I_1\rangle$ which are encoded in the strip is in line with the definition of similarity between two FRQI images in Equation (3.12), where $f(\sigma_{k,t}^0, \sigma_{k,t}^1, \dots, \sigma_{k,t}^{2^{2n}-1}) = \frac{1}{2^{2n}} \sum_{i=0}^{2^{2n}-1} \cos \sigma_{0,1}^i$.

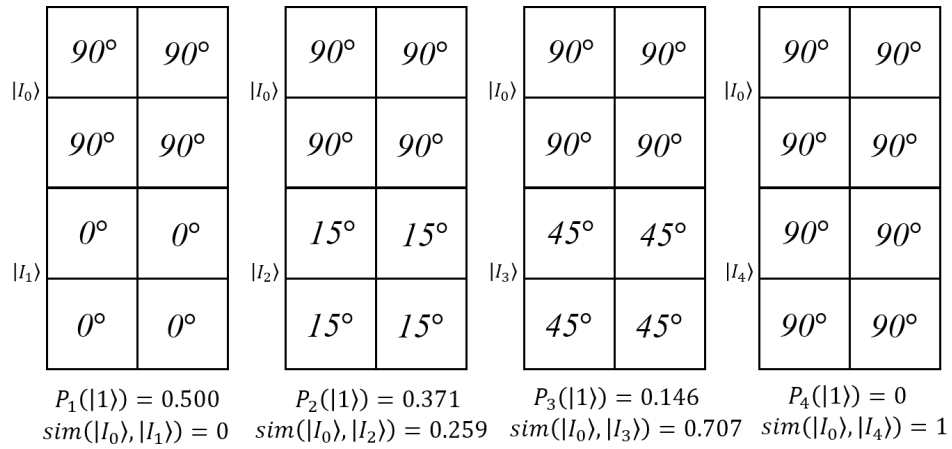


Figure 3.4: Four strips where each comprises two images are considered in order to compare the four pairs of images.

An example to compare the image $|I_0\rangle$ with $|I_1\rangle$, $|I_2\rangle$, $|I_3\rangle$ and $|I_4\rangle$ is presented in Figure 3.4. The probabilities of the readouts on strip wire s_0 , $P_{s_0}(|1\rangle)$ in Equation (3.19), from each pair of images are shown with $P_1(|1\rangle)$, $P_2(|1\rangle)$, $P_3(|1\rangle)$, and $P_4(|1\rangle)$ on the first row below the strip in the figure, and it is followed by the similarity value between the two images in the strip. It is trivial that $\text{sim}(|I_0\rangle, |I_1\rangle) < \text{sim}(|I_0\rangle, |I_2\rangle) < \text{sim}(|I_0\rangle, |I_3\rangle) < \text{sim}(|I_0\rangle, |I_4\rangle)$, actually, the images $|I_0\rangle$ and $|I_4\rangle$ have the same content.

3.3.3 A parallel comparison of multiple pairs of images in a strip

The parallel computation on quantum computer leads us to find a way that comparing many pairs of images in parallel. The proposal of the strip comprising 2^m images as defined in Definition 2.1 provides us a crucial condition to make it possible because the operation

on the strip wires can transform the information in every image simultaneously. The generalized circuit structure of comparing $2^m - 1$ pairs of quantum images in parallel is presented in Figure 3.5. By applying a Hadamard operation on the r^{th} strip wire in the circuit, s_r , the mathematical expressions between the two images being compared are realized. The final step in the procedure consists of m measurements from which the similarity can be retrieved in each pair of images.

Due to the representation of the strip and the property of Hadamard operation, only the specified pairs of images in the strip can be compared, which is the k^{th} image, $|I_k\rangle$, and the $(k+2^r)^{th}$ image, $|I_{k+2^r}\rangle$ (r is the index of s_r in the circuit). Therefore, the m FRQI state of the strip when $2^m - 1$ pairs of images are compared is

$$\begin{aligned} |S(m, n)\rangle &= \frac{1}{2^{m/2}} \sum_{s=0}^{2^m-1} |I_s(n)\rangle \otimes |s\rangle \\ &= \frac{1}{2^{m/2}} \sum_{z=1}^{2^{m-r-1}} \sum_{k=g(z)}^{\frac{1}{2}g(2z)-1} (|I_k\rangle \otimes |k\rangle + |I_{k+2^r}\rangle \otimes |k+2^r\rangle), \end{aligned} \quad (3.21)$$

$$g(z) = (z - 1)2^{r+1}, \quad (3.22)$$

where $m \geq 2$, $|s\rangle = |s_{m-1}, \dots, s_{r+1}, s_r, s_{r-1}, \dots, s_0\rangle$, $s_r \in \{0, 1\}$.

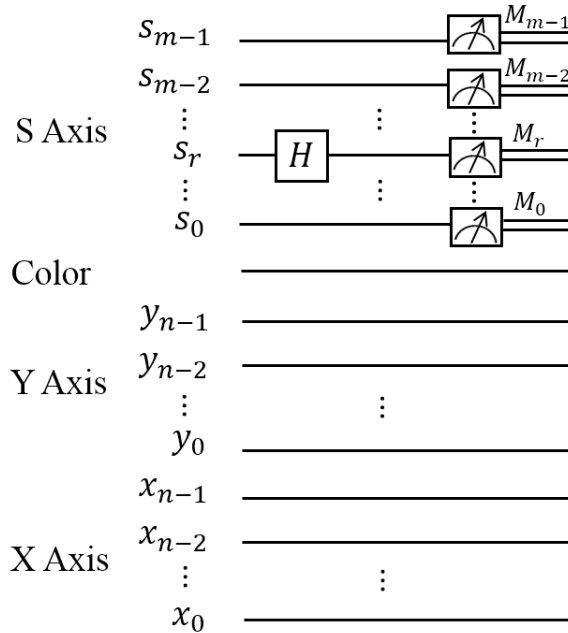


Figure 3.5: Generalized circuit structure for a parallel comparison of $2^m - 1$ pairs of images.

Applying the Hadamard gate that maps the basis state $|0\rangle$ to $(|0\rangle + |1\rangle)/\sqrt{2}$ and $|1\rangle$ to $(|0\rangle - |1\rangle)/\sqrt{2}$ as mentioned in Section 3.3.2, on the strip wire s_r (expressed by $H_r|S(m, n)\rangle$) transforms the state of the strip into:

$$\begin{aligned}
 H_r|S(m, n)\rangle &= \frac{1}{2^{m/2}} \sum_{s=0}^{2^m-1} |I_s(n)\rangle \otimes |s_{m-1}, \dots, s_{r+1}\rangle \otimes H|s_r\rangle \otimes |s_{r-1}, \dots, s_0\rangle \\
 &= \frac{1}{2^{m/2}} \sum_{z=1}^{2^{m-r-1}} \sum_{k=g(z)}^{\frac{1}{2}g(2z)-1} |I_k(n)\rangle \otimes |s_{m-1}, \dots, s_{r+1}\rangle \otimes H|0\rangle \otimes |s_{r-1}, \dots, s_0\rangle \\
 &+ \frac{1}{2^{m/2}} \sum_{z=1}^{2^{m-r-1}} \sum_{k=g(z)}^{\frac{1}{2}g(2z)-1} |I_{k+2^r}(n)\rangle \otimes |s_{m-1}, \dots, s_{r+1}\rangle \otimes H|1\rangle \otimes |s_{r-1}, \dots, s_0\rangle \\
 &= \frac{1}{2^{(m+1)/2}} \sum_{z=1}^{2^{m-r-1}} \sum_{k=g(z)}^{\frac{1}{2}g(2z)-1} (|I_k(n)\rangle + |I_{k+2^r}(n)\rangle) \otimes |s_{m-1}, \dots, s_{r+1}, 0, s_{r-1}, \dots, s_0\rangle \\
 &+ \frac{1}{2^{(m+1)/2}} \sum_{z=1}^{2^{m-r-1}} \sum_{k=g(z)}^{\frac{1}{2}g(2z)-1} (|I_k(n)\rangle - |I_{k+2^r}(n)\rangle) \otimes |s_{m-1}, \dots, s_{r+1}, 1, s_{r-1}, \dots, s_0\rangle,
 \end{aligned} \tag{3.23}$$

where

$$\begin{aligned}
 |I_k(n)\rangle \pm |I_{k+2^r}(n)\rangle &= \frac{1}{2^n} \sum_{i=0}^{2^{2n}-1} (|c_{k,i}\rangle \pm |c_{k+2^r,i}\rangle) \otimes |i\rangle \\
 &= \frac{1}{2^n} \sum_{i=0}^{2^{2n}-1} [(\cos \theta_{k,i} \pm \cos \theta_{k+2^r,i})|0\rangle + (\sin \theta_{k,i} \pm \sin \theta_{k+2^r,i})|1\rangle] \otimes |i\rangle
 \end{aligned} \tag{3.24}$$

The probability of the readouts from the m measurements are given by

$$\begin{aligned}
 P_{s_r}(|s_{m-1}, \dots, s_{r+1}, 0, s_{r-1}, \dots, s_0\rangle) &= \frac{1}{2^{m+2n}} \sum_{z=1}^{2^{m-r-1}} \sum_{k=g(z)}^{\frac{1}{2}g(2z)-1} \sum_{i=0}^{2^{2n}-1} 1 + \cos(\theta_k - \theta_{k+2^r}) \\
 &= \frac{1}{2} + \frac{1}{2^{m+2n}} \sum_{z=1}^{2^{m-r-1}} \sum_{k=g(z)}^{\frac{1}{2}g(2z)-1} \sum_{i=0}^{2^{2n}-1} \cos \sigma_{k,k+2^r}^i.
 \end{aligned} \tag{3.25}$$

In the same way, that of state $|s_{m-1}, \dots, s_{r+1}, 1, s_{r-1}, \dots, s_0\rangle$ on s_r is given by

$$P_{s_r}(|s_{m-1}, \dots, s_{r+1}, 1, s_{r-1}, \dots, s_0\rangle) = \frac{1}{2} - \frac{1}{2^{m+2n}} \sum_{z=1}^{2^{m-r-1}} \sum_{k=g(z)}^{\frac{1}{2}g(2z)-1} \sum_{i=0}^{2^{2n}-1} \cos \sigma_{k,k+2^r}^i. \tag{3.26}$$

From this, it becomes evident that

$$P_{s_r}(|s_{m-1}, \dots, s_{r+1}, 0, s_{r-1}, \dots, s_0\rangle) + P_{s_r}(|s_{m-1}, \dots, s_{r+1}, 1, s_{r-1}, \dots, s_0\rangle) = 1. \quad (3.27)$$

The states $|s_{m-1}, \dots, s_{r+1}, 0, s_{r-1}, \dots, s_0\rangle$ and $|s_{m-1}, \dots, s_{r+1}, 1, s_{r-1}, \dots, s_0\rangle$ represent all the images that are at the k^{th} and $(k+2^r)^{th}$ position of the strip, respectively. In order to determine the similarity of every pair of images, the generalized representation of the probability of $|I_{k+2^r}(n)\rangle$ in the strip is given by

$$\begin{aligned} P_{s_r}(|k+2^r\rangle) &= \frac{1}{2^{m+2n}} \sum_{i=0}^{2^{2n}-1} 1 - \cos(\theta_k - \theta_{k+2^r}) \\ &= \frac{1}{2^m} - \frac{1}{2^{m+2n}} \sum_{i=0}^{2^{2n}-1} \cos \sigma_{k,k+2^r}^i, \end{aligned} \quad (3.28)$$

In addition, the similarity between $|I_k(n)\rangle$ and $|I_{k+2^r}(n)\rangle$ can be presented as

$$\begin{aligned} sim(|I_k\rangle, |I_{k+2^r}\rangle) &= 1 - 2^m P_{s_r}(|k+2^r\rangle) \\ &= \frac{1}{2^{2n}} \sum_{i=0}^{2^{2n}-1} \cos \sigma_{k,k+2^r}^i, \end{aligned} \quad (3.29)$$

where $|I_k\rangle$ and $|I_{k+2^r}\rangle$ are the two images being compared in the strip, $P_{s_r}(|k+2^r\rangle)$ is defined in Equation (3.28), and $sim(|I_k\rangle, |I_{k+2^r}\rangle) \in [0, 1]$. The similarity between $|I_k\rangle$ and $|I_{k+2^r}\rangle$ which are encoded in the strip comprising 2^m images is also determined in accordance with Definition 3.3, where $f(\sigma_{k,t}^0, \sigma_{k,t}^1, \dots, \sigma_{k,t}^{2^{2n}-1}) = \frac{1}{2^{2n}} \sum_{i=0}^{2^{2n}-1} \cos \sigma_{k,k+2^r}^i$.

Two examples to demonstrate how two pairs of images can be compared and the implication of applying the Hadamard gate on different strip wires s_0 or s_1 are presented in Figure 3.6. A strip comprising of four images $|I_0\rangle$, $|I_1\rangle$, $|I_2\rangle$, and $|I_3\rangle$ with the differences between their content captured by their varying color angles is presented on the left in Figure 3.6. On the right of the same figure, the circuit in Figure 3.6 (a) is used to compare $|I_0\rangle$ with $|I_1\rangle$ and $|I_2\rangle$ with $|I_3\rangle$ by applying a Hadamard gate on the strip wire s_0 , while the circuit in Figure 3.6 (b) is served to compare $|I_0\rangle$ with $|I_2\rangle$ and $|I_1\rangle$ with $|I_3\rangle$ by applying a Hadamard gate on the strip wire s_1 .

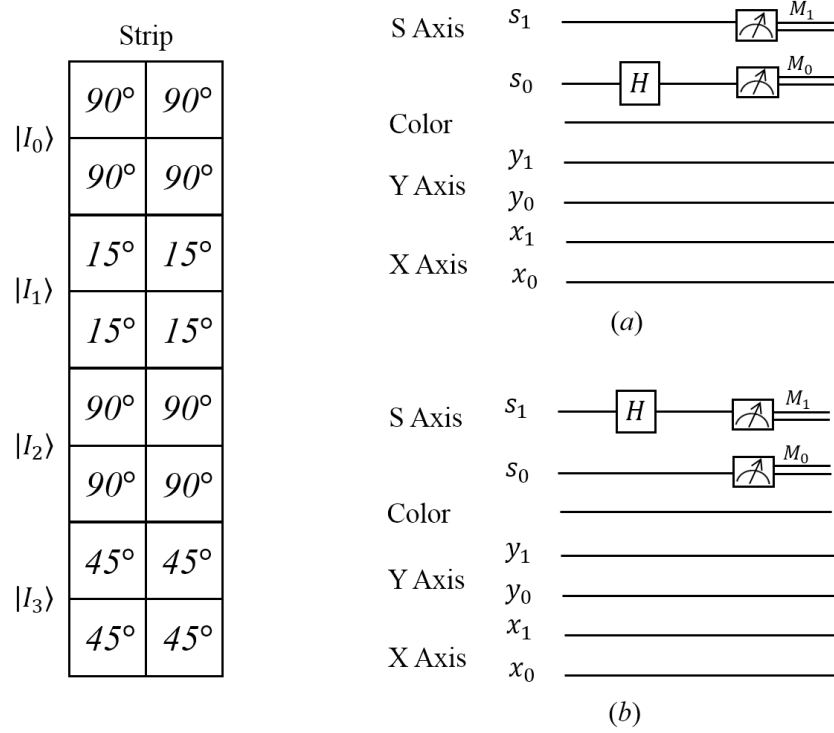


Figure 3.6: An example to realize the simultaneous comparison of two pairs of images.

According to Equation (3.4), the m FRQI state of this strip ($m = 2$, $n = 1$) is given by

$$|S(2, 1)\rangle = \frac{1}{2}(|I_0\rangle \otimes |00\rangle + |I_1\rangle \otimes |01\rangle + |I_2\rangle \otimes |10\rangle + |I_3\rangle \otimes |11\rangle). \quad (3.30)$$

The difference between applying the Hadamard gate on strip wire s_0 and s_1 is elaborated in Table 3.1. The table also shows the transformed state, the probability of the state on strip wires, and the similarity between the images being compared. The probability and similarity are calculated using Equations (3.28) and (3.29) where $m = 2$, $n = 1$, $r = 0$ or 1, respectively.

From the discussion in this sub-section and results from the example in Figure 3.6 as well as Table 3.1, it is evident that different pairs of images can be compared by simply moving the Hadamard operation from one wire on the S-axis to another. However, comparing some pairs of images such as $|I_0\rangle$ with $|I_3\rangle$, and $|I_1\rangle$ with $|I_2\rangle$ in Figure 3.6, is difficult to accomplish in this manner because they do not satisfy the relationship defined earlier in Equation (3.21). Hence, a new strategy is required to deal how to compare two

Table 3.1: Image comparison by applying Hadamard operation on different strip wires.

Image comparison	Circuit	Transformed state	Probability	Similarity
$ I_0\rangle, I_1\rangle$	Figure 3.6(a)	$\frac{1}{2\sqrt{2}}[(I_0\rangle + I_1\rangle) 00\rangle$ $+ (I_0\rangle - I_1\rangle) 01\rangle$ $+ (I_2\rangle + I_3\rangle) 10\rangle$ $+ (I_2\rangle - I_3\rangle) 11\rangle$	$P_{s_0}(01) = 0.185$	$sim(I_0\rangle, I_1\rangle) = 0.259$
$ I_2\rangle, I_3\rangle$			$P_{s_0}(11) = 0.073$	$sim(I_2\rangle, I_3\rangle) = 0.707$
$ I_0\rangle, I_2\rangle$	Figure 3.6(b)	$\frac{1}{2\sqrt{2}}[(I_0\rangle + I_2\rangle) 00\rangle$ $+ (I_1\rangle + I_3\rangle) 01\rangle$ $+ (I_0\rangle - I_2\rangle) 10\rangle$ $+ (I_1\rangle - I_3\rangle) 11\rangle$	$P_{s_1}(10) = 0$	$sim(I_0\rangle, I_2\rangle) = 1$
$ I_1\rangle, I_3\rangle$			$P_{s_1}(11) = 0.033$	$sim(I_1\rangle, I_3\rangle) = 0.866$

arbitrary images in a strip and is the main focus in Section 3.3.4.

3.3.4 Comparison between two arbitrary quantum images and the sub-blocks

As mentioned in Section 3.3.3, the position of the two images being compared, which are the k^{th} and $(k + 2^r)^{th}$ images in the strip (r is the index of s_r in the circuit), in a strip is relatively fixed. In order to compare two arbitrary quantum images and/or contents of their sub-blocks from a strip, some geometric transformation and control-conditions are applied to the quantum system. In this sub-section, the more complicated cases of quantum image comparison are discussed such as comparing arbitrary pairs of images, and comparing sub-blocks from two images in a strip. The circuit structure for realizing such processes is presented in Figure 3.7.

The input of this circuit is the m FRQI state as defined in Equation (3.21) (expressed by $|S_I\rangle$ in the circuit), the operation G_S that is applied on the strip wires is the geometric operation which can swap two images in the strip when two arbitrary images are supposed to be compared. A notation ‘ \oslash ’ to indicate for ‘0’ or ‘1’ control-condition is adopted throughout the discussion. The additional control-conditions on either of the position axis (Y Axis or X Axis) are necessary in order to confine this Hadamard operation to the

required sub-blocks from the images that are being compared. The operation G_I is needed when the sub-blocks being compared are at different positions from the two images. The state in the circuit after applying the Hadamard gate on the r^{th} strip wire is transformed into $H_r G_s |S_{G_I}\rangle$ as shown in Figure 3.7.

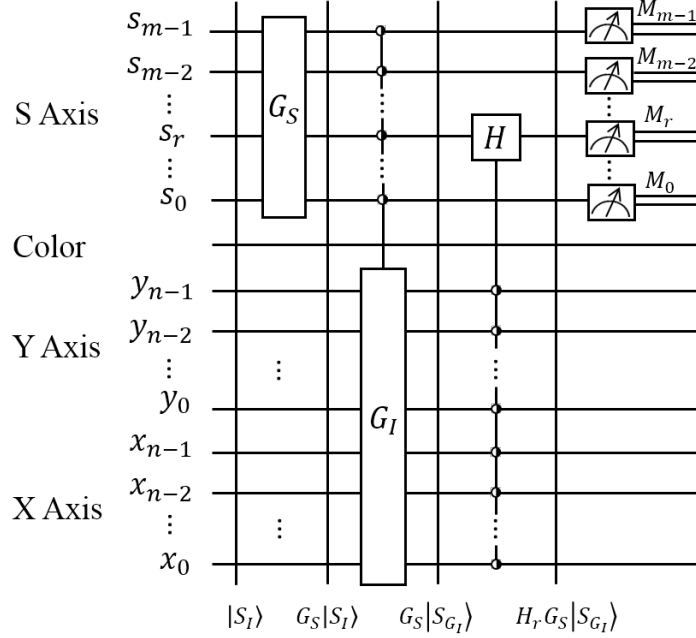


Figure 3.7: Generalized circuit structure for parallel comparison of FRQI images.

The similarity between the sub-blocks from two FRQI images encoded in a strip is

$$\text{sim}(|i_k\rangle, |i_{t \rightarrow k+2^r}\rangle) = 1 - \frac{2^m p}{q} P_{s_r}(|k+2^r\rangle), \quad (3.31)$$

where $|i_k\rangle$ and $|i_{t \rightarrow k+2^r}\rangle$ are the sub-blocks from the two images $|I_k\rangle$ and $|I_{t \rightarrow k+2^r}\rangle$ in the strip, $|I_{t \rightarrow k+2^r}\rangle$ is the image from the position t to $k+2^r$ using the geometric transformation on the strip wires, p is the area of the image $|I_k\rangle$ or $|I_{t \rightarrow k+2^r}\rangle$, and q is the area of the sub-block $|i_k\rangle$ or $|i_{t \rightarrow k+2^r}\rangle$ in the two images, $P_{s_r}(|k+2^r\rangle)$ is the probability of the readouts in the measurements from the state $|k+2^r\rangle$ as discussed in Equation (3.28), $\text{sim}(|i_k\rangle, |i_{t \rightarrow k+2^r}\rangle) \in [0, 1]$.

The procedure to determine the similarity of images in a strip in parallel has already been elaborated in Section 3.3.3. Here, only an example in Figure 3.8 suffices to illustrate the comparison between two sub-blocks from two arbitrarily located FRQI images.

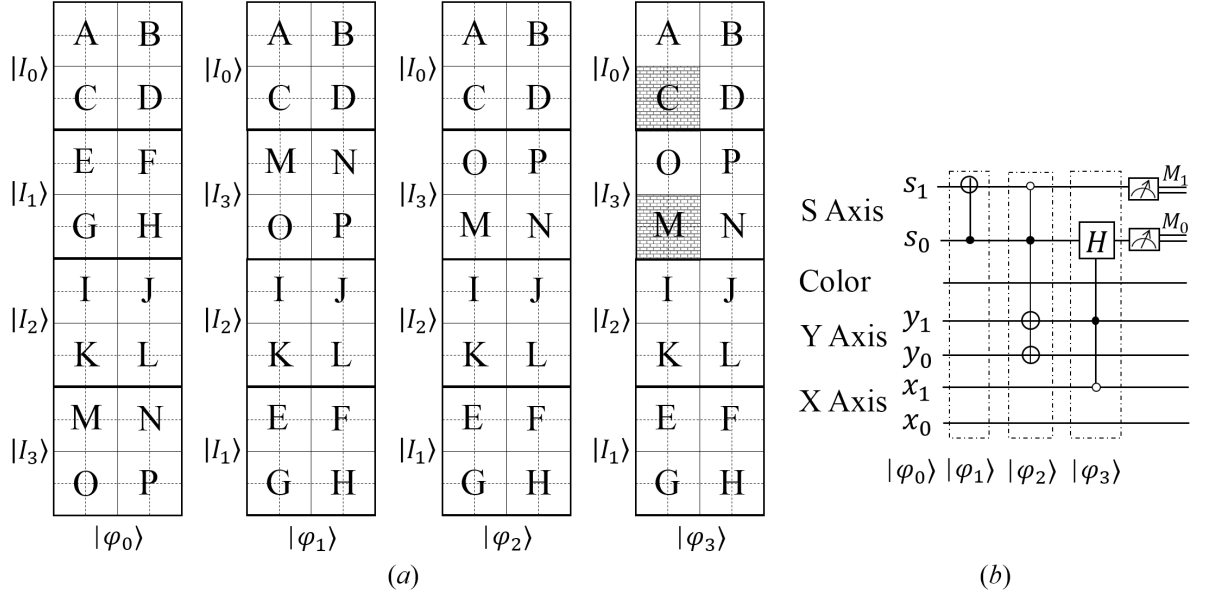


Figure 3.8: Comparison of two sub-blocks, ‘C’ and ‘M’ from images $|I_0\rangle$ and $|I_3\rangle$ in strip $|\varphi_0\rangle$. Strip $|\varphi_1\rangle$, $|\varphi_2\rangle$, and $|\varphi_3\rangle$ in (a) are the midterm states when applying the circuit in (b).

The sub-block ‘C’ from $|I_0\rangle$ is compared with sub-block ‘M’ from $|I_3\rangle$ in $|\varphi_0\rangle$. The midterm states and the corresponding circuit are also presented in the figure. The procedure to accomplish this comparison is:

$|\varphi_0\rangle$: The original strip comprising four qautnum images;

$|\varphi_1\rangle$: Swap the position between $|I_1\rangle$ and $|I_3\rangle$ using the C-NOT gate on the strip wires;

$|\varphi_2\rangle$: Flip the position of ‘M’ with ‘O’, ‘N’ with ‘P’ in $|I_3\rangle$ along the X-axis;

$|\varphi_3\rangle$: Compare the two sub-blocks ‘C’ and ‘M’ through applying the Hadamard gate on s_0 .

As explained in Figure 3.6 in Section 3.3.3, another way to realize the comparison between the sub-blocs ‘C’ and ‘M’ is by first swapping the images $|I_2\rangle$ and $|I_3\rangle$, then flipping the position of sub-block ‘M’ with ‘O’, ‘N’ with ‘P’ in $|\varphi_3\rangle$ along X-axis. Finally, the sub-blocks ‘C’ and ‘M’ are compared by applying the Hadamard gate on s_1 .

3.4 Simulation experiments to assess the similarity of quantum images

In the absence of the physical quantum hardware to implement the image comparison, a conventional desktop computer with Intel Core i7, 2 Duo 2.80 GHz CPU, 4GB RAM and 64bit operating system is used to simulate the experiments. The simulation is based on linear algebra with complex vectors as quantum states and unitary matrices as unitary transforms using Matlab, and the program is realized by means of equations as well as the definitions which are introduced in the preceding sub-sections. The final step is that of measurement which converts the quantum information to the classical form as probability distributions. Extracting and analyzing the distributions gives information for comparing quantum images.

3.4.1 Comparison of two synthetic quantum images

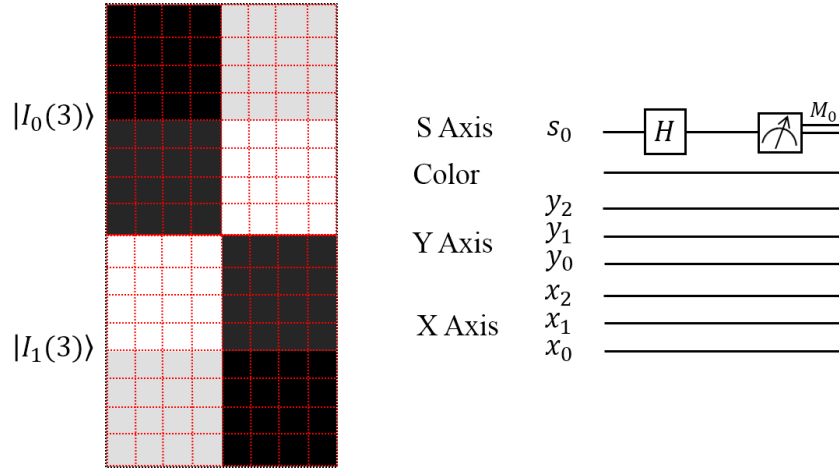
The first experiment is that to compare two 8×8 synthetic images and two 256×256 synthetic images both having 4 grey levels, comprising of black, dark, light, and white colors respectively, as shown on the left in Figure 3.9 and 3.10. The purpose of this experiment is to analyze the relationship between the similarity of two images and the size of them.

The comparison between the two 8×8 images is executed using the circuit on the right side in Figure 3.9. The circuit comprises of 8 qubits of which 6 qubits are used to address location of the content of the image, 1 qubit stores the color information, and the remaining 1 qubit represents the strip wire where the Hadamard and measurement operations are performed. Using the definition in Equation (3.20), a similarity of 0.314 is obtained for these two images. On the other hand, the similarity value between the two 256×256 images, whose circuit consists of 17 wires as shown on the right in Figure 3.10, is 0.253. The information retrieved from comparing these two sets of images are summarized in Table 3.2. These results indicate that the similarity between two quantum images increases with increase in the size of the images. As shown in Figures 3.9 and

Table 3.2: Summary of comparison results for synthetic images in Figures 3.9 and 3.10.

Image comparison	No. of qubits (wires)	Probability	Similarity
$ I_0(3)\rangle, I_1(3)\rangle$	8	$P_{s_0}(1\rangle) = 0.343$	$sim(I_0\rangle, I_1\rangle) = 0.314$
$ I_0(8)\rangle, I_1(8)\rangle$	18	$P_{s_0}(1\rangle) = 0.374$	$sim(I_0\rangle, I_1\rangle) = 0.253$

3.10, the operation to compare two images is realized by using only a single Hadamard gate. Accomplishing such a task on a classical computer requires that the color of every position in the image be compared one at a time. Hence, the proposed method offers a significant speed-up compared to how it is performed using classical computing resources.


Figure 3.9: Two synthetic 8×8 FRQI images and the circuit structure for their comparison.

3.4.2 Parallel comparison of four quantum images in a strip

In the second experiment, a data set consisting of four 512×512 images comprising of the Blonde Lady, Dark-haired Lady, Bridge, and Plane is considered. These images are prepared as $|I_0\rangle$, $|I_1\rangle$, $|I_2\rangle$, and $|I_3\rangle$, respectively and combined to form a strip. For brevity, we represent the strip with only labels of these images as seen on the left in Figure 3.11. The aim of this experiment is to simultaneously compare $|I_0\rangle$ with $|I_1\rangle$, and $|I_2\rangle$ with $|I_3\rangle$.

Similar to the circuit in Figure 3.6 (a), the circuit to simultaneously compare these

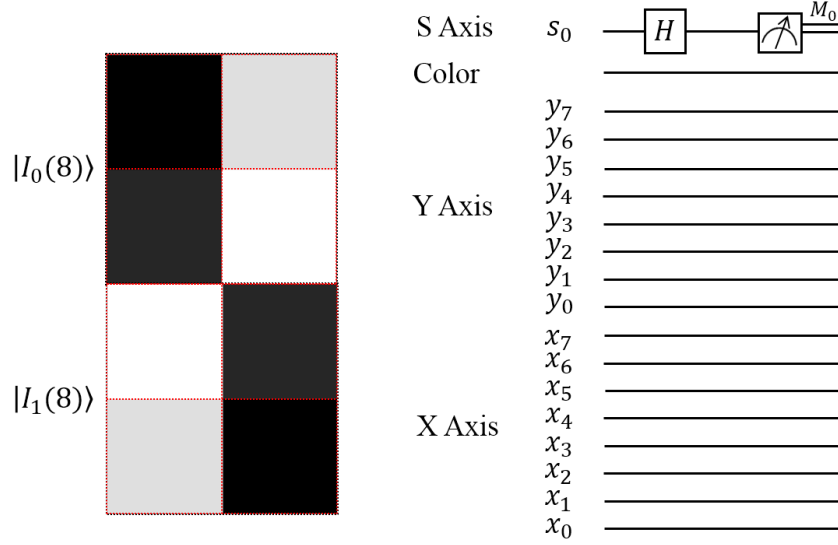


Figure 3.10: Two synthetic 256×256 FRQI images and the circuit structure for their comparison.

Table 3.3: Comparison results for the images encoded in the strip in Figure 3.11.

Image comparison	Probability	Similarity
$ I_0\rangle, I_1\rangle$	$P_{s_0}(01\rangle) = 0.029$	$sim(I_0\rangle, I_1\rangle) = 0.883$
$ I_2\rangle, I_3\rangle$	$P_{s_0}(11\rangle) = 0.040$	$sim(I_2\rangle, I_3\rangle) = 0.839$

two pairs of images is presented in Figure 3.12. The probabilities of getting the readouts (in *log* scale) on the strip wires in the measurements are presented in Figure 3.13. The similarities between different pairs of images being compared are shown in the Table 3.3, all of which suggest $|I_0\rangle$ and $|I_1\rangle$ are more similar to each other than $|I_2\rangle$ and $|I_3\rangle$. A simulation of a single Hadamard gate and two measurement operations are used to obtain the similarities for these two pairs of images. This further demonstrates the low computational requirements of the proposed method in comparison with performing the same task on traditional computing devices.

3.4.3 Comparison of sub-blocks from two quantum images

The aim of the last experiment is to realize the comparison between two sub-blocks from two arbitrary images in a strip. As shown in Figure 3.14, we intend to compare the

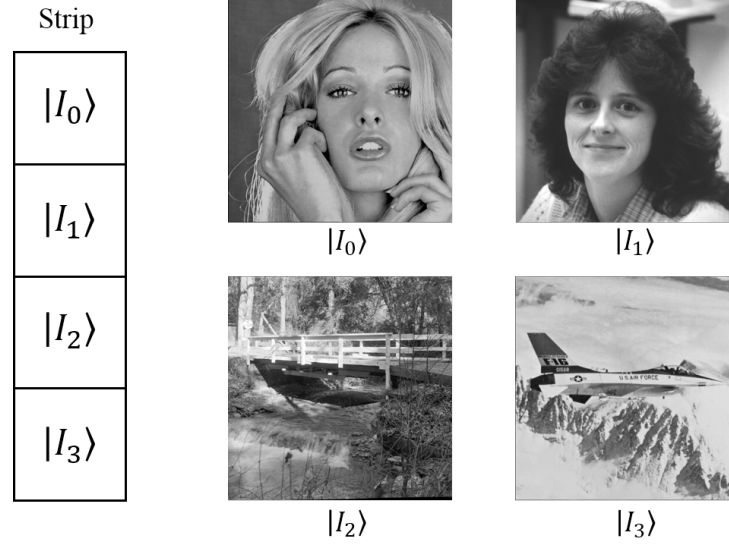


Figure 3.11: *The strip on the left and the images being compared in the strip.*

Lena image in the bottom left of the image in $|I_0\rangle$ (labelled as $|i_0^3\rangle$) with the watermarked Lena image in the top right of the image in $|I_3\rangle$ (labelled as $|i_3^2\rangle$), and the Man image (labelled as $|i_1^3\rangle$) with the processed Man image (labelled as $|i_2^3\rangle$) at the same position in $|I_1\rangle$ and $|I_2\rangle$, respectively. The enlarged versions of these four images that are being compared are presented in the bottom row of the Figure 3.14. For brevity, the four 1024×1024 images are indicated by only their labels $|I_0\rangle$, $|I_1\rangle$, $|I_2\rangle$, and $|I_3\rangle$ in the strip on the left in the same figure.

The corresponding circuit structure to compare them is presented in Figure 3.15. There are four steps to accomplish this comparison:

Step 1: Swap the position between $|I_1\rangle$ and $|I_3\rangle$ using the C-NOT gate on the strip wires;

Step 2: Swap the position of the watermarked Lena image with baboon in $|I_3\rangle$;

Step 3: Compare the two Lena images and two ‘Man’ images in parallel by applying the Hadamard gate on s_0 with appropriate control-condition operations to confine the operation to the desired sub-blocks;

Step 4: Observe the readouts from the quantum measurements to build up a histogram which can reflect the similarity of the two pairs of images.

As discussed in Figure 3.9 in Section 3.3.4, another way to execute the same comparison is applying Hadamard gate on strip wire s_1 after swapping the position of $|I_2\rangle$ and $|I_3\rangle$ in

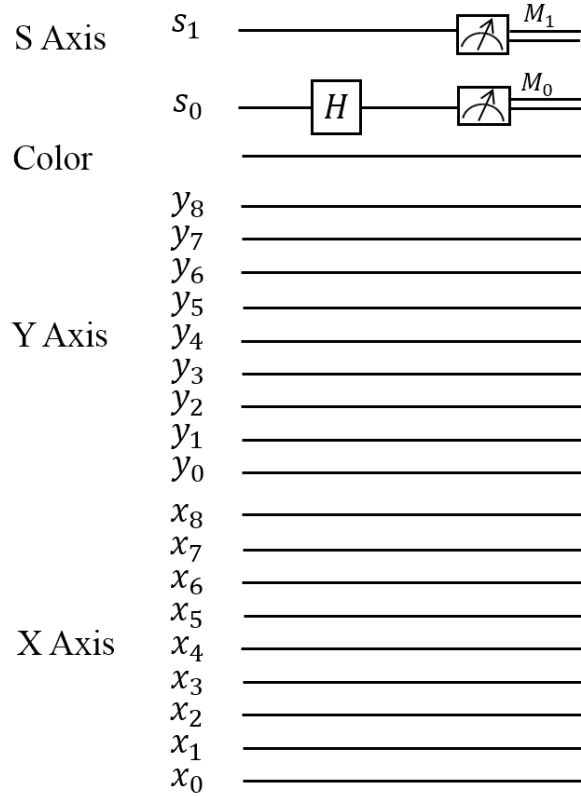


Figure 3.12: Circuit structure of comparing the images in Figure 3.11.

the strip.

The probabilities of getting the readouts (in *log* scale) on the strip wires in the measurements are presented in Figure 3.16, and the similarities among different pairs of images being compared are shown in the Table 3.4, from which the similarity between the original Lena image and the watermarked Lena image is 0.936. Moreover, the watermarking and authentication of quantum images [29][32] introduced how to realize the watermarked quantum image, however, the use of the Peak-Signal-to-noise-ratio (PSNR) as an evaluation metric for the fidelity between the original image and the watermarked image needs to be reconsidered in order to atone for the presence of errors in the preparation of the quantum image as well as the procedure to encode and decode the images. Using the proposed comparison scheme, a more accurate comparison can be made between the original quantum image and its watermarked version.

The results as indicated in this section show that the comparison of quantum images is both feasible and practical. Therefore, the proposed method provides the foundation for

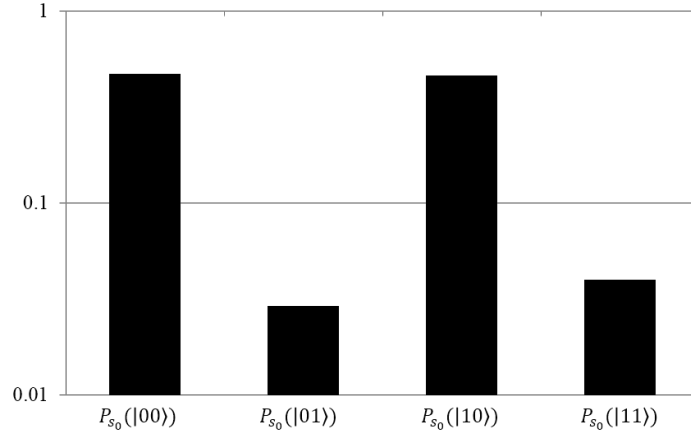


Figure 3.13: Histogram of the probabilities of the readouts in the measurements.

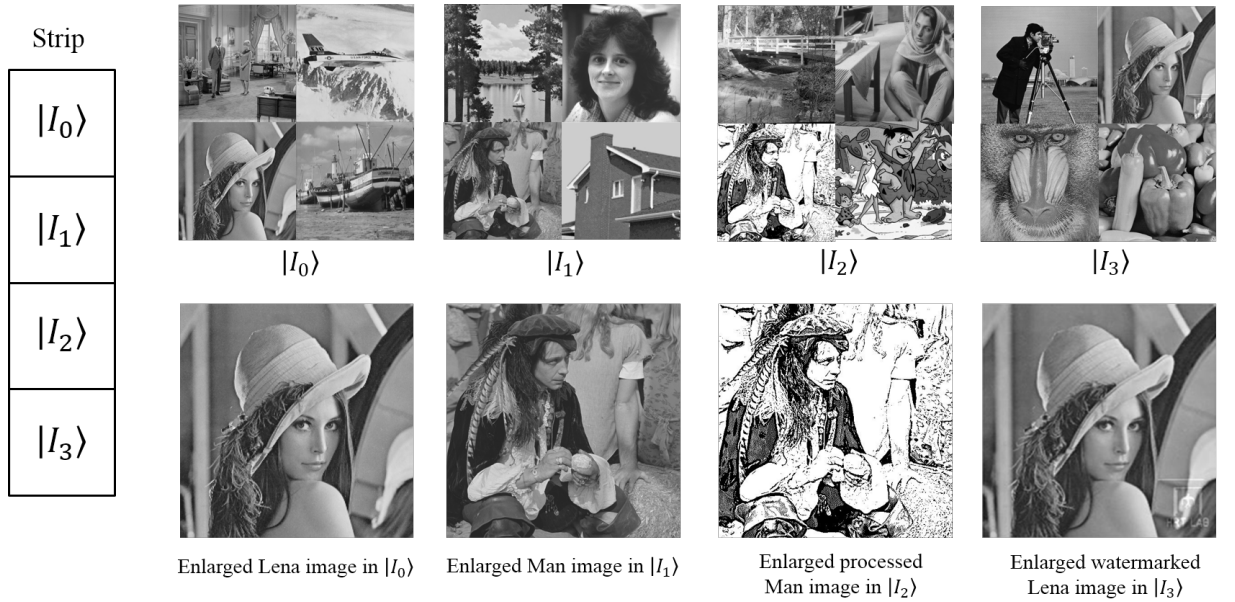


Figure 3.14: Parallel comparison of two Lena images and two ‘Man’ images.

quantum image database search, which is one of the next steps in FRQI image processing.

3.5 Conclusion

A method to evaluate the similarity between FRQI images of equal size is proposed. According to the representation of the strip, which combined by 2^m (m qubits) quantum images being compared and the basic operations in the quantum computation, a similarity value is estimated on the basis of the probability distributions of the readouts from quantum measurements. The proposed method is proven to require less computational

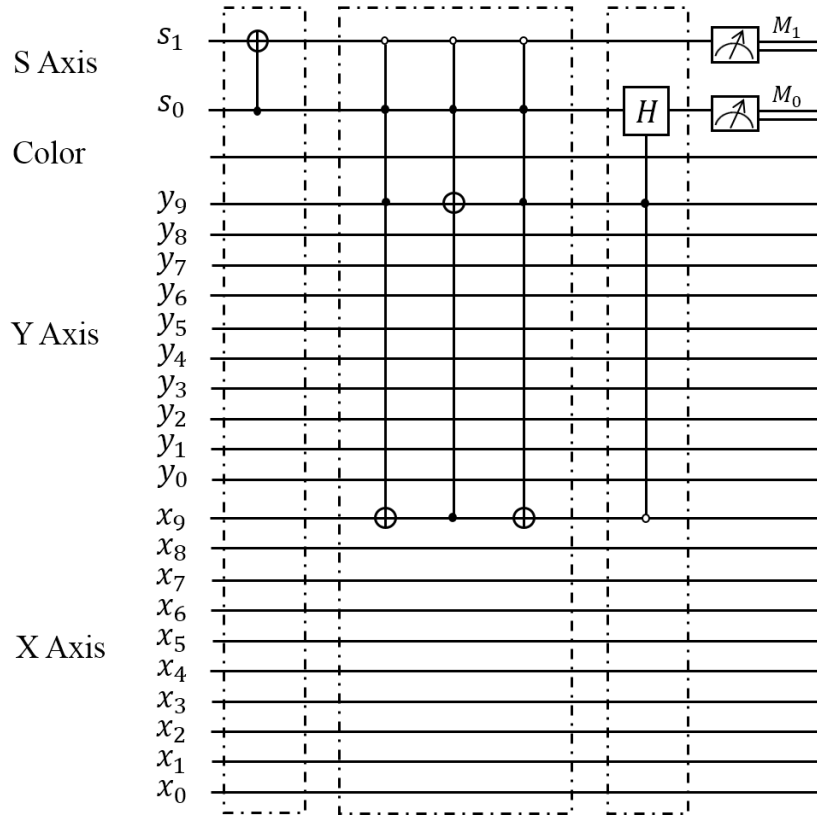


Figure 3.15: Circuit structure for realizing the comparison in Figure 3.14.

Table 3.4: Comparison results for the sub-blocks from two images.

Image comparison	Probability	Similarity
$ i_0^3\rangle, i_3^2\rangle$	$P_{s_0}(01\rangle) = 0.004$	$sim(i_0\rangle, i_3\rangle) = 0.936$
$ i_1^3\rangle, i_2^3\rangle$	$P_{s_0}(11\rangle) = 0.013$	$sim(i_1\rangle, i_2\rangle) = 0.787$

resources, and hence, offers a significant speed-up in comparison to performing the same task on traditional computing devices. This is possible because only a single Hadamard gate as well as several control-conditions (when the sub-blocks are compared) is required to simultaneously transform the entire information encoding the quantum images in a strip.

Three simulation-based experiments are implemented using Matlab on a classical computer by means of linear algebra with complex vectors as quantum states and unitary matrices as unitary transformations provide a reasonable estimation to the image com-

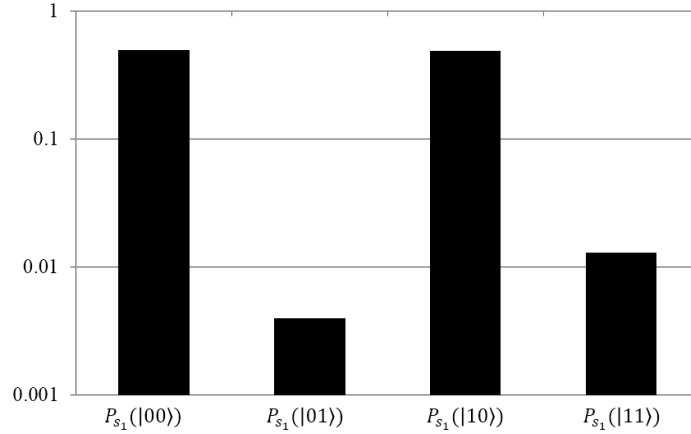


Figure 3.16: Histogram of the probabilities of the readouts in the measurements.

parison. Parallel comparison of quantum images is executed by constituting the new quantum system with the additional wires (strips). By utilizing appropriate geometric transformation operations on the strip wires as well as the required control conditions to the position wires, the comparison between two arbitrary FRQI images in the strip and the comparison between the sub-blocks from two different images can be realized. As a consequence, the work presented has shown that the similarity between two quantum images depends on the entire information in the both images instead of some parts of them, and furthermore, it is related to the size of the two images.

As for future work, the results in this chapter will be extended in the following directions. Firstly, the comparison between two quantum images in this chapter is based on the cosine function of pixel difference at every position of the images. Quantum Fourier Transform [12] or Wavelet transform [21] could also be applied on FRQI images in order to create different function so as to finish the quantum image comparison. Secondly, the proposal offers a first step towards image database search on quantum computers whereby an image could be retrieved as a search result from a database based on the extent of its similarity in comparison with the particular reference image. To realize such a search procedure, a reconstitution of the quantum system by adding some additional wires to the circuit in order to represent the images in the database and the reference images together might be necessary. Then the comparison is performed between the images to get the best result as the image with highest similarity value to the reference image. Exploiting

the parallelism inherent to quantum computation, it is envisaged that quantum image database search will be significantly faster than those on classical computers. Thirdly, besides the ability to measure the difference between the original image and the watermarked image which is suggested earlier, the proposed comparison method presented in this chapter can also be applied to the quantum movie [33] in order to enhance the smoothness and continuity of the frame to frame transition between scenes, and also to make the quantum movie trailers. These extensions will open new directions for efficient image and video processing using quantum computing hardware.

Chapter 4

Quantum image searching based on probability distributions

4.1 Introduction

Inspired by the image searching on conventional computers, the research on quantum image searching is also an indispensable field in quantum image processing [26][34]. In order to improve the limitation of the traditional searching, e.g. only text based and time consuming, the quantum image searching on the strength of the content of the images can be executed in parallel to realize more efficient computation.

On the basis of Flexible Representation of Quantum Image (FRQI) and the method to analyze the similarity between two FRQI images of the same size which is proposed in Chapter 3, a quantum image searching method is proposed whereby an image could be retrieved as a search result from a database based on the extent of its similarity in comparison with the particular test image. The searching result is provided by the probability distributions from two types of quantum measurements, the first of which, Z-axis measurement, represents the similarity between two current images being compared; the second type, S-axis measurements, gives the position of the comparing results in Z-axis measurement. Succinctly put, the main contributions of this work include the analysis of the similarity between multiple pairs of images simultaneously and the proposal of the whole scheme for the image searching on quantum mechanical systems.

The searching process is based on “parallel comparison”, where $2^m + 1$ pairs of quantum images are compared in parallel. In addition, the method is executed using low computational resources in comparison with performing the same task on traditional computing devices, since only a single Hadamard gate as well as $m + 1$ quantum measurement operations could transform the entire information encoding the quantum images in a strip simultaneously.

The Z-strip is defined based on the Flexible Representation of Quantum Images (FRQI) in Section 4.2. The proposed scheme to realize image searching on quantum mechanical systems is presented in Section 4.3. The simulation experiment and its discussion are shown in Section 4.4.

4.2 Representation of Z-strip to indicate multiple FRQI images

For the quantum image processing, a good deal of operations are done by relying on the corresponding processing in classical images as reference [37][5]. The Flexible Representation for Quantum Images, FRQI [37][41], which is similar to the pixel representation for images in conventional computers, captures the essential information about the colors as well as the corresponding positions of every point in an image and integrates them into a quantum state having its formula as

$$|I(n)\rangle = \frac{1}{2^n} \sum_{i=0}^{2^{2n}-1} |c_i\rangle \otimes |i\rangle, \quad (4.1)$$

where

$$|c_i\rangle = \cos \theta_i |0\rangle + \sin \theta_i |1\rangle, \quad (4.2)$$

$$\theta_i \in [0, \frac{\pi}{2}], i = 1, 2, \dots, 2^{2n} - 1, \quad (4.3)$$

where $|i\rangle$, $i = 1, 2, \dots, 2^{2n} - 1$, are $2n$ -D computational basis quantum states and $\theta = (\theta_0, \theta_1, \dots, \theta_{2^{2n}-1})$ is the vector of angles encoding colors.

A dexterous property of Z-strip representation encoding 2^{m+1} -ending FRQI images is its ability to utilize the parallelism inherent to quantum computation in order to transform multiple images using very few quantum resources. The Z-strip representation is defined in Definition 4.1.

Definition 4.1 A Z-strip, $|Z(m, n)\rangle$, is a horizontal combination of two strips [33], which are located on the left and right side, respectively. The state of Z-strip is defined by

$$|Z(m, n)\rangle = \frac{1}{2^{(m+1)/2}} \sum_{s=0}^{2^m-1} (|L_s(n)\rangle \otimes |0\rangle + |R_s(n)\rangle \otimes |1\rangle) \otimes |s\rangle, \quad (4.4)$$

where $|L_s(n)\rangle$ and $|R_s(n)\rangle$ are FRQI images as defined in Equations (4.5) and (4.6),

$$|L_s(n)\rangle = \frac{1}{2^n} \sum_{i=0}^{2^{2n}-1} |c_{l,s,i}\rangle \otimes |i\rangle, \quad (4.5)$$

$$|R_s(n)\rangle = \frac{1}{2^n} \sum_{i=0}^{2^{2n}-1} |c_{r,s,i}\rangle \otimes |i\rangle, \quad (4.6)$$

$$|c_{l,s,i}\rangle = \cos_{l,s,i} |0\rangle + \sin_{l,s,i} |1\rangle, \quad (4.7)$$

$$|c_{r,s,i}\rangle = \cos_{r,s,i} |0\rangle + \sin_{r,s,i} |1\rangle, \quad (4.8)$$

$$\theta_{l,s,i}, \theta_{r,s,i} \in [0, \frac{\pi}{2}], \quad (4.9)$$

$$i = 0, 1, \dots, 2^{2n} - 1, s = 0, 1, \dots, 2^m - 1. \quad (4.10)$$

As seen in Figure 4.1, the size of a Z-strip in the representation captures the input state comprising 2^{m+1} quantum images. The Z-axis differentiates the strip which is located on the left and the right position. Each image in the Z-strip is an FRQI state while the combination of such states in the Z-strip is best represented as a Z-FRQI state.

The Z-FRQI state represents 2^{m+1} quantum images using only $m+2n+2$ qubits since all of the images are of the same size on this Z-strip. A notation ‘o’ for ‘0’ or ‘●’ for ‘1’ control-condition on Z-axis or S-axis, is sufficient to specify any quantum image in the Z-strip. In addition, combining with the control-conditions from the position $|y\rangle|x\rangle$ to the color wire; every pixel in this strip can be accessed. The representation also facilitates

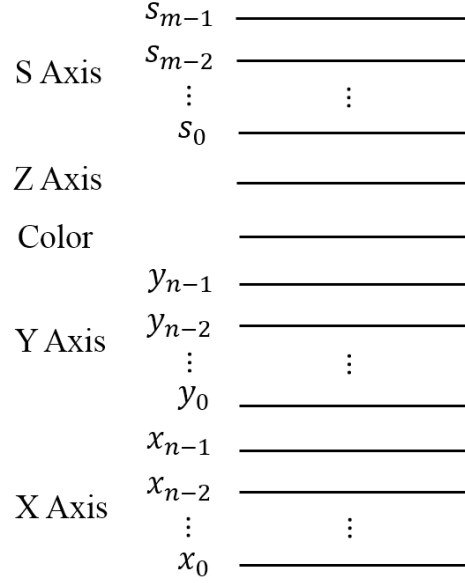


Figure 4.1: Circuit structure to encode the Z-strip input.

the quantum operation to all the images in this strip.

An example that has two 2×2 images on both the left and right side of the Z-strip, respectively, including its circuit structure and Z-FRQI state is shown in Figure 4.2.

4.3 Image searching on quantum mechanical systems

Quantum image searching from a database is an important research field inspired by the database searching on classical computers. A first step towards realizing that would be to propose a scheme so as to evaluate the extent to which two or more images are similar to one another. The parallel computation on quantum computers allows us to find a way that comparing many pairs of images in parallel. The proposal of the Z-strip comprising $2^m + 1$ images in the Definition 4.1 provides us a crucial condition to make the parallel comparison of quantum images possible because the operation on the strip wires can transform the information in every image simultaneously. The generalized circuit structure of comparing 2^m pairs of FRQI images in parallel is presented in Figure 4.3.

The input of this circuit is the Z-FRQI state as defined in Equation (4.4), a Hadamard gate, which maps the basis state $|0\rangle$ to $(|0\rangle + |1\rangle)/\sqrt{2}$ and $|1\rangle$ to $(|0\rangle - |1\rangle)/\sqrt{2}$, is applied on the Z-axis to obtain the new mathematical expressions between the two images being

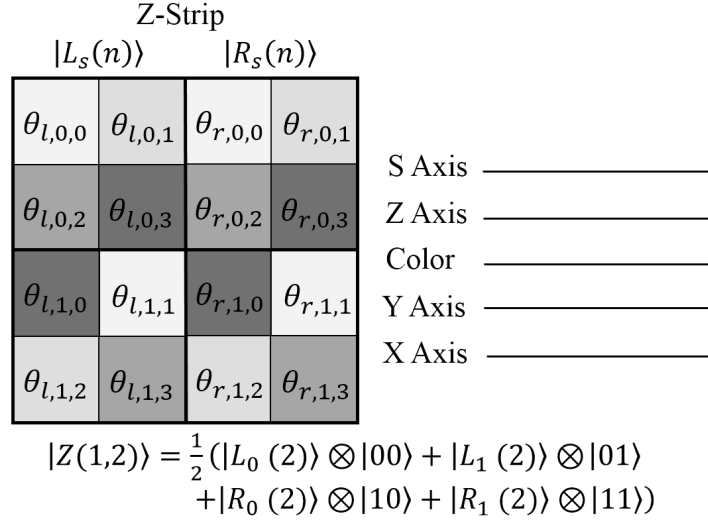


Figure 4.2: An example of Z-strip, its circuit structure and Z-FRQI state.

compared. The final step in the circuit consists of $m+1$ measurements from which the similarity can be retrieved in each pair of images.

When n experiments are performed, the measurement results on the Z-axis follow a binomial distribution. The probability of obtaining k readouts of 1 in n experiments is given by the probability mass function

$$Pr(X = k) = C_n^k p^k (1 - p)^{n-k}, \quad (4.11)$$

where X is the incident that the result of measurement is 1, p is the probability of 1 when the results on the Z-axis are measured, $k = 0, 1, \dots, n$.

Meanwhile, the measurement results on the S-axis, $s_{m-1} \dots s_r \dots s_0, s_r \in \{0, 1\}$, give the position of probabilities of the measurements on the Z-axis. According to the readouts on both the measurements, the similarity between each pair of images on the Z-strip can be assessed, from which the quantum image searching can be realized.

Corresponding to the circuit shown in Figure 4.3, the state of quantum system after applying the Hadamard gate on the strip wire can be shown in Equations (4.12) and

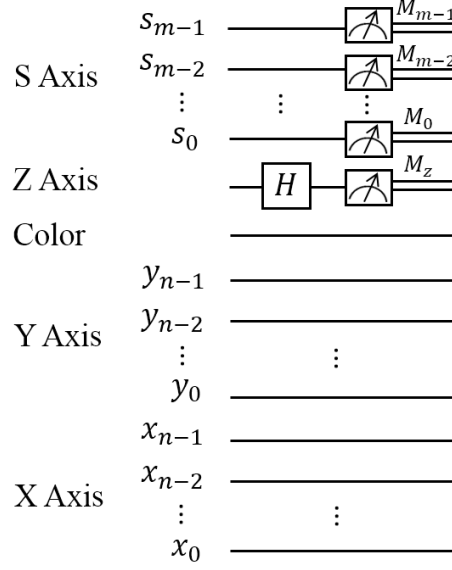


Figure 4.3: Generalized circuit structure for parallel comparison of quantum images in Z-strip.

(4.13).

$$\begin{aligned}
 H_z|Z(m, n)\rangle &= \frac{1}{2^{m/2}} \sum_{s=0}^{2^m-1} (|L_s(n)\rangle \otimes \frac{(|0\rangle + |1\rangle)}{\sqrt{2}} + |R_s(n)\rangle \otimes \frac{(|0\rangle - |1\rangle)}{\sqrt{2}}) \otimes |s\rangle \\
 &= \frac{1}{2^{(m+1)/2}} \sum_{s=0}^{2^m-1} [(|L_s(n)\rangle + |R_s(n)\rangle)|0\rangle + (|L_s(n)\rangle - |R_s(n)\rangle)|1\rangle] \otimes |s\rangle,
 \end{aligned} \tag{4.12}$$

where

$$|L_s(n)\rangle \pm |R_s(n)\rangle = \frac{1}{2^n} \sum_{i=0}^{2^{2n}-1} [(\cos \theta_{l,s,i} + \cos \theta_{r,s,i})|0\rangle \pm (\sin \theta_{l,s,i} + \sin \theta_{r,s,i})|1\rangle] \otimes |i\rangle. \tag{4.13}$$

Obviously, the result of the measurement depends on the disparities between $|L_s(n)\rangle$ and $|R_s(n)\rangle$. The probability of state $|0\rangle$ on the Z-axis at position $|s_{m-1}, s_{m-2}, \dots, s_0\rangle$ is shown by

$$P_s(|0\rangle) = \frac{1}{2} + \frac{1}{2^{2n+1}} \sum_{i=0}^{2^{2n}-1} \cos(\theta_{l,s,i} - \theta_{r,s,i}). \tag{4.14}$$

In the same manner, that of state $|1\rangle$ on the same wire is

$$P_s(|1\rangle) = \frac{1}{2} - \frac{1}{2^{2n+1}} \sum_{i=0}^{2^{2n}-1} \cos(\theta_{l,s,i} - \theta_{r,s,i}). \tag{4.15}$$

The probabilities of these two states sum up to 1, $P_s(|0\rangle) + P_s(|1\rangle) = 1$, as they should.

Definition 4.2 Pixel difference in position i , $\sigma_{s,i}$, is defined by

$$\sigma_{s,i} = |\theta_{l,s,i} - \theta_{r,s,i}|, \sigma_{s,i} \in [0, \frac{\pi}{2}] \quad (4.16)$$

where $\theta_{l,s,i}$ and $\theta_{r,s,i}$ represent the color information at position i of the two images which are at the s^{th} position of the Z-strip, respectively.

It is apparent that, arising from Equations (4.15) and (4.16), the pixel difference $\sigma_{s,i}$ is related to the probability of getting readout of 1 from the Z-axis, $P_s(|1\rangle)$, in the measurement and $P_s(|1\rangle)$ will increase when pixel difference increases. Furthermore, the similarity between the two images, which is the function of the pixel differences at every position, depends on $P_s(|1\rangle)$ as given by

$$\begin{aligned} sim(|L_s(n)\rangle, |R_s(n)\rangle) &= 1 - 2P_s(|1\rangle) \\ &= \frac{1}{2^{2n}} \sum_{i=0}^{2^{2n}-1} \cos \sigma_{s,i}, \end{aligned} \quad (4.17)$$

where $|L_s(n)\rangle$ and $|R_s(n)\rangle$ are the two images being compared, $P_s(|1\rangle)$ is defined in Equation (4.15), and $sim(|L_s(n)\rangle, |R_s(n)\rangle) \in [0, 1]$.

Two special cases of the similarity between two quantum images are listed as follows:

- if $\forall i, \sigma_{s,i} = \pi/2$, then $sim(|L_s(n)\rangle, |R_s(n)\rangle) = 0$, two images are totally different;
- if $\forall i, \sigma_{s,i} = 0$, then $sim(|L_s(n)\rangle, |R_s(n)\rangle) = 1$, two images are exactly the same,

where $i = 0, 1, \dots, 2^{2n} - 1$, $\sigma_{s,i}$ is the pixel difference at position i as defined in Definition 4.2.

Based on the comparison method and the probability distributions introduced above, the scheme to accomplish the image searching on quantum mechanical systems is presented in Figure 4.4.

The quantum images are prepared from the classical images using FRQI representation [37][69][33][29]. The color information as well as the corresponding positions of every point in the classical image is integrated into the quantum state, and $2^m + 1$ quantum images

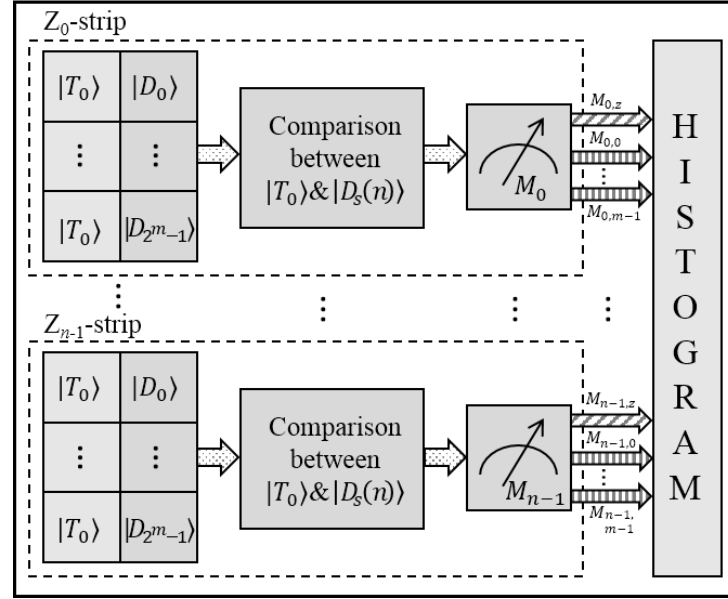


Figure 4.4: Block diagram of scheme to realize image searching on quantum mechanical systems.

being compared are combined as a Z-strip. Because of the superposition property of quantum computation, such a work can be realized using only a few quantum resources.

The Z-strip prepared in the preceding period is transformed using a gate array comprising of geometric, GTQI [38], and color, CTQI [39], transformations on all the images in the strip. For this particular application, the transformations are built in a way to allow the recovery of the pixel difference as defined in Equation (4.16). This transformation unit combines with measurement operations that follow it to convert the quantum information into the classical form as probability distributions. The Z-strip is prepared $n(n > 1)$ times to compare the similarity between two quantum images in parallel since a measurement would destroy the superposition state in the quantum system [49]. Extracting and analyzing the distributions gives information that the similarity values between the quantum images being compared, so that the image with the highest similarity to the particular test image could be retrieved as a result from the database.

The operation to search image on quantum mechanical systems is realized by using only a single Hadamard gate and several measurements. Such an image searching scheme, however, can only be achieved on a classical computer by comparing one pair of images at a time. Hence, the proposed method offers a significant speed-up compared to how it

is performed using classical computing resources.

4.4 A simulation experiment to search quantum images from database

A conventional desktop computer with Intel Core i7, 2 Duo 2.80 GHz CPU, 4GB RAM and 64bit operating system is used to simulate the experiment. The simulation experiment is executed based on linear algebra using Matlab and the program is encoded by means of equations as well as the definitions that are introduced in earlier sections of this chapter. The purpose of this experiment is that to search the image from a database which has the highest similarity with the test image. An original database which includes sixty-four 4×4 binary image data is used, then the Z-strip comprising of $|D_0(2)\rangle, |D_1(2)\rangle, \dots, |D_{63}(2)\rangle$, and sixty-four $|T(2)\rangle$ s is constituted as shown in Figure 4.5.

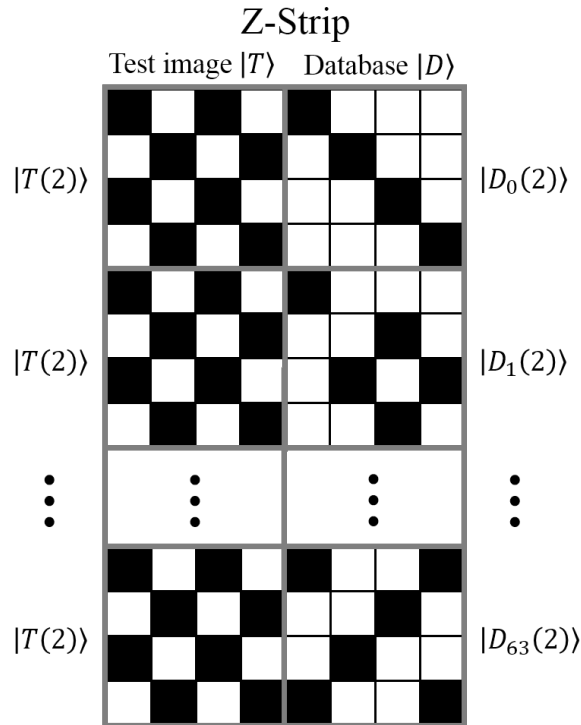


Figure 4.5: Image searching from database $|D\rangle$.

The corresponding circuit structure to realize such an image searching is presented in Figure 4.6. There are three steps to achieve this comparison:

Step 1: The test images $|T(2)\rangle$ is prepared from the classical version using FRQI representation and integrated to a Z-strip state with the images $|D\rangle$ in the database;

Step 2: A Hadamard operation is applied on the Z-axis in order to compare the test image $|T(2)\rangle$ with $|D_0(2)\rangle, |D_1(2)\rangle, \dots, \text{ and } |D_{63}(2)\rangle$;

Step 3: The measurements which convert the quantum information to the classical form are used on the S-axis and Z-axis to distribute the readouts from which the histogram is built to reflect the similarity of the sixty-four pairs of images.

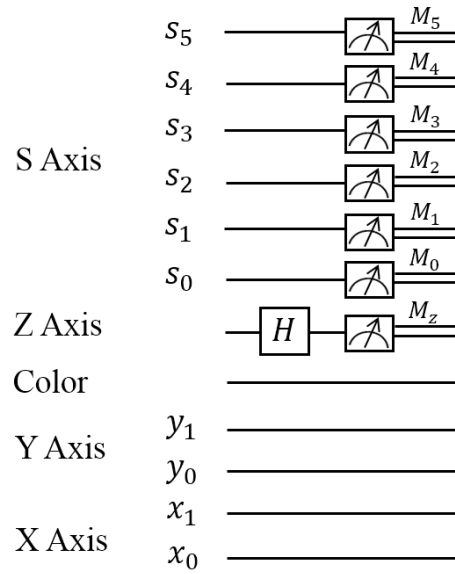


Figure 4.6: Circuit structure for realizing the image searching in Figure 4.5.

The circuit comprises of 12 qubits of which 6 are used to address positions of the image, 1 qubit is reserved for storing the information about the colors, and the remaining qubits are prepared for representing the Z-strip wire where the Hadamard gate and measurement M_z are applied. A simulation of a single Hadamard gate and seven measurement operations are used to obtain the similarities for these 64 pairs of images based on the probabilities of getting the readouts on the Z-axis and S-axis in the measurements as shown in the Figure 4.7. From the histogram, the image $|D_{37}(2)\rangle$, which manifests the highest similarity value of 0.93 to the test image $|T(2)\rangle$ is retrieved as the searching result. There is only one different grid between the test image and $|D_{37}(2)\rangle$, which are shown in Figure 4.8. It is testified from that the quantum image searching is based on the pixel difference between the test image and the images in the database.

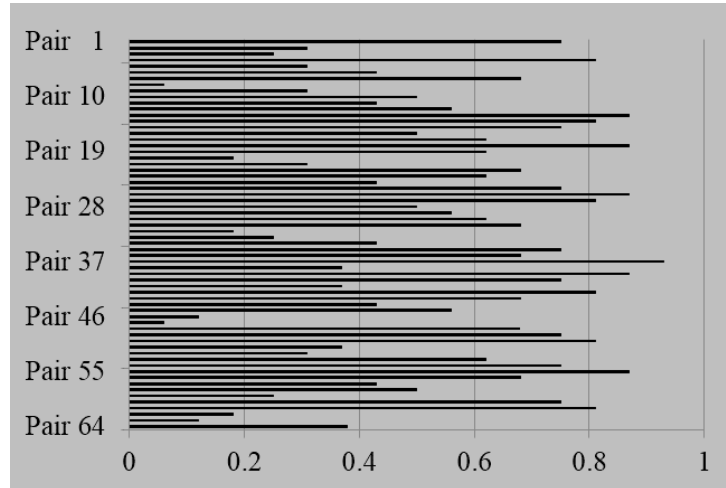


Figure 4.7: Similarities among different pairs of images in Z-strip.

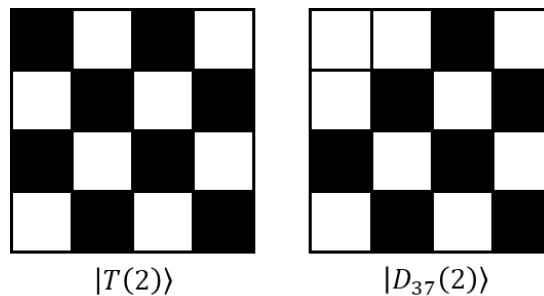


Figure 4.8: The test image $|D(2)\rangle$ and the retrieved image $|D_{37}(2)\rangle$.

The foregoing experiment provides the foundation for the next step in quantum image processing based on the FRQI representation. The results as indicated in this section show that the quantum image searching on quantum mechanical systems is feasible and practical. Furthermore, the target area to apply the proposed method is the development of the search engine on quantum computing devices.

4.5 Conclusion

The simulation experiment is performed to search for a target image from an original database comprising of sixty-four (64) binary images. There are 12 qubits which encodes each image in the Z-strip and 7 quantum measurements which are for converting the quantum information to the classical form as probability distributions in the circuit. According to the readouts from the measurements, the similarity of each pair between

the test image and the images in the database is calculated. For the simulation-based database used in this chapter, the 38th image, $|D_{37}(2)\rangle$, with the highest similarity value of 0.93 is retrieved as search result. It is concluded that the more images in the database, the better the ability of the proposed method. This is because m qubits on the strip wires can represent 2^m quantum images in the Z-strip, and only one qubit on the Z-axis can represent the images on both the left and right side of Z-strip. This further demonstrates the low computational resources of the proposed method compared to performing the same task on traditional computing devices.

As for future work, the proposal will be applied on designing a search engine on such quantum computing devices that the image in the database is retrieved based on its similarity to the test image. Most of the search engines recently are only based on the text to realize the searching [54]. Even some searching is developed based on the content of the images. It is, however, usually time-consuming. This work, which realizes the searching based on the content of the images and is executed in parallel, proposes a basic step for the quantum image searching, especially when a database comprising of a huge amount of data is confronted.

Chapter 5

A double-key, double-domain watermarking strategy for multi-channel quantum images

5.1 Introduction

To process color images on quantum computers, a Multi-Channel representation for Quantum Image (MCQI) is proposed to capture RGB channel information and these multi-channel information is stored in quantum states simultaneously [60][59]. Through such an representation, the Channel of Interest (CoI) and Channel Swapping (CS) [60][59] can be realized. Arising from the quantum image representations, researchers start to investigate watermarking strategies, which embeds the specific symbolic information into quantum images, in order to protect the copyright of the quantum images [22][23][70][61]. The watermarking and authentication of quantum images (WaQI) [30][29] was proposed, which is secure, keyless, and blind, but it could be only used to authenticate whether the carrier image belongs to a certain one or not because we have to know the content of watermark image first so as to design the quantum circuit for the authentication. Another quantum image watermarking strategy which embeds the logo information into Quantum Fourier Transform (QFT) coefficients was discussed in [71]. The illegal users can not understand what the watermarked information means even though they extract it from

the watermarked image, however, it is still dangerous if the ‘fixed’ key is stolen by them. In addition, both of these two watermarking strategies are used for dealing with grey scale quantum images only.

A new Multi-Channel Watermarking strategy for Quantum Images (MC-WaQI) is proposed where the double-key and double-domain idea makes the watermarking more secure. It is designed based on the MCQI representation [60][59] which is used to represent the color watermark image and carrier image. Specifically, the main contributions of this chapter are three-fold:

- The adoption of MCQI representation makes MC-WaQI strategy possible to deal with color quantum images;
- The double-key scheme produces the double protection on the watermark image, and the color information key from the quantum measurement is ‘unfixed’;
- The watermark image is embedded into both spatial domain and frequency domain which improves the anti-attack capability of watermarked images.

The Multi-Channel representation for Quantum Images (MCQI) is introduced in Section 5.2, which is the basis of the MC-WaQI strategy. The details of the MC-WaQI strategy is describe in Section 5.3. In Section 5.4, the experiment results are presented and analyzed.

5.2 General schematic of watermarking strategy for MCQI images

Based on the pixel representation for images on conventional computers and FRQI representation [37], the Multi-Channel representation for Quantum Images (MCQI) is proposed in [60] to capture RGB channels information, which is accomplished by assigning three qubits to encode color information of images and the mathematical expression is presented as

$$|I(n)_{mc}\rangle = \frac{1}{2^{n+1}} \sum_{i=0}^{2^{2n}-1} |C_{RGB}^i\rangle \otimes |i\rangle, \quad (5.1)$$

where the color information $|C_{RGB}^i\rangle$ encoding the information of R, G, and B channels is defined as

$$\begin{aligned}
 |C_{RGB}^i\rangle = & \cos \theta_R^i |000\rangle + \cos \theta_G^i |001\rangle + \cos \theta_B^i |010\rangle + \cos \theta_O |011\rangle \\
 & + \sin \theta_R^i |100\rangle + \sin \theta_G^i |101\rangle + \sin \theta_B^i |110\rangle + \sin \theta_O |111\rangle,
 \end{aligned} \tag{5.2}$$

where $\{\theta_R^i, \theta_G^i, \theta_B^i\} \in [0, \pi/2]$ are three angles encoding the colors of the R, G, and B channels of the i^{th} pixel, respectively. θ_O is set as 0 to make the two coefficients constant ($\cos \theta_O = 1$ and $\sin \theta_O = 0$) to carry no information [60][59].

In this chapter, a double-key, double-domain Multi-Channel Watermarking strategy for Quantum Images (MC-WaQI) is proposed, which can be used to increase the security of quantum images. The general framework for the proposal is shown in Figure 5.1, which is delineated into two broad divisions, the first of that comprises of all the data available to the copyright owner, i.e. the publisher of the watermarked image, and the other consists of the information published for the public users. Therefore, the tasks such as preprocessing, embedding, and extracting are handled by the copyright owner who has exclusive permission to access these data. In addition, the scheme is also divided into classical domain and quantum domain from the view of research field.

In detail, this strategy could be realized by the following three steps:

(1) Preprocessing procedure

- prepare for MCQI images $|I\rangle$ and $|W\rangle$ from the classical version of them I and W ;
- create two watermark information $|FW\rangle$ and $|SW\rangle$ from the original watermark image $|W\rangle$ for the embedding into both frequency domain and spatial domain of the carrier image;
- apply measurement operation on image $|SW\rangle$ to obtain retrieved image M ;
- generate the Color Information Key (CIK) from image M by means of the encoding rule;
- execute operations on $|SW\rangle$ using CIK to get image $|SW'\rangle$;

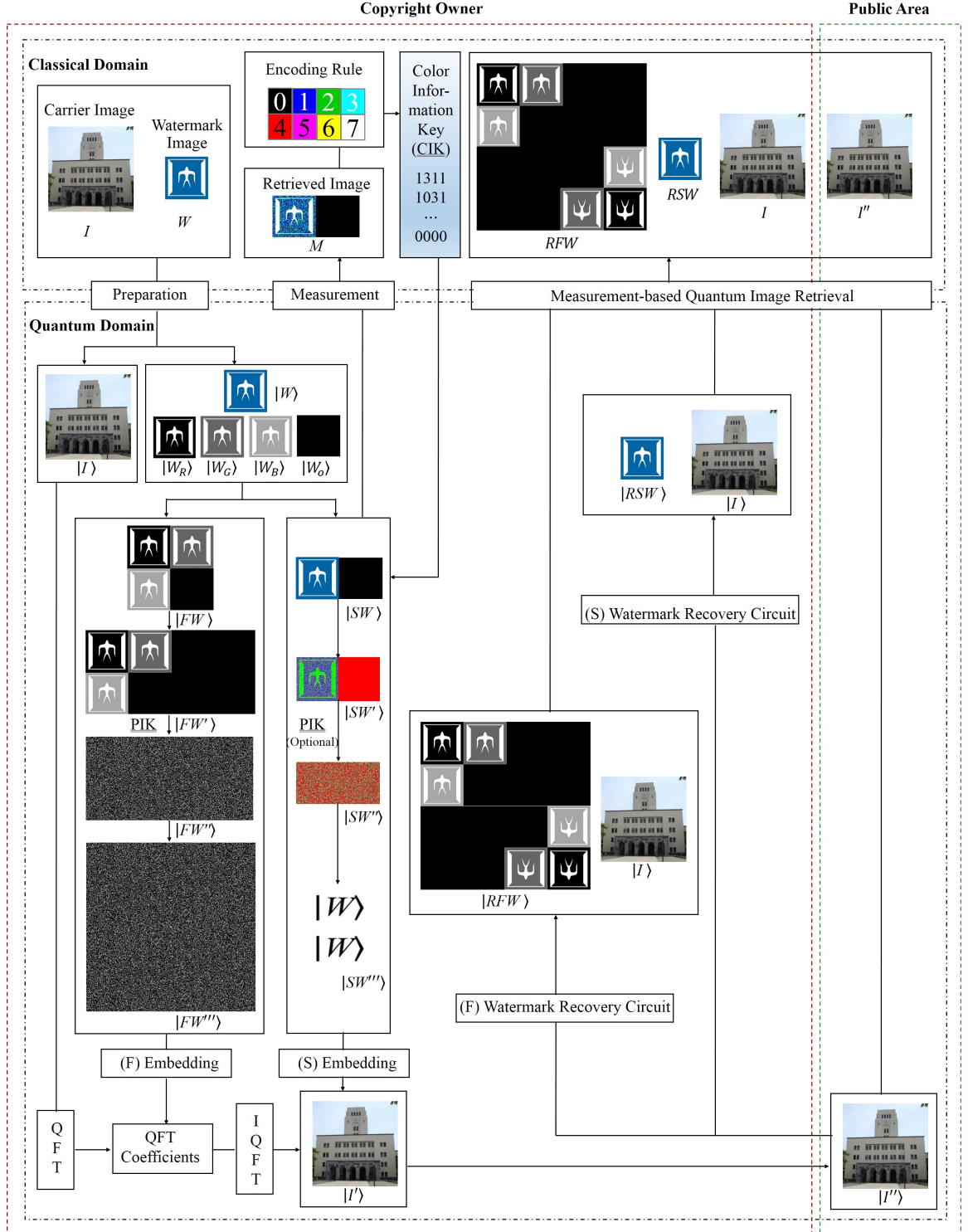


Figure 5.1: General schematic for MC-WaQI.

- compose image $|FW'\rangle$ from image $|FW\rangle$;
- scramble image $|FW'\rangle$ to obtain image $|FW''\rangle$ by applying Position Information Key (PIK) operation, and it is an optional operation to scramble image

$|SW'\rangle$ to $|SW''\rangle$;

- resize image $|FW''\rangle$ and $|SW''\rangle$ to get image $|FW'''\rangle$ and $|SW'''\rangle$.

(2) Embedding procedure

- embed image $|FW'''\rangle$ into the QFT coefficients of carrier image to transform image $|I\rangle$ to image $|I'\rangle$;
- embed image $|SW'''\rangle$ into the spatial domain of image $|I'\rangle$ to generate image $|I''\rangle$.

(3) Extracting procedure

- extract watermark image $|RFW\rangle$ from frequency domain using PIK;
- extract watermark image $|RSW\rangle$ from spatial domain using CIK (probably with PIK depending on preprocessing procedure).

Quantum computers are usually initialized in well-prepared states, as a result, the preparation which transforms quantum computers from the initialized state (assuming $|00\dots0\rangle$) to MCQI state is enumerated as the first step [60][37]. Two watermark information are created from the original watermark image for embedding it into both frequency domain and spatial domain of the carrier image in order to strengthen the power of resisting invalid attack. Meanwhile, two keys are generated in the procedure that one of them (Color Information Key or briefly CIK) is randomly updated by the quantum measurement to protect the color information of the watermark image and the other (Position Information Key or briefly PIK) is fixedly assigned by the owner [71] to scramble the position information of the watermark image. After the preprocessing, the two watermark information are embedded into the frequency domain and the spatial domain of carrier image, respectively. Finally, the watermarked quantum image could be extracted from these two domains by means of the proposed watermark recovery circuit, which is only available to the embedder. Furthermore, the quantum images can be retrieved to the classical version of them on the basis of quantum measurement.

5.3 Double-key generation and double-domain embedding procedure

5.3.1 Two watermark information generation

In MC-WaQI strategy, the watermark information is requested to be embedded into both frequency domain and spatial domain of the carrier image. In order to realize it, the watermark image with half size of the carrier image are processed to two kinds of log information. Assuming the size of carrier image is $n \times n$, the size of the watermark image is supposed to be $n/2 \times n/2$, otherwise, the embedder will polish the watermark image to half the size of carrier image [71]. The MCQI image is a multiple channel quantum image with the original RGB channels and O channel for processing the color information as shown in Equations (5.1) and (5.2), so the watermark images in different channels are presented in Figure 5.2, where O channel is the redundant channel with all black pixels.

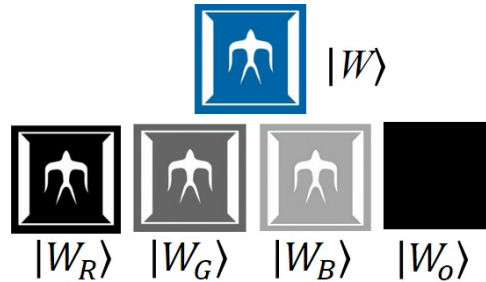


Figure 5.2: The watermark image and its separations in 4 channels.

In order to embed the watermark information into the spatial domain of the carrier image, a new logo information $|SW\rangle$ should be composed by combining the original watermark image $|W\rangle$ with its separation in O channel, image $|W_O\rangle$, horizontally as shown in Figure 5.3.



Figure 5.3: Watermark image $|SW\rangle$ in spatial domain.

After the preparation of watermark information in spatial domain, the separations of watermark information in R, G, B, and O channels are combined to generate a grey scale image $|FW\rangle$ for the watermarking in frequency domain as presented in Figure 5.4(a). Then a double sized image $|FW'\rangle$ as shown in Figure 5.4(b) is obtained by adding a black image with the same size adjoint to the right border of image $|FW\rangle$ so that the watermark information can be embedded into QFT coefficients of the carrier image.

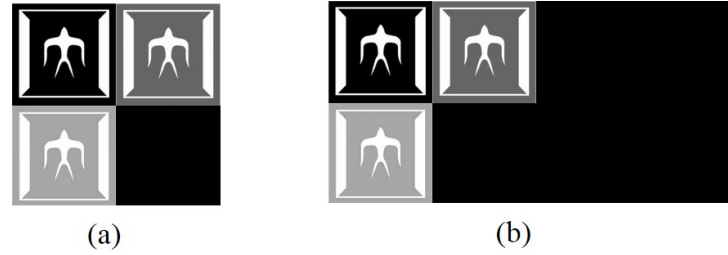


Figure 5.4: (a) Watermark image $|FW\rangle$ and (b) resized version $|FW'\rangle$ in frequency domain.

5.3.2 Spatial domain embedding and CIK generation

The Color Information Key (CIK) is an unfixed key, which is updated by applying quantum measurement on watermark image. A measurement applied on a superposition state $\alpha|0\rangle + \beta|1\rangle$ will lead to the collapse of this state to produce the result 0 with probability of α^2 or 1 with probability of β^2 , where $\alpha^2 + \beta^2 = 1$. An simple example presented in Figure 5.5 shows how a CIK can be generated.

First of all, the watermark image is prepared and stored as quantum state [37][60], then it is preprocessed to have the same row number and double column number. The processed watermark image contains the original watermark information located at the left and the right part is filled with black pixels (0,0,0). A quantum measurement is applied on each channel of the watermark image to lead the different color information collapsed to a certain color as shown in the post-measurement image [15]. Take a purple quantum pixel as an example, it could be decomposed to R (128), G (64), and B (128), however, we can only obtain black and white with probabilities on each channel after the measurement on these three channels according to the quantum state collapse property

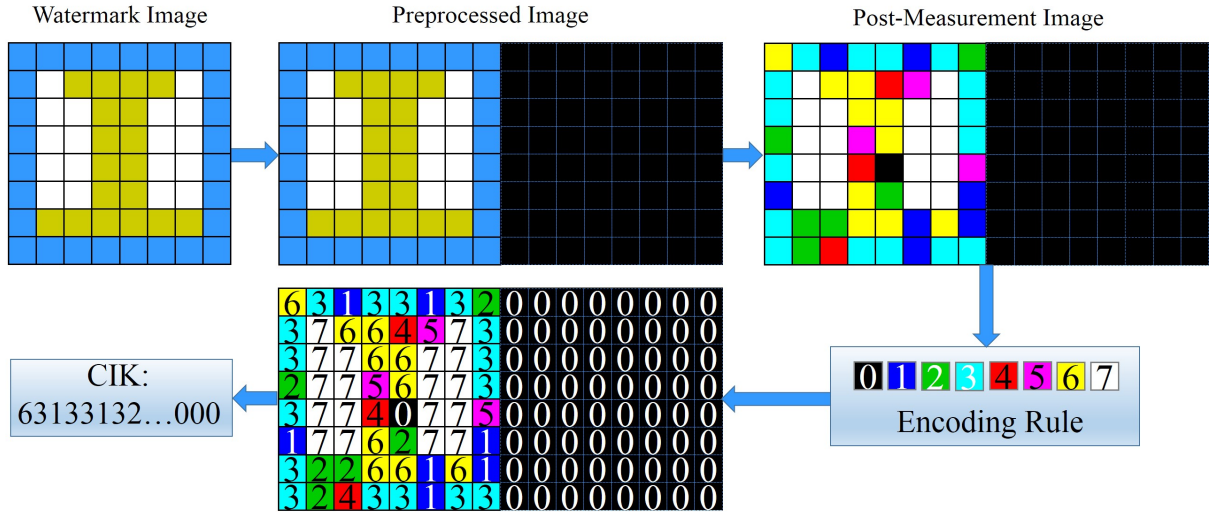


Figure 5.5: Generation procedure of CIK.

as we introduced earlier. Undoubtedly, there are only eight possible colors in the post-measurement image and we assign eight natural numbers from 0 to 7 for them to make an encoding rule, from that a CIK is generated as presented in Figure 5.6. The CIK is obtained by the quantum measurement and the length of CIK is the same with the number of the pixels in post-measurement image. For example, the length of CIK in Figure 5.5 is 128, which is the same size with resized watermark image, and the first element in CIK is 6, the second is 3, the third is 1, and so on. We give each number in CIK a different operation based on a specified Channel of Interest (CoI) or Channel Swapping (CS) operation [60][45] so that the color information in the watermark image could be transformed. The rule of relationship between the value of element of CIK and the color operation as well as the explanation of the operations is also shown in Figure 5.6. Specifically, the CoI operation (CoI_R , CoI_G , or CoI_B) changes the grey scale value of one channel (R, G, or B) of an image and the CS operation (CS_{RG} , CS_{RB} , or CS_{GB}) swaps the grey scale value between two channels (RG, RB, or GB).

Using the CIK generation with related operations, the watermark image $|SW\rangle$ is processed to $|SW'\rangle$ as presented in Figure 5.7(b). It is clear that the color information of image $|SW\rangle$ has been protected, however, the position information is still exposed. A Position Information Key (PIK) will be introduced in the following sub-section which can


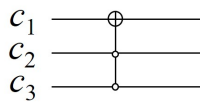

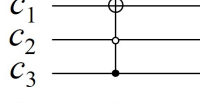

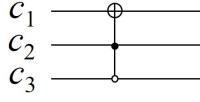

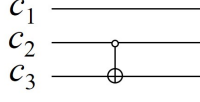

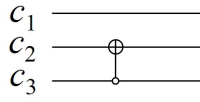

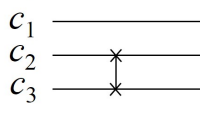

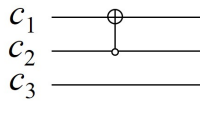

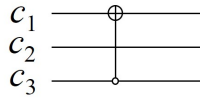
Element of CIK	Color Operation	Color Operation	Explanation	
	0	CoI_R	 c_1 — \oplus — c_2 — \circ — c_3 — \circ —	Invert the greyscale value of R channel
	1	CoI_G	 c_1 — \oplus — c_2 — \circ — c_3 — \bullet —	Invert the greyscale value of G channel
	2	CoI_B	 c_1 — \oplus — c_2 — \bullet — c_3 — \circ —	Invert the greyscale value of B channel
	3	CS_{RG}	 c_1 — \circ — c_2 — \circ — c_3 — \oplus —	Swap the greyscale value of R&G channel
	4	CS_{RB}	 c_1 — \circ — c_2 — \oplus — c_3 — \circ —	Swap the greyscale value of R&B channel
	5	CS_{GB}	 c_1 — \circ — c_2 — \times — c_3 — \times —	Swap the greyscale value of G&B channel
	6	$CoI_R CoI_G$	 c_1 — \oplus — c_2 — \circ — c_3 — \circ —	Invert the greyscale value of R&G channel
	7	$CoI_R CoI_B$	 c_1 — \oplus — c_2 — \circ — c_3 — \circ —	Invert the greyscale value of R&B channel

Figure 5.6: The rule of applying CIK operations.

scramble the position information of $|SW'\rangle$ when it is needed. Such a spatial domain embedding method makes sure that a different key will be updated every time when we produce watermark information, which means the illegal users can only get the image this time even though they steal the key. It is different from the previous research [71], where the key used to scramble the watermark image is fixedly assigned by the copyright owner.

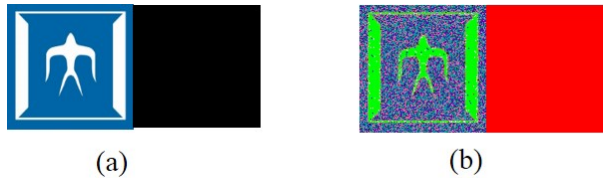


Figure 5.7: (a) Watermark image $|SW\rangle$ and (b) result image $|SW'\rangle$ by applying CIK operations.

5.3.3 Frequency domain embedding and PIK generation

The position information protection method is designed by applying Position Information Key (PIK) on watermark image [71]. Given a image sized by $m \times n$, there are two random permutations denoted by A and B (A and B build up the PIK) with the size of m and n , respectively. The pixel $(A(i),B(j))$ of image $|FW'\rangle$ in Figure 5.4 replaces the pixel at position (i,j) in the same image, where $A(i)$ and $B(j)$ are the i^{th} and j^{th} elements of A and B, respectively. After performing this algorithm on all pixels of image $|FW'\rangle$, the position information of the image is scrambled to produce a meaningless image $|FW''\rangle$ as shown in Figure 5.8(a). In addition, sequel to the discussion about watermark information in spatial domain, image $|SW'\rangle$ can be scrambled again by applying PIK and the result of it, image $|SW''\rangle$, is presented in Figure 5.8(b).

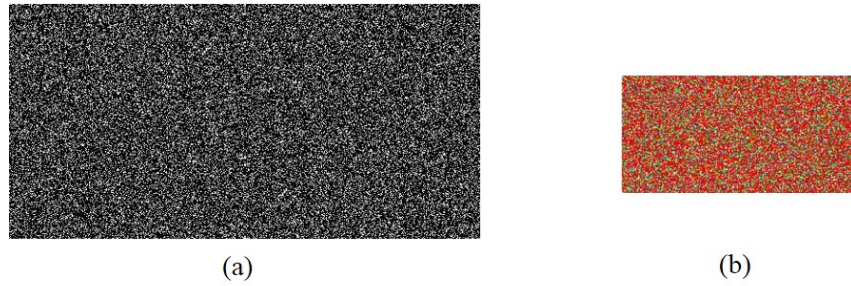


Figure 5.8: (a) Scrambled image $|FW''\rangle$ and (b) scrambled image $|SW''\rangle$.

5.3.4 Embedding and extracting procedure of watermark image

A color image consists of many pixels and the color information of each pixel can be separated into three channels. According to the Equation (5.2), a quantum image can be rewritten as

$$|I(\theta)_{mc}\rangle = \sum_{i=0}^{N-1} (X_R^i|0\rangle + X_G^i|1\rangle + X_B^i|2\rangle + X_O|3\rangle)|i\rangle, \quad (5.3)$$

where i is the position information, N is the number of pixels in the image, X_R^i , X_G^i , and X_B^i are color channel information, and X_O is made to carry no information. The watermark image will be embedded into both frequency domain (QFT coefficients) and spatial domain (RGB channels), so we discuss the embedding and extracting procedure

from these two domains.

1. Embedding procedure:

(1) Embedding in frequency domain. In order to guarantee the pixels' value of the embedded carrier image ($|I'\rangle$) are still real, the revised value of the QFT coefficients should be symmetrical [71]. Suppose the size of carrier image is $m \times n$, the revised value of the QFT coefficients should meet the conditions that $CE_X(i, j) = CE_X(m - 1 - i, n - 1 - j)$, $X \in \{R, G, B, O\}$, where $CE_X(i, j)$ is the revised value of QFT coefficients in X channel of the carrier image. Accordingly, the watermark image $|W\rangle$ to be embedded into the carrier image should also be symmetrical that $W_X(i, j) = W_X(m - 1 - i, n - 1 - j)$. In addition, image $|W\rangle$ used for the embedding in frequency domain should be doubly sized with image $|I\rangle$ because of QFT [64][12], while it used for the embedding in spatial domain should be uniform-sized with image $|I\rangle$ according to MCQI representation, that is the reason why we resized the watermark image $|W\rangle$. The final processed watermark images $|FW'''\rangle$ and $|SW'''\rangle$ are obtained from image $|FW''\rangle$ and $|SW''\rangle$ by symmetrically setting the lower half part of them. The whole procedure of embedding in frequency domain is as:

- preprocessing on watermark image ($W \rightarrow |W\rangle \rightarrow |FW\rangle \rightarrow |FW'\rangle \rightarrow |FW''\rangle \rightarrow |FW'''\rangle$);
- execute QFT on the carrier image and get its QFT coefficients;
- embed each channel of image $|FW'''\rangle$ into each channel of QFT coefficients of image $|I\rangle$ and obtain image $|I'\rangle$. The details about the embedding and extracting in QFT coefficients is thoroughly discussed in [71].

(2) Embedding in spatial domain. As stated in the previous two sub-sections, the whole procedure of embedding in spatial domain is listed as:

- preprocessing on watermark image ($W \rightarrow |W\rangle \rightarrow |SW\rangle \rightarrow |SW'\rangle \rightarrow |SW''\rangle \rightarrow |SW'''\rangle$);
- embed each channel of image $|SW'''\rangle$ into image $|I'\rangle$ to obtain the final watermarked image $|I''\rangle$.

2. Extracting procedure:

As the anti-operation of embedding procedure, we design two kinds of circuits that (F)watermark recovery circuit and (S)watermark recovery circuit as shown in Figure 5.1.

The whole procedure of extracting is presented as:

- recover the watermarked image $|I''\rangle$ to get image $|RFW\rangle$ and image $|I\rangle$ using (F)watermark recovery circuit;
- recover the watermarked image $|I''\rangle$ to get image $|RSW\rangle$ and image $|I\rangle$ using (S)watermark recovery circuit.

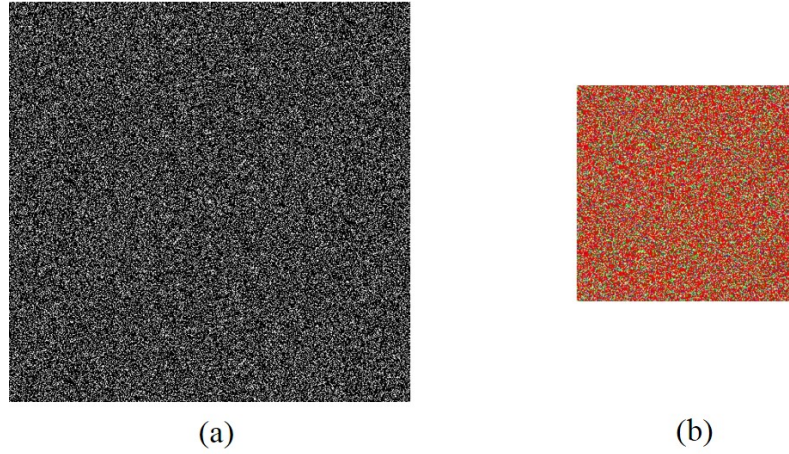


Figure 5.9: (a) Resized image $|FW'''\rangle$ and (b) resized image $|SW'''\rangle$.

5.4 Simulation experiments of watermarking for M-CQI images

The experiments are carried out on a desktop computer with Intel Core i7, 2 Duo 2.80 GHz CPU, 4GB RAM and 64bit operating system. The simulations are based on linear algebra with complex vectors as quantum states and unitary matrices as unitary transforms using QLIB [44][27] (A Matlab package for quantum information). Nine building images are used as carrier image and a Tokyo Tech logo is treated as the watermark image. To evaluate the quality of the embedded images, average RGB Peak Signal-to-Noise

Ratio (RGB-PSNR) [43][1][16] is used, which is defined as

$$PSNR_{RGB} = (PSNR_R + PSNR_G + PSNR_B)/3, \quad (5.4)$$

where

$$PSNR_X = 20 \log_{10} \left(\frac{255}{\sqrt{MSE}} \right), X \in \{R, G, B\}, \quad (5.5)$$

$$MSE = \frac{1}{mn} \sum_{i=0}^{m-1} \sum_{j=0}^{n-1} [I''(i, j) - I(i, j)]^2, \quad (5.6)$$

Here, MSE is the Mean Squared Error between the carrier image $I(i, j)$ and the embedded image $I''(i, j)$, where m and n are the number of pixels in the image. The size of the carrier images in the experiments are all 256×256 as shown in Figure 5.10 and one specific embedding and extracting experiment is presented in Figure 5.11.

5.5 Conclusion

A new Multi-channel Watermarking strategy for Quantum Images (MC-WaQI) is proposed where the double-key and double-domain idea makes the watermarking more secure. The MC-WaQI strategy is designed based on the MCQI representation [60] to represent the watermark image and the carrier image to realize the color quantum image watermarking. The simulation results of the embedding and extracting experiments show that the average RGB-PSNR between each carrier image and its embedded image is bigger than the previous researches. The logo representing the copyright owner can be retrieved by using CIK and PIK, and also the experiment proves that the illegal users are difficult to get or destroy the logo, which further ensures the security of the proposed strategy.

For the future works, on the one hand, we will do the watermarking job to a strip of quantum images instead of one image once using the quantum parallel computing ability, which will significantly increase the efficiency; on the other hand, the MC-WaQI strategy will be used for quantum data protection.



Figure 5.10: All the carrier images in the simulation experiments.

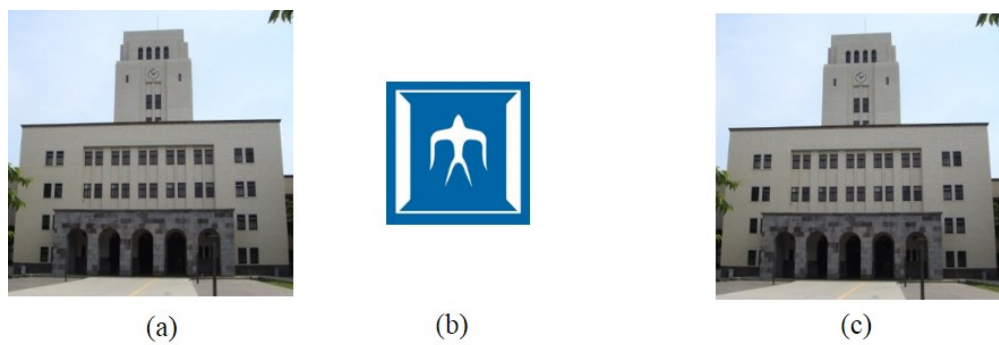


Figure 5.11: (a) The carrier image, (b) watermark image, and (c) watermarked image.

Chapter 6

Bloch sphere based representation for quantum emotion space

6.1 Introduction

Inspired by the research on quantum image processing, we extend our research topic to the emotion space in quantum computing domain. Emotion expression, where an emotion space is always used to represent the emotion in terms of quantitative analysis and visualization, is important to facilitate a smooth communication in face-to-face communication [53][46][66]. In 1997, pleasure-arousal judgment space [53] was proposed as a “psychological judgment space” for affective feelings, in which the two dimensions that are associated with general characters of emotion, represents not only specific emotions but also continuous variations in emotions. Each emotion can be placed in the pleasure-arousal space when the stimuli are translated into appropriate values in the coordinate system. In 2001, a three-dimensional mental space [46] was defined as the mental model of the robot based on the pleasure-arousal space. A certainty axis, which is a continuous value ranging from -1 to +1, was added to this new space to produce smooth and effective communication between humans and robots. Later on, in order to take into account the rapid variations in the mentality state due to real time human-robot interaction, affinity pleasure-arousal space [66], where the affinity axis was used to describe the transition from one mentality state to another according to the progress of the conversation and

repetitive interaction was proposed. The pleasure-displeasure and arousal-sleep axis in the space are related to the favor of the interlocutor and liveliness in communication, respectively.

Most of the emotion space representations and discussions are, however, based on the conventional arithmetic relying purely on the use of mathematical expressions and calculations. Often, it is difficult to visualize the emotion space needed to provide an intuitional impression to the observer and even more complex to find a ‘sensor’ to track the emotional transition. In terms of the development of quantum computation and information, as well as the overwhelming superiority in quantum processing, such as parallel computation and invertible property [49], a quantum emotion space representation is considered to realize more practical and efficient operations. In addition, inspired by the color expression in wheel of emotions [50] and quantum sphere of emotions [52], Bloch Sphere based Emotion Space (BSES) is proposed, where two angles φ ($0 \leq \varphi < 2\pi$) which represents the emotion (such as happiness, surprise, anger, sadness, expectation, and relaxation) and θ ($0 \leq \theta \leq \pi$) which indicates its intensity are determined. The set (φ, θ) , which corresponds to a specific qubit, can be used to express any emotion. Such a representation makes it easy to visualize the emotion space using the saturation and brightness of color information based on the psychological perspective [19][35]. Therefrom, the current status of a human’s emotional state is easily observable. In addition, the emotion space is extended to the quantum computing domain, where the properties of quantum computation could be fully utilized to track human’s emotional transition using quantum gates.

In the experiment, a human’s facial expressions with different emotions are photographed in order to express them in BSES space. According to the intensity of the human emotion, pleasure and arousal are scored by the difference between the same face showing the configuration minus the rating of the same face showing no visible Action Units using FACS [53][18]. The scores are transformed from the two-dimension ‘pleasure-arousal plane’ to the Bloch sphere using the preset formula in order to represent the emotions visually in BSES space.

A Bloch sphere based emotion representation method is proposed in Section 6.2. The quantum emotion and how to generate it from stimulus are introduced in Section 6.3. The experiments to represent and interpret human emotion using the BSES space are presented in Section 6.4.

6.2 Bloch sphere based emotion space

Emotion space is intended to extend to quantum domain so as to realize the quantum affective computing. The qubit and quantum gates are reviewed in this section firstly. In addition, Bloch Sphere based Emotion Space (BSES) which represents human emotion in quantum computing domain is proposed based on the potential relation between the qubit representation and human emotion.

6.2.1 Qubit and human emotion

A quantum computer is a physical machine that can accept input states which represent a coherent superposition of many different inputs and subsequently evolve them into a corresponding superposition of outputs [33]. The smallest unit of information in a quantum system, a qubit, is a unit vector in a two-dimensional Hilbert space that can exist in a superposition state, $|\varphi\rangle = \alpha|0\rangle + \beta|1\rangle$, which is formed by linear combinations of computational basis states $|0\rangle$ and $|1\rangle$, where α and β are complex numbers. It only ever gives ‘0’ or ‘1’ as the measurement result probabilistically when a qubit is measured [49]. These are analogous to the human’s behavior where although there are a number of emotions inside human mind, the final action of them represents only one emotion [52]. Linear operator on a Hilbert space, U_f , which manipulates the qubit is a unitary matrix as $U_f U_f^\dagger = I$, where U_f^\dagger is the Hermitian conjugate or adjoint of U_f . These three matrices are represented as

$$U_f = \begin{pmatrix} a_{00} & a_{01} \\ a_{10} & a_{11} \end{pmatrix}, U_f^\dagger = \begin{pmatrix} a_{00}^* & a_{10}^* \\ a_{01}^* & a_{11}^* \end{pmatrix}, \text{ and } I = \begin{pmatrix} 1 & 0 \\ 0 & 1 \end{pmatrix}, \quad (6.1)$$

where a_{ij}^* is the complex conjugate of a_{ij} , $i, j \in \{0,1\}$ [65]. The unitary transformation U_f possesses the reversibility that enables a transformed qubit state $|f(x)\rangle$ to be recovered from the original state $|x\rangle$ after applying the adjoint matrix as

$$U_f : |x\rangle \rightarrow |f(x)\rangle, U_f^\dagger : |f(x)\rangle \rightarrow |x\rangle. \quad (6.2)$$

In the quantum circuit models of computation, designing efficient circuits is necessary to realize and analyze any quantum algorithm. The main resources that make up these circuits consist of a succession of basic unitary gates that act on one or two qubits only. Many elementary gates including single qubit gates, Pauli gates, Controlled-NOT or CNOT, and Toffoli gates for quantum computation are introduced in [68][67]. These quantum gates are tools to track and recover the human's emotional transition in BSES space.

6.2.2 Representation of BSES space

In the 'pleasure-arousal judgment space' [53], the two-dimensional plane has a pleasure-displeasure axis and an arousal-sleep axis. The cross point is regarded as the neutral expression, and from which the level of happiness will increase along the pleasure direction, and vice versa. On the arousal-sleep axis, the liveliness of a human emotion will become stronger from the cross point along the arousal direction. Based on the discussion above, the four quadrants are settled with 'Excitement', 'Stress', 'Depression', and 'Calm'. These two dimensions represent not only specific emotions but also continuous variations in emotions. Several typical emotions are enumerated as shown in Figure 6.1, the emotion 'Surprise' is taken as an example, which has a higher liveliness, but also owns both possibilities for pleasure and displeasure. In the same way, any emotional stimulus-faces, words, tones of voice, postures, emotion-eliciting situations, and actions can be represented by emotional states in the pleasure-arousal space.

In addition, inspired by the color expression in wheel of emotions [50], a disc with color gradient on the pleasure-arousal plane is adopted to vividly represent the continuously

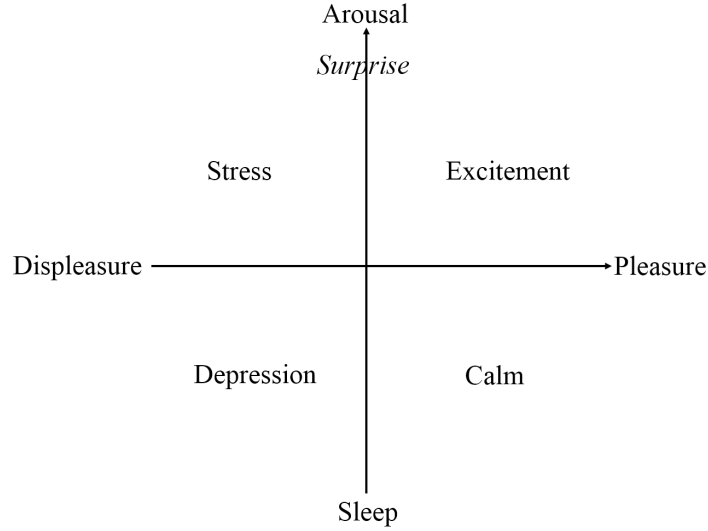


Figure 6.1: *Pleasure-arousal judgment space for affective feelings.*

Table 6.1: *Different emotions expressed by colors [50][19][35].*

Color	Red	Yellow	Green	Blue	Indigo	Purple
Emotion	Anger	Surprise	Happiness	Relaxation	Expectation	Sadness

variable emotions, instead of using the discrete point in the coordinate system, as shown in Figure 6.2. The angle φ ($0 \leq \varphi < 2\pi$) from the pleasure-displeasure axis's positive axis is used to represent the different emotions. The upper bound of the angle φ can be either in each color area or the overlapped parts, which means the angle φ can represent different emotions even a mixture of two emotions. Besides, the saturation of the color from the original point to the edge of the disc is gradually changed in order to take into account the intensity of the current emotion. Based on [50], five representative emotions are selected from the general features in pleasure-arousal space, which are 'Anger', 'Surprise', 'Happiness', 'Relaxation', and 'Sadness', are used to represent basic human emotions. Another emotion, which is supposed to be around the neutral expression, 'Expectation', is made to make a pair with surprise. The color information also corresponds to the selected emotions according to some literature on psychology [50][19][35]. The colors on the disc and the corresponding emotions are presented in Table 6.1.

Additionally, because of the potential relation between the qubit representation and

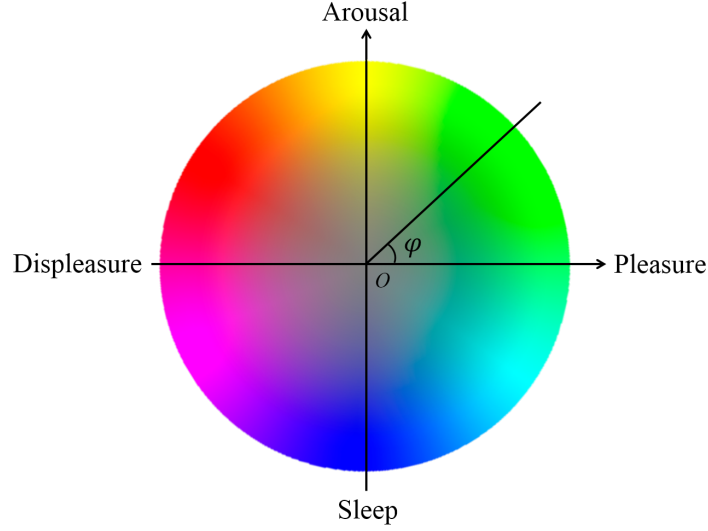


Figure 6.2: *Pleasure-arousal judgment space with continuous color disc for affective feelings.*

human emotion as presented in Section 6.2.1, a qubit is considered to be used to represent human emotion which is defined as the following geometric representation:

$$|\phi\rangle = \cos \frac{\theta}{2} |0\rangle + e^{i\varphi} \sin \frac{\theta}{2} |1\rangle \quad (6.3)$$

where θ and φ are real numbers that define a point on the unit three-dimensional sphere, i.e. Bloch sphere [49] which provides a useful means of visualizing the state of a single qubit, and often gives an excellent foundation for quantum computation and quantum information. It is obvious that we can always find a projection of the point on the sphere surface from equator plane which means the Bloch sphere representation of qubit is appropriate to represent the emotions of human as shown in Figure 6.3.

To construct a model of human emotion in the BSES space, three hypotheses are put forward as follows:

- Each emotion subspace, i.e. the space that each emotion covers follows a Gaussian distribution;
- Each emotion subspace has a limited boundary, and the projections of all subspaces on the ‘equator plane’ are combined to a complete plane;
- The center of each subspace represents its category.

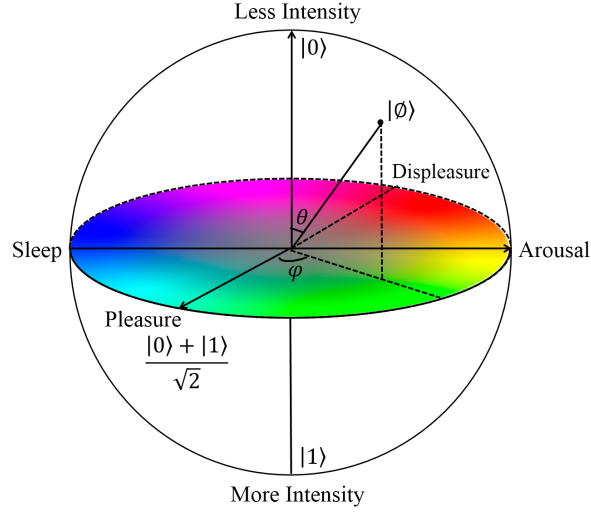


Figure 6.3: Human emotional space expressed using the Bloch sphere.

The angle φ ($0 \leq \varphi < 2\pi$) in the BSES space is used to represent the human emotion, and the angle θ ($0 \leq \theta \leq \pi$) indicates the intensity of the current emotion. Therefore, the set (φ, θ) corresponds to a specific qubit, which can be used to express the human emotion. There are several special cases to represent different emotions as follows:

1. $\theta=0$ represents a neutral emotion, which is useful for the initialization;
2. $\theta=\pi/2$ represents the emotion, which is determined by the angle φ , in mid-level intensity, for example, $(\varphi, \theta)=(3\pi/2, \pi/2)$, on the Bloch sphere represents the mid-level surprise emotional state;
3. $\theta=\pi$ represents all the maximum emotional states.

The BSES space extends emotion space to the quantum computing domain, where the properties of quantum computation could be fully utilized, for example, the quantum gate would be regarded as the emotional transition matrix to track the changes in human emotion.

6.3 Quantum Emotion in BSES space

The notion of Quantum Emotion (QE), which essentially translates the representation of human emotion in terms of the quantum mechanical properties of quantum computa-

tion, is discussed in this section. It is followed by the discussion on how to generate the QE from stimulus such as faces, words, and voice.

6.3.1 Definition of quantum emotion

As we know, human emotion is time-dependent [42]; therefore, the state of the human's Quantum Emotion (QE) is supposed to be a continuous and time-related variable. In other words, at time t , the transfer of the state of the QE is related to the state of the QE at time $t-1$. Because in BSES space, the emotional change can be attributed to the rotation about the y axis and (or) x axis, it is feasible to use a 2×2 unitary matrix, $ET_t(\varphi, \theta)$, which is defined as an emotional transition matrix, to track the process. Therefore, QE can be defined as

$$|QE(t)\rangle = \begin{cases} \cos \frac{\theta}{2}|0\rangle + e^{i\varphi} \sin \frac{\theta}{2}|1\rangle, & t = 1 \\ ET_t(\varphi, \theta)|QE(t-1)\rangle, & t = 2, 3, \dots, m \end{cases} \quad (6.4)$$

where φ is the current human emotion, and θ is its intensity, $|QE(t-1)\rangle$ is the quantum emotion at time $t-1$, $ET_t(\varphi, \theta)$ is the emotional transition matrix which plays a significant role in transmitting the emotion from time $t-1$ to time t .

In line with the frequently used quantum gates in quantum computation as reviewed in Section 6.2.1, several special emotional transition matrixes to track the human's emotional change are listed as below:

1. ETZ corresponding to $Z \equiv \begin{pmatrix} 1 & 0 \\ 0 & -1 \end{pmatrix}$, which leaves the state $|0\rangle$ unchanged, and flips the sign of $|1\rangle$ to give $-|1\rangle$, changes the emotion completely, but the intensity is unchanged;
2. ETX corresponding to $X \equiv \begin{pmatrix} 0 & 1 \\ 1 & 0 \end{pmatrix}$, which transforms the emotion state to a new one where role of $|0\rangle$ and $|1\rangle$ have been interchanged, changes the intensity to the inversed corresponding position, but doesn't change the current emotion;

Table 6.2: Quantum emotion scores for single Action Units adapted from [53].

AU	FACS Name	(Pleasure, Arousal)	$QE(\varphi, \theta)$
1	Inner brow raised	(-1.92, -0.85)	(3.56, 1.16)
2	Outer brow raised	(1.85, 2.11)	(0.85, 1.56)
4	Brow furrowed	(-2.00, 1.23)	(2.59, 1.30)
5	Upper eyelid raised	(-1.19, 3.04)	(1.94, 1.81)
6	Cheek raised	(1.46, 0.73)	(0.46, 0.91)
7	Lower eyelid raised	(-1.85, 0.58)	(2.84, 1.08)
9	Nose wrinkled	(-2.33, 2.33)	(2.35, 1.83)
10	Upper lip raised	(-3.67, 1.97)	(2.65, 2.31)
15	Lip corner depressed	(-2.26, -0.63)	(3.41, 1.30)
17	Chin raised	(-0.93, 0.60)	(2.57, 0.61)
46	Wink	(1.19, 0.54)	(0.43, 0.72)

3. *ETH* corresponding to $H \equiv 1/\sqrt{2} \begin{pmatrix} 1 & 1 \\ 1 & -1 \end{pmatrix}$, makes the emotion do a rotation of the sphere about the y axis by 90° , followed by a 180° rotation about the x axis.

Human emotion is constantly changing as the time goes by, compared to the initial state, therefore, we can compute the Emotional Transition matrix (ET) from the quantum emotion at time t . ET is an important parameter to describing the tendency and magnitude of changes in a human's emotional state. For example, how much extent one person changes his emotion from happiness to sadness. Because $ET_t(\varphi, \theta)$ is a unitary matrix in the definition of quantum emotion $|QE(t)\rangle = ET_t(\varphi, \theta)|QE(t-1)\rangle$, we can use its adjoint matrix, ET^\dagger , to recover the current emotion $|QE(t)\rangle$ to the proceeding state $|QE(t-1)\rangle$ for some special issues.

6.3.2 Generation of quantum emotion

The representation of BSES space, where humans' multifarious emotions are expressed using a Bloch sphere and the quantum emotion generated in such a space were introduced earlier. The next question should be 'How to generate the emotions in BSES space' from the emotion stimulus. Several stimuli such as faces, words, voice, and postures are usually used for the analysis of human emotion. In this chapter, we will only focus on how to translate the emotion to the 'pleasure-arousal plane' from the facial movement using Facial Action Coding System (FACS) [18]. FACS is a system to taxonomize human facial movements by their appearance on the face that defines the Action Units (AUs), which are contractions or relaxations of one or more facial muscles. Pleasure and arousal scores for single Action Units are evaluated by values are those obtained from a face with the Action Unit minus the same face with no Action Unit [53]. Each scale is numbered from 1 to 9. Thus, the potential range of the difference would be from -8 to +8. In practice, the neutral face falls near the middle of the scale; thus, the effective range of the difference is from -4 to +4. In order to match the standard of pleasure and arousal scores, the radius of the Bloch sphere is set to be 4.

According to the coordinate system conversions from the Cartesian coordinate to spherical coordinate system, the emotion, φ , is determined using anti-trigonometric function calculation. The intensity of this emotion, θ , is decided based on the distance from the original point to the projection of the current emotion in the pleasure-arousal plane. The coordinate transformation from the two-dimensional 'pleasure-arousal plane' to the BSES space is stated as

$$\varphi = \arctan y/x \quad (6.5)$$

$$\theta = \pi/4\sqrt{2}\sqrt{x^2 + y^2} \quad (6.6)$$

where x is the length from the original point to the projection of QE on the pleasure-displeasure axis; y is the length from the original point to the projection of QE on the arousal-sleep axis. The value of φ and θ could also be adjusted in depending on which quadrant the point is located. Therefore, we can express the information of any particular

emotion in BSES space. The process of generating human emotion in BSES space is shown in Figure 6.4.

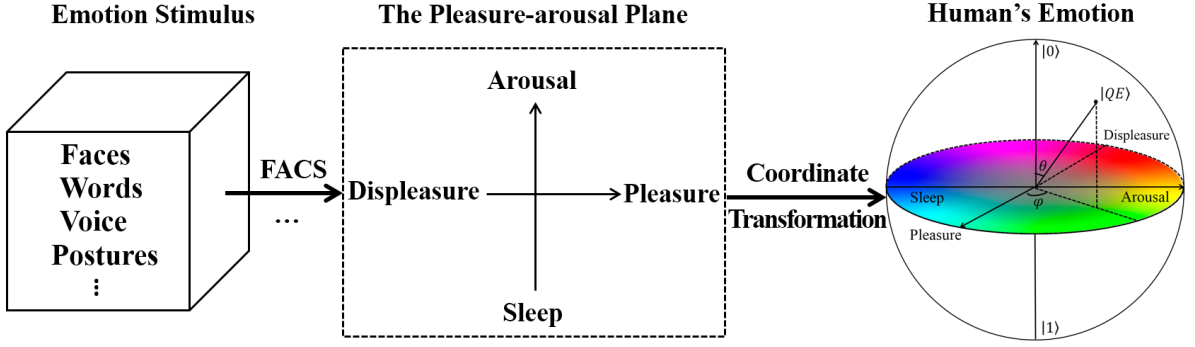


Figure 6.4: Generation of human emotion in BSES space.

Some representative facial features which are attributed to different AUs are shown in Table 6.2. FACS name represents the emotional description of AU. The pleasure and arousal are evaluated and scored from [53], while the quantum emotion transformed from that is shown as $QE(\varphi, \theta)$.

6.4 Experiment of representing human emotion in BSES space

In the experiment, a person's faces with different expression are photographed while the subject's expression is changing, which are used for the analysis and representation using the Bloch sphere based emotion spaces. We focus on the subject's initial and final emotional state (happiness and sadness, respectively), from which the emotional transition matrix is analyzed for tracking the tendency and magnitude of his emotional change. The basic emotions are presented as the combination of the Action Units according to the emotional FACS. The intensities of FACS are annotated by appending letters A-E (for minimal-maximal intensity) to the Action Unit number in order to represent the intensity of movements of individual facial muscles, i.e. A (Trace), B (Slight), C (Marked or Pronounced), D (Severe or Extreme), and E (Maximum) [18].

Referring to the description of emotional features in FACS, we assign the two emotions

Table 6.3: Quantum emotion scores for the two emotions in Figures 6.5 and 6.6.

Emotion	Description of emotional features	(Pleasure, Arousal)	$QE(\varphi, \theta)$
Happiness (AU6C + AU12D)	Cheek raised (Marked) + Lip Corner puller (Severe)	(3.23, 2.18)	(0.42, 2.16)
Sadness (AU1B + AU4B + AU15D)	Inner brow raised (Slight) and furrowed (Slight) + Lip corner depressed (Severe)	(-2.76, 0.31)	(3.03, 1.54)

in Figures 6.5 and 6.6 AU expressions with appropriate intensities. Based on the principle of scoring emotions in [53] and [18], where pleasure and arousal are scored by the difference between the face showing the configuration minus the rating of the same face showing no visible Action Units using FACS, we evaluate the pleasure and arousal scores of the two current emotions in the two-dimensional ‘pleasure-arousal plane’. Then, the scores are transformed from the two-dimensional plane to the BSES space using the preset Equations (6.5) and (6.6). The emotion, description of emotional features, and the coordinate value for ‘pleasure-arousal plane’ as well as BSES space are presented in Table 6.3.

The initial quantum emotion state $|QE(1)\rangle$ (happiness) and the final quantum emotional state $|QE(t)\rangle$ (sadness) are presented using BSES space in Figures 6.5 and 6.6 based on the QE values in Table 6.3, respectively. The state of quantum system is usually described as a vector in a Hilbert space in quantum mechanical notation as reviewed in Section 6.2.1. Therefore, the initial quantum emotion is presented as

$$|QE(1)\rangle = \cos \frac{\theta_1}{2} |0\rangle + e^{i\varphi_1} \sin \frac{\theta_1}{2} |1\rangle = \begin{pmatrix} 0.47 \\ 0.8 + 0.36i \end{pmatrix} \quad (6.7)$$

from which, we represent the final state as

$$|QE(t)\rangle = \cos \frac{\theta_t}{2} |0\rangle + e^{i\varphi_t} \sin \frac{\theta_t}{2} |1\rangle = \begin{pmatrix} 0.72 \\ -0.69 + 0.08i \end{pmatrix} \quad (6.8)$$

where θ_1 , θ_t , φ_1 , and φ_t are human emotions and their intensities in initial and final state

as listed in Table 6.3, which has an almost exact match to the emotion distribution as presented earlier in Figure 6.1. The happiness (AU6C + AU12D) occurs in our pleasure and arousal space when pleasure is high and arousal slightly above neutral. Sadness (AU1B + AU4B + AU15D) coincides with low pleasure and slightly raised arousal [24].

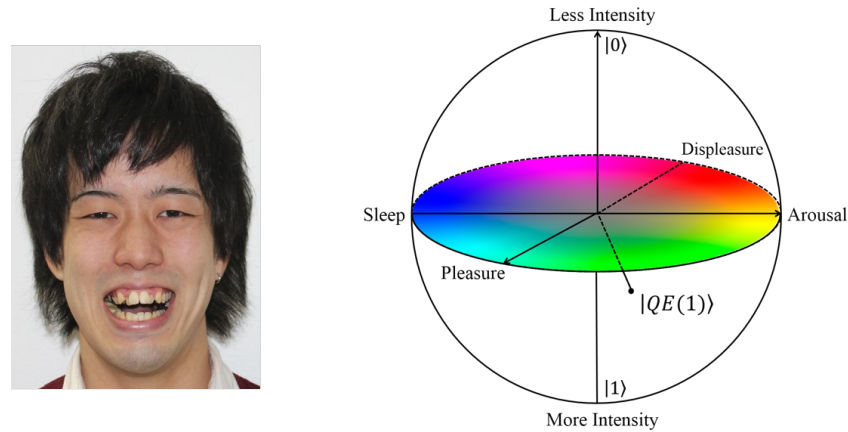


Figure 6.5: ‘Happy’ emotion and its representation in the BSES space.

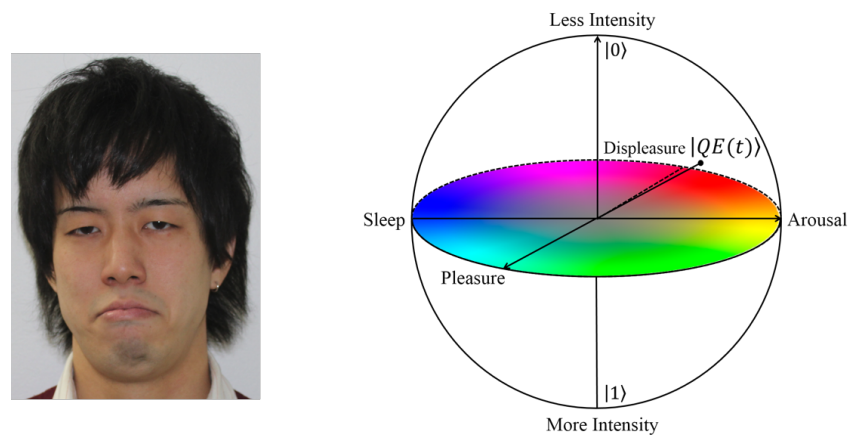


Figure 6.6: ‘Sad’ emotion and its representation in the BSES space.

As discussed earlier, the emotion is transmitted from happiness to sadness. From the representation of current emotion in BSES space, it is found that the current emotion represents an overlap between the angry and sadness emotions, which indicates that the person is sad with traces of anger at that particular instant. This further suggests that using angle with color information to represent the emotion and intensity, and make them relatively independent would make the emotional analysis more flexible and visible.

Finally, we are supposed to find the emotional transition matrix to track such an emotional change. According to the definition of QE , the emotional transition matrix is presented as

$$ET_t(\varphi, \theta) = f(|QE(1)\rangle, |QE(t)\rangle) = \begin{pmatrix} 1.53 & 0 \\ -1.84 & 0.22 \end{pmatrix} \quad (6.9)$$

The emotional transition matrix could be regarded as a ‘sensor’ to trace human’s emotional change, which could be also applied on the human-robot interaction scenario in order to make the robot adaptive to the human emotion. In addition, using the adjoint matrix of ET , i.e. ET^\dagger , to make the robot responsive to the human emotion.

6.5 Conclusion

A Bloch Sphere based Emotion Space (BSES) is proposed to extend the representation of human emotion space to the quantum computing domain wherein the color information is used to visualize the emotion and quantum gates are applied as emotional transition matrix to track the changes in emotion. A human emotion with happiness and sadness are analyzed via FACS and scored according to the preset emotional transmission model in the experiment. The emotions are visually presented in BSES space respectively, where the current emotion and its intensity are totally expressed. An emotional transition matrix is used to track the changes from the initial through to the final emotion states in order to account for how the emotion changed.

As for future work, the results in this chapter will be extended to the application on the human-robot interaction. The BSES space presented in this proposal could also be used to represent a robot’s emotion. The emotional transition matrix that tracks the human’s emotional change could then be used to control robots after they are initialized. Besides the adaptability, the adjoint matrix of emotional transition matrix could be used to make the robot responsive to the human emotion, for example, the robot could be used to cheer the human up when (s)he is upset. Another direction that the proposal could be extended is its integration into the fuzzy atmosfield [42], to capture the emotional atmosphere among multiple human beings. Here, the quantum mechanical properties

of superposition and entanglement could be used to fuse multiple human emotions, and better express the atmosfield model in order to make the robots more responsive to the choice of appropriate operations to suit the atmosphere.

Chapter 7

Conclusions

The number of transistors on integrated circuits doubles approximately every eighteen months, which makes the components inside our calculation devices are becoming smaller and more sophisticated. At a certain level of this process, another kind of computing machine will undoubtedly appear to replace the current classical computer, which is supposed to be quantum computer according to its powerful computing capacity. ‘Quantum computers have the potential to solve problems that would take a classical computer longer than the age of the universe,’ Professor David Deutsch said. Throughout the history of quantum computer development, so many institutes and enterprises are focusing on the quantum algorithms and application-specific quantum computing hardware. Specifically, a 512-qubit quantum computing system was born in 2012, which is proved that the amazing computation speed and superiority to solve problems in comparison with the same task on the conventional machines.

Different from the quantum computing hardware realization, our research is focused on what we can do if the quantum computer is completed. In the thesis, we proposed the quantum computation based image data searching, image watermarking, and representation of emotion space. The research started with the review of a Flexible Representation of Quantum Images (FRQI) which captures and stores two fundamental information about the color and position of every point in an images as a normalized quantum state and its related transformations on the position and color information as presented in Chapter 2. The transformations serve as foundation blocks for algorithms that would facilitate

higher-level quantum image processing applications. Exploiting the flexible features of the FRQI representation and transformations on it, a method to compare multiple pairs of quantum images in parallel, where the similarities of the images are estimated according to the probability distributions of the readouts from quantum measurements, is proposed in Chapter 3 that offers a significant speed-up in comparison to performing the same task on traditional computing devices by means of a single Hadamard gate with control-conditions to transform the entire information encoding the quantum images in a strip. Three simulation-based experiments are implemented using Matlab on a classical computer by means of linear algebra with complex vectors as quantum states and unitary matrices as unitary transformations provide a reasonable estimation to the image comparison. The comparison between two arbitrary FRQI images in the strip and the comparison between the sub-blocks from two different images can be realized by utilizing appropriate geometric transformation operations on the strip wires as well as the required control conditions to the position wires. On the basis of such a quantum image comparison strategy, a quantum image searching method is proposed in Chapter 4 which is achieved by using low computational resources which are only a single Hadamard gate combined with $m + 1$ quantum measurement operations. A simulation experiment is performed to search for a target image from an original database comprising of sixty-four binary images. According to the readouts from the measurements, the similarity of each pair between the test image and the images in the database is calculated. It is concluded that the more images in the database, the better the ability of the proposed method. This is because m qubits on the strip wires can represent 2^m quantum images in the Z-strip, and only one qubit on the Z-axis can represent the images on both the left and right side of Z-strip. As an extension of FRQI representation, and in order to protect the quantum image information, a new Multi-Channel Watermarking strategy for Quantum Images (MC-WaQI) is proposed where the double-key and double-domain idea makes the watermarking more secure. The simulation results of the embedding and extracting experiments show that the average RGB-PSNR between each carrier image and its embedded image is bigger than the previous researches. Inspired by the research on quantum image processing, we

attempt to extend the representation of emotion space to quantum computing domain. In Chapter 5, a Bloch Sphere based Emotion Space (BSES) is proposed wherein the color information is used to visualize the emotion and quantum gates are applied as emotional transition matrix to track the changes in emotion. A human emotion with happiness and sadness are analyzed via FACS and scored according to the preset emotional transmission model in the experiment. The emotions are visually presented in BSES space with both the current emotion and its intensity being totally expressed. An emotional transition matrix is used to track the changes from the initial through to the final emotion states in order to account for how the emotion changed. Overall, our proposals in the thesis to encode the images and various algorithmic frameworks together with the extensions that are suggested in the various chapters provide the road-map towards the realization of secure and efficient image and emotion-related processing on quantum computers.

As discussed in the thesis, we focus on the quantum computation based image data searching, image watermarking, and representation of emotion space. New applications and extensions can be discovered by new contributions in each of the three components. Therefore, the research can be extended to the following directions:

- The proposal in Chapters 3 and 4 will be applied on designing a search engine on such quantum computing devices that the image in the database is retrieved based on its similarity to the test image. Most of the search engines recently are realizing the data searching only based on the text. Even though some of them are developed based on the content of the images, it is usually time-consuming though. These proposals give a basic step for the quantum image searching especially when a database comprising of a huge amount of data is confronted, because the searching is based on the content of the images and executed in parallel.
- The watermarking strategy proposed in Chapter 5 will be improved to deal with a strip of quantum images simultaneously instead of one image once using the quantum parallel computing ability, which will significantly increase the efficiency of processing. What's more, the MC-WaQI strategy will be used for the protection of quantum data transmission and processing.

- The results in Chapter 6 will be extended to the application on the human-robot interaction. The emotional transition matrix that tracks the human's emotional change could be used to control robots and the adjoint matrix of it could be used to make the robot more responsive to the human emotion. In addition, the integration of the proposed idea into the fuzzy atmosfield to capture the emotional atmosphere among multiple human beings is also a good research topic. The quantum mechanical properties of superposition and entanglement could be used to fuse multiple human emotions to better express the atmosfield model so that the robots are more responsive to the choice of appropriate operations to suit the atmosphere.

Quantum computing research still has a long way to go, therefore, more researches in quantum image processing and other various related fields are necessary to be thoroughly studied for the preparation of our next generation computing devices.

Bibliography

- [1] A. Al-Nu'aimi and R. Qahwaji. Robust self embedding watermarking technique in the dwt domain for digital colored images. *Journal of Digital Information Management*, 5(4):211–219, 2007.
- [2] J. Anders, D. Oi, K. Kashefi, B. D.E., and A. E. Ancilla-driven universal quantum computation. *Physical Review A*, 82(020301), 2010.
- [3] A. Barenco, C. Bennett, R. Cleve, D. Divincenzo, N. Margolus, P. Shor, T. Sleator, J. Smolin, and H. Weinfurter. Elementary gates for quantum computation. *Physical Review A*, 52(5):3457–3467, 1995.
- [4] G. Beach, C. Lomont, and C. Cohen. Quantum image processing (quip). In *Proceedings of the 32nd Applied Imagery Pattern Recognition Workshop*, pages 39–44, 2003.
- [5] R. Bennink, S. Bentley, and R. Boyd. Quantum and classical coincidence imaging. *Physical Review Letters*, 92(6):1–4, 2004.
- [6] T. Beth and M. Rotteler. Quantum algorithms: applicable algebra and quantum physics. *Springer Tracts in Modern Physics*, 173:96–150, 2001.
- [7] E. Biham, G. Brassard, D. Kenigsberg, and T. Mor. Quantum computing without entanglement. *Theoretical Computer Science*, 320(1):15–33, 2004.

-
- [8] A. Broadbent and E. Kashefi. Parallelizing quantum circuits. *Theoretical Computer Science*, 410(26):2489–2510, 2009.
- [9] S. Caraiman and V. Manta. New applications of quantum algorithm to computer graphics the quantum random sample consensus algorithm. In *Proceedings of the 6th ACM conference on Computing frontiers*, pages 81–88, 2009.
- [10] A. Childs, D. Leung, and M. Nielsen. Unified derivations of measurement-based schemes for quantum computation. *Physical Review A*, 71(3):1–14, 2005.
- [11] J. M. Chow, A. D. Corcoles, J. M. Gambetta, C. Rigetti, B. Johnson, J. Smolin, S. Merkel, S. Poletto, J. Rozen, R. M.B., G. Keefe, M. Ketchen, and M. Steffen. High-fidelity gates towards a scalable super-conducting quantum processor. In *American Physical Society*, 2012.
- [12] R. Cleve and J. Watrous. Fast parallel circuits for the quantum fourier transform. In *Proceedings of 41st Annual Symposium on Foundations of Computer Science*, pages 526–536, 2000.
- [13] D. Cory, R. Laflamme, E. Knill, L. Viola, T. Havel, N. Boulant, G. Boutis, E. Fortunato, S. Lloyd, R. Martinez, C. Negrevergne, M. Pravia, Y. Sharf, G. Teklemariam, Y. Weinstein, and W. Zurek. Nmr based quantum information processing: achievements and prospects. *Fortschritte der Physik*, 48(9-11):875–907, 2000.
- [14] D. Curtis and D. Meyer. Towards quantum template matching. *Proceedings of the SPIE*, 5161:134–141, 2004.
- [15] W. Debbie. Quantum computation by measurement. *International Journal of Quantum Information (IJQI)*, 2(1):33–43, 2004.
- [16] F. Di Martino, V. Loia, and S. Sessa. Direct and inverse fuzzy transforms for coding/decoding color images in yuv space. *Journal of Uncertain Systems*, 3(1):11–30, 2009.

-
- [17] J. Dodd, T. Ralph, and G. Milburn. Experimental requirements for grover's algorithm in optical computing. *Physical Review A*, 68(4):1–8, 2003.
- [18] P. Ekman, W. Friesen, and J. Hager. *Facial Action Coding System*. A Human Face: Salt Lake City, USA, 2002.
- [19] Eric, John, and Paraag. *Color psychology*. <http://library.thinkquest.org/27066/psychology/nlcolorpsych.html>, 2007.
- [20] R. Feynman. Simulating physics with computers. *International journal of theoretical physics*, 21(6-7):467–488, 1982.
- [21] A. Fijany and C. Williams. Quantum wavelet transforms fast algorithms and complete circuits. *Lecture Notes in Computer Science*, 1509:10–33, 1999.
- [22] M. Gabriella. Hiding data in a qimage file. *International Journal of Multimedia and Ubiquitous Engineering (IJMUE)*, 4(2):13–19, 2005.
- [23] J. Gea-Banacloche. Hiding messages in quantum data. *Journal of Mathematical Physics*, 43(4531):4531–4536, 2002.
- [24] K. Grammer and E. Oberzaucher. The reconstruction of facial expression in embodied systems new approaches to an old problem. *ZIF Mitteilungen*, 2:14–31, 2006.
- [25] L. Grover. A fast quantum mechanical algorithm for database search. In *Proceedings of the 28th Annual ACM Symposium on Theory of Computing*, pages 212–219, 1996.
- [26] L. Grover. Quantum mechanics helps in searching for a needle in a haystack. *Physical Review Letters*, 79(2):325–328, 1997.
- [27] K. Heylen and T. Dams. An image watermarking tutorial tool using matlab. In *Proceeding of the SPIE*, volume 7075, 2008.
- [28] A. Ilyasu. Towards realising secure and efficient image and video processing applications on quantum computers. *Entropy*, 15:2874–2974, 2013.

-
- [29] A. Ilyasu, P. Le, F. Dong, and K. Hirota. Watermarking and authentication of quantum images based on restricted geometric transformations. *Information Sciences*, 9(6):1459–1497, 2011.
- [30] A. Ilyasu, P. Le, D. F., and K. Hirota. Restricted geometric transformations and their applications for quantum image watermarking and authentication. In *Proceeding of the 10th Asian Conference on Quantum Information Sciences (AQIS 2010)*, pages 96–97, 2010.
- [31] A. Ilyasu, P. Le, F. Yan, B. Sun, J. Garcia, F. Dong, and K. Hirota. Insights into the viability of using available photonic quantum technologies for efficient image and video processing applications. *International Journal of Unconventional Computing*, 9(1-2):125–151, 2013.
- [32] A. Ilyasu, P. Le, F. Yan, B. Sun, J. Garcia, F. Dong, and K. Hirota. A two-tier scheme for greyscale quantum image watermarking and recovery. *International Journal of Innovative Computing and Applications*, 5(2):85–101, 2013.
- [33] A. M. Ilyasu, P. Q. Le, F. Dong, and K. Hirota. A framework for representing and producing movies on quantum computers. *International Journal of Quantum Information*, 9(6):1459–1497, 2011.
- [34] M. Inoue. On the need for annotation-based image retrieval. In *Proceedings of the ACM-SIGIR Workshop on Information Retrieval in Context*, pages 44–46, 2004.
- [35] D. Johnson. *Color psychology*. <http://infoplease.com/spot/colors1.html>, 2007.
- [36] J. I. Latorre. *Image compression and entanglement*. arXiv: quant-ph/0510031, 2005.
- [37] P. Le, F. Dong, and K. Hirota. A flexible representation of quantum images for polynomial preparation, image compression, and processing operations. *Quantum Information Processing*, 10(1):63–84, 2011.
- [38] P. Le, A. Ilyasu, F. Dong, and K. Hirota. Fast geometric transformations on quantum images. *IAENG International Journal of Applied Mathematics*, 40(3):113–123, 2010.

-
- [39] P. Le, A. Ilyasu, F. Dong, and K. Hirota. Efficient colour transformations on quantum image. *Journal of Advanced Computational Intelligence and Intelligent Informatics*, 15(6):698–706, 2011.
- [40] P. Le, A. Ilyasu, F. Dong, and K. Hirota. Strategies for designing geometric transformations on quantum images. *Theoretical Computer Science*, 412(15):1406–1418, 2011.
- [41] P. Le, A. M. Ilyasu, F. Dong, and K. Hirota. A flexible representation and invertible transformations for images on quantum computers. *New Advances in Intelligent Signal Processing: Studies in Computational Intelligence*, 372:179–202, 2011.
- [42] Z. Liu, M. Wu, D. Li, L. Chen, F. Dong, Y. Yamazaki, and K. Hirota. Concept of fuzzy atmosfield for representing communication atmosphere and its application to humans-robots interaction. *Journal of Advanced Computational Intelligence and Intelligent Informatics*, 17(1):3–17, 2012.
- [43] F. Luthon, B. Beaumesnil, and N. Dubois. Lux color transform for mosaic image rendering. In *IEEE International Conference on Automation Quality and Testing Robotics (AQTR)*, volume 3, pages 1–6, 2010.
- [44] S. Machnes. *QLib-A Matlab Package for Quantum Information Theory Calculations with applications*. arXiv:0708.0478, 2007.
- [45] S. Maity and M. Kundu. Perceptually adaptive spread transform image watermarking scheme using hadamard transform. *Information Sciences*, 181(3):450–465, 2011.
- [46] H. Miwa, T. Umetsu, A. Takanishi, and H. Takanobu. Robot personality based on the equations of emotion defined in the 3d mental space. In *Proceedings of the 2001 IEEE International Conference on Robotics & Automation*, pages 2602–2607, 2001.
- [47] C. Moore and M. Nilsson. Parallel quantum computation and quantum codes. *SIAM Journal on Computing*, 31(3):799–815, 2001.

-
- [48] M. Nagy and S. Akl. Quantum computation and quantum information. *International Journal of Parallel, Emergent and Distributed Systems*, 21(1):1–59, 2006.
- [49] M. Nielsen and I. Chuang. *Quantum computation and quantum information*. Cambridge University Press, United Kingdom, 2000.
- [50] R. Plutchik. *Plutchik's wheel of emotions*. <http://www.fractal.org/Bewustzijns-Besturings-Model/Nature-of-emotions.htm>, 1980.
- [51] A. Politi, J. Matthews, and J. O'Brien. Shor's quantum factoring algorithm on a photonic chip. *Science*, 325(5945):1221–1222, 2009.
- [52] A. Raghuvanshi and M. Perkowski. Fuzzy quantum circuits to model emotional behaviors of humanoid robots. In *IEEE Congress on Evolutionary Computation (CEC)*, pages 1–8, 2010.
- [53] J. Russell and J. Fernandez-Dols. *Reading emotion from and into faces, The Psychology of Facial Expression*. Cambridge University Press, United Kingdom, 1997.
- [54] C. R.V., D. Lakshmi, and K. Sunitha. Image searching based on image mean distance method. In *2012 International Conference on Radar, Communication and Computing (ICRCC)*, pages 199–201, 2012.
- [55] T. Schenkel, C. Lo, C. Weis, A. Schuh, A. Persaud, and J. Bokor. Critical issues in the formation of quantum computer test structures by ion implantation. *Nuclear Instruments and Methods in Physics Research Section B: Beam Interactions with Materials and Atoms*, 267(16):2563–2566, 2009.
- [56] P. Shor. Algorithms for quantum computation: discrete logarithms and factoring. In *Proceedings of the 35th Annual Symposium on Foundations of Computer Science*, pages 124–134, 1994.
- [57] B. Sun, A. Iliyasa, Y. F., J. Garcia, D. F., A. Al-Asmari, and K. Hirota. Quantum computation based color information transformation on multi-channel image. In *The*

-
- Ninth China-Japan International Workshop on Information Technology and Control Applications*, pages 19–26, 2013.
- [58] B. Sun, A. Ilyasu, Y. F., J. Garcia, D. F., A. Al-Asmari, and K. Hirota. Multi-channel information operations on quantum images. *Journal of Advanced Computational Intelligence and Intelligent Informatics*, 18(4), 2014.
- [59] B. Sun, A. Ilyasu, F. Yan, F. Dong, and K. Hirota. An rgb multi-channel representation for images on quantum computers. *Journal of Advanced Computational Intelligence and Intelligent Informatics*, 17(3):404–417, 2013.
- [60] B. Sun, P. Le, A. Ilyasu, Y. F., J. Garcia, D. F., and K. Hirota. A multi-channel representation for images on quantum computers using the rgba color space. In *IEEE 7th International Symposium on Intelligent Signal Processing (WISP)*, pages 1–6, 2011.
- [61] H. Tsai and L. Chang. Secure reversible visible image watermarking with authentication. *Journal of Image Communication*, 25(1):10–17, 2010.
- [62] S. Venegas-Andraca and J. Ball. Processing images in entangled quantum systems. *Quantum Information Processing*, 9(1):1–11, 2010.
- [63] S. Venegas-Andraca and S. Bose. Storing, processing and retrieving an image using quantum mechanics. In *Proceedings of SPIE Conference of Quantum Information and Computation*, volume 5105, pages 134–147, 2003.
- [64] Y. Weinstein, M. Pravia, E. Fortunato, S. Lloyd, and D. Cory. Implementation of the quantum fourier transform. *Implementation of quantum fourier transform*, 86(9):1889–1891, 2001.
- [65] P. Xia. Quantum computing. *Journal of computer research and development*, 38(10):1153–1171, 2001.
- [66] Y. Yamazaki, Y. Hatakeyama, F. Dong, K. Nomoto, and K. Hirota. Fuzzy inference based mentality expression for eye robot in affinity pleasure-arousal space. *Journal*

-
- of *Advanced Computational Intelligence and Intelligent Informatics*, 12(3):304–313, 2008.
- [67] F. Yan, A. Ilyasu, C. Fatichah, M. Tangel, J. Betancourt, F. Dong, and K. Hirota. Quantum image searching based on probability distributions. *Journal of Quantum Information Science*, 2(3):55–60, 2012.
- [68] F. Yan, A. Ilyasu, P. Le, B. Sun, F. Dong, and K. Hirota. A parallel comparison of multiple pairs of images on quantum computers. *International Journal of Innovative Computing and Applications*, 5(4):1–26, 2014.
- [69] F. Yan, P. Le, A. Ilyasu, B. Sun, J. Garcia, F. Dong, and K. Hirota. Assessing the similarity of quantum images based on probability measurements. In *IEEE Congress on Evolutionary Computation (CEC)*, pages 1–6, 2012.
- [70] F. Zhang, X. Zhang, and H. Zhang. Digital image watermarking capacity and detection error rate. *Pattern Recognition Letters*, 28:1–10, 2008.
- [71] W. Zhang, F. Gao, B. Liu, Q. Wen, and H. Chen. A watermark strategy for quantum images based on quantum fourier transform. *Quantum Information Processing*, 12(2):793–803, 2013.

Related Publications

- **Journal Papers**

- J1** Fei Yan, Abdullah M. Ilyasu, Phuc Q. Le, Bo Sun, Fangyan Dong, and Kaoru Hirota, A parallel comparison of multiple pairs of images on quantum computers. *International Journal of Innovative Computing and Applications*, 5(4), 2014.
- J2** Fei Yan, Abdullah M. Ilyasu, Chastine Fatichah, Martin L. Tangel, Janet P. Betancourt, Fangyan Dong, and Kaoru Hirota, Quantum image searching based on probability distributions. *Journal of Quantum Information Science*, 2(3):55-60, 2012.
- J3** Fei Yan, Bo Sun, Abdullah M. Ilyasu, Phuc Q. Le, Fangyan Dong, and Kaoru Hirota, A double-key, double-domain watermarking strategy for multi-channel quantum images. *Quantum Information Processing, In Preparation*.
- J4** Fei Yan, Abdullah M. Ilyasu, Zhentao Liu, Janet P. Betancourt, Fangyan Dong, and Kaoru Hirota, Representation for quantum emotion space using Bloch sphere. *Journal of Advanced Computational Intelligence and Intelligent Informatics, Under review*.
- J5** Abdullah M. Ilyasu, Phuc Q. Le, Fei Yan, Bo Sun, Adrian S. Garcia, Fangyan Dong, and Kaoru Hirota, Insights into the viability of using available photonic quantum technologies for efficient image and video processing applications, *International Journal of Unconventional Computing*, 9(1-2):125-151, 2013.

- J6** Abdullah M. Ilyasu, Phuc Q. Le, **Fei Yan**, Bo Sun, Adrian S. Garcia, Fangyan Dong, and Kaoru Hirota, A two-tier scheme for greyscale quantum image watermarking and recovery, *International Journal of Innovative Computing and Applications*, 5(2):85-101, 2013.
- J7** Bo Sun, Abdullah M. Ilyasu, **Fei Yan**, Fangyan Dong, and Kaoru Hirota, An RGB multi-channel representation for images on quantum computers, *Journal of Advanced Computational Intelligence and Intelligent Informatics*, 17(3):1-13, 2013.
- J8** Bo Sun, Abdullah M. Ilyasu, **Fei Yan**, Jesus A. Garcia, Fangyan Dong, Awad Kh. Al-Asmari, and Kaoru Hirota, Multi-channel information operations on quantum images, *Journal of Advanced Computational Intelligence and Intelligent Informatics*, 18(4), 2014.

• International Conference Papers

- C1** **Fei Yan**, Phuc Q. Le, Abdullah M. Ilyasu, Bo Sun, Jesus A. Garcia, Fangyan Dong, and Kaoru Hirota, Assessing the similarity of quantum images based on probability measurements. *2012 IEEE World Congress on Computational Intelligence (IEEE CEC)*, 1-6, 2012.
- C2** **Fei Yan**, Abdullah M. Ilyasu, Zhentao Liu, Janet P. Betancourt, Fangyan Dong, and Kaoru Hirota, Bloch sphere based representation for quantum emotion space. *2014 IEEE World Congress on Computational Intelligence (FUZZ-IEEE)*, Under review.
- C3** Bo Sun, Phuc Q. Le, Abdullah M. Ilyasu, **Fei Yan**, Adrian S. Garcia, Fangyan Dong, and Kaoru Hirota, A multi-channel representation for images on quantum computers using RGB color space, *2011 IEEE International Symposium on Intelligent Signal Processing*, 1-6, 2011.
- C4** Bo Sun, Abdullah M. Ilyasu, **Fei Yan**, Jesus A. Garcia Sanchez, Fangyan Dong, Awad Kh. Al-Asmari, and Kaoru Hirota, Quantum Computation based Color Information Transformation on Multi-Channel Image, *The Ninth China-*

Japan International Workshop on Information Technology and Control Applications, 19-26, 2013.